The Dissertation Committee for Thomas Matthew Murphy Certifies that this is the approved version of the following dissertation:

Physical Aging of Glassy Polymers in Confined Environments

Committee:

Donald R. Paul, Co-Supervisor

Benny D. Freeman, Co-Supervisor

Christopher J. Ellison

David A. Vanden Bout

Isaac C. Sanchez

Physical Aging of Glassy Polymers in Confined Environments

by

Thomas Matthew Murphy, B.S.Ch.E.

Dissertation

Presented to the Faculty of the Graduate School of

The University of Texas at Austin

in Partial Fulfillment

of the Requirements

for the Degree of

Doctor of Philosophy

The University of Texas at Austin

December 2012

Dedication

To my family, both current and future

Acknowledgements

Most students who enter graduate school with an idealized vision of how their studies will proceed are soon confronted with a much different reality once they begin their research. The road leading to a Ph.D. is not always as smooth as one would hope. A substantial amount of careful thought and planning, coupled with a tremendous amount of diligence and perseverance, is required. It is difficult to imagine finishing a doctoral program without the help and support of many people. I want to extend my sincere thanks to Dr. Don Paul and Dr. Benny Freeman for serving as my research advisors. I consider myself fortunate to have been under their guidance during my studies at the University of Texas. They have encouraged me, shared with me their accumulated wisdom, and offered many useful suggestions that have helped me in my work. I have a tremendous amount of personal and professional respect for both of them.

I would also like to acknowledge my fellow research group members. Special thanks are due to my CLiPS colleagues Dan Miller, Grant Offord, and Kevin Tung, with whom I entered the program and shared many memorable experiences. I thank Dr. Brandon Rowe, Dr. Norman Horn, Dr. Lili Cui, and Dr. Rajkiran Tiwari for their help and suggestions related to research-specific issues. I am grateful for my interactions with all of the current and former members of the Paul and Freeman research groups, and I wish all of them the best in life and work. I would also like to thank our colleagues at Case Western Reserve University, especially Dr. Mike Ponting and Dr. Deepak Langhe, who provided me with materials that I used in my work and helped in the characterization of layered films. I would like to acknowledge the National Science Foundation, which provided funding for the CLiPS program and financial support for my studies. Thanks

are also due to Dr. Eric Baer and the late Dr. Anne Hiltner, who directed the NSF CLiPS program.

The roommates with whom I have lived during graduate school deserve mention as well, so I would like to thank Dr. Marty Gran, Dr. Mark Pond, Dr. Sean Carroll, Col. Peter Frailie, Doug French, and Justin Harris for their friendship and for the good times we shared. As luck would have it, I also met my fiancée, Helen, during my time in Austin. She has been a constant source of encouragement and has helped me through a number of tough times, both personal and work-related. I would not be the person I am today without her love and support, and for those things I am truly grateful. I would also like to specially thank my parents, John and Debbie Murphy, and my sisters, Erin and Maura, who have always been there to offer support and encouragement to me in everything I do. I am so fortunate to have been blessed with the family that I have.

Physical Aging of Glassy Polymers in Confined Environments

Thomas Matthew Murphy, Ph.D.

The University of Texas at Austin, 2012

Supervisors: Donald R. Paul and Benny D. Freeman

This research project investigated the physical aging of glassy polymers in confined environments. Many recent studies of aging in glassy polymers have observed that aging behavior is often strongly affected by confinement. Understanding aging in confined environments (e.g., thin polymer films and nanocomposites) is vital for predicting long-term performance in applications that use confined glassy polymers, such as gas separation membranes and advanced nanocomposite materials.

Aging in bulk and layered films produced via layer-multiplying co-extrusion was studied using gas permeability measurement and differential scanning calorimetry (DSC). The layered films consisted of polysulfone (PSF) and a rubbery co-layering material, with PSF layers ranging in thickness from ~185 nm to ~400 nm. Gas permeation aging studies at 35 °C revealed that the PSF layers in layered films aged in a manner that was similar to bulk PSF and independent of layer thickness. This finding differs from what was observed previously in freestanding PSF films, in which aging depended strongly on thickness and was accelerated relative to bulk.

Isothermal aging studies at 170 °C and cooling rate studies were performed on both bulk and layered samples using DSC. The aging of the PSF layers was similar to aging in bulk PSF for films having PSF layer thicknesses of ~640 nm and ~260 nm, while

the film with 185 nm PSF layers showed a slightly higher aging rate than that of bulk PSF. The results of the DSC studies generally support the conclusions of our gas permeation aging studies. The absence of strong thickness dependence in aging studies of layered films tends to support the idea that the effect of film thickness on physical aging stems from interfacial characteristics and not merely thickness per se.

The physical aging of thin polystyrene (PS) films at 35 °C was also investigated using gas permeation techniques. PS films of 400 nm and 800 nm did not exhibit aging behavior that was highly accelerated relative to bulk or strongly dependent on film thickness. At the thicknesses and aging temperature considered, the aging of PS shows much weaker thickness dependence than that seen in polymers like PSF and Matrimid.

Table of Contents

List of Tables

List of Figures

Chapter 1: Introduction

1.1 INTRODUCTION

"Physical aging" refers to changes in the properties of a non-equilibrium glassy material as it approaches equilibrium *via* structural rearrangement.[1,2] Physical aging occurs in all types of glassy materials, but it is perhaps most commonly studied in polymers. Aging results in densification of a polymer sample, which leads to increased brittleness, increased refractive index, decreased gas permeability, decreased enthalpy, and a host of other property changes.[3–7] Though physical aging in bulk polymer glasses has been widely studied, there have been many recent investigations into the aging behavior of polymers in confined environments (*e.g.*, thin films and nanocomposites). Many of these studies have found that aging in confinement is often significantly different from that of bulk.[3,5,6,8–17] Interest in the aging of confined polymers stems from the wide variety of applications that utilize polymers in confined geometries, such as gas separation membranes and nanocomposite materials, among others.[5,6,16–19] Gas separation membranes often have a 50-100 nm glassy "skin" layer, so understanding the aging of thin films is necessary for predicting the long-term performance of a membrane module. Many studies of aging in confinement have thus used gas permeability measurement at near-ambient temperatures to track aging in polymers that are of interest as gas separation membrane materials. These studies have generally found that aging in thin films is accelerated relative to bulk and dependent on film thickness, with noticeable deviations from bulk behavior beginning at film thicknesses on the order of 1-3 μm.[4–6,8,10,20–24] Studies of the glass transition in thin films have generally shown that measurable deviations from the bulk T_g begin when the film thickness is on the order of ~100 nm or less,[25–28] which is roughly an order of magnitude less than the thickness at which aging behavior modifications have been observed in gas permeation studies.

Other aging studies have used techniques such as ellipsometry, fluorescence spectroscopy, dielectric spectroscopy, and differential scanning calorimetry to study physical aging in thin films of various polymers.[12–15,29–32] These studies have found that the effect of confinement on aging depends on the aging temperature and the nature of the interfacial interactions (*i.e.*, polymer-substrate interactions or free surfaces). Different types of interfacial interactions can lead to enhanced, suppressed, or invariant physical aging rates with decreasing film thickness.[12,13,29,30,33]

The diversity of experimental findings in studies using different polymers, experimental techniques, and temperature ranges suggest that there are many questions about physical aging in confinement that remain unanswered. Thus, from a purely fundamental scientific point of view, the aging and dynamics of glasses in confinement is an interesting topic of study; however, understanding aging and its effects has practical relevance for gas separation membranes, microelectronics, nanocomposites, and other applications that use glassy polymers in confinement.

1.2 GOALS AND ORGANIZATION OF THIS DISSERTATION

The primary goal of this research was to develop a better understanding of the physical aging behavior of polymers in confined environments. Multilayered films with thin polysulfone layers and freestanding thin films of polystyrene were both studied. It was of particular interest to investigate the role played by interfaces (free surfaces and polymer-polymer interfaces) during physical aging. The effect of aging on the gas permeability of polystyrene, a polymer with a more flexible backbone than previously studied membrane materials, was also explored. The data gathered during this work was

compared and contrasted with published results in order to provide context for our findings.

This dissertation is divided into eight chapters, including this introduction. Chapter 2 provides a more detailed description of physical aging and its effects. A portion of this chapter is dedicated to summarizing the work of other researchers who have investigated physical aging in confined polymer systems using a variety of techniques. Layer-multiplying co-extrusion is also discussed. The materials and experimental methods that were used in performing the work described in this dissertation are discussed in chapter 3.

Chapter 4 presents comparisons of the permeability and selectivity of Engage 8100 (a rubbery material used to produce the layered films discussed in Chapter 5 and Appendix A) to similar materials that have been studied previously. The measured values for Engage 8100 (EO) were found to be reasonable based on these comparisons, so these values were used to calculate the polysulfone (PSF) layer permeability for aging experiments involving PSF/EO films.

Chapter 5 presents the results of gas permeation aging experiments for layered PSF/EO and PSF/Infuse 9007 (PSF/OBC) films. The aging behavior of the PSF layers in both types of layered films was largely similar to that of bulk PSF films and did not show a strong dependence on films thickness. Chapter 6 discusses DSC studies of PSF/OBC films. Both isothermal aging studies and cooling rate studies were performed. The results of these studies were found to be in general agreement with those presented in Chapter 5, in which the behavior of the layered films displayed little thickness dependence and was similar to bulk. Chapter 7 presents the results from aging studies of thin and bulk films of PS. These studies revealed that, in contrast to previously studied gas separation polymers like PSF and Matrimid, PS films do not appear to show aging

behavior that is strongly dependant on film thickness or highly accelerated relative to bulk.

Chapter 8 provides a summary of the main conclusions from this research and discusses recommendations for future work related to the physical aging of glassy polymers in confined environments.

1.3 REFERENCES

1. Hutchinson JM. Physical aging of polymers. *Progress in Polymer Science* **1995**, 20(4): 703–760.

2. Hodge IM. Physical aging in polymer glasses. *Science* **1995**, 267(5206): 1945–1947.

3. Struik LCE. *Physical Aging in Amorphous Polymers and Other Materials*. Amsterdam, Elsevier, 1978.

4. Huang Y, Paul DR. Physical Aging of Thin Glassy Polymer Films Monitored by Optical Properties. *Macromolecules* **2006**, 39(4): 1554–1559.

5. Rowe BW, Freeman BD, Paul DR. Physical aging of ultrathin glassy polymer films tracked by gas permeability. *Polymer* **2009**, 50(23): 5565–5575.

6. Huang Y, Paul DR. Physical aging of thin glassy polymer films monitored by gas permeability. *Polymer* **2004**, 45(25): 8377–8393.

7. Simon SL, Sobieski JW, Plazek DJ. Volume and enthalpy recovery of polystyrene. *Polymer* **2001**, 42(6): 2555–2567.

8. Huang Y, Paul DR. Effect of Temperature on Physical Aging of Thin Glassy Polymer Films. *Macromolecules* **2005**, 38(24): 10148–10154.

9. Cui L, Qiu W, Paul DR, Koros WJ. Physical aging of 6FDA-based polyimide membranes monitored by gas permeability. *Polymer* **2011**, 52(15): 3374–3380.

10. Pfromm PH, Koros WJ. Accelerated physical ageing of thin glassy polymer films: evidence from gas transport measurements. *Polymer* **1995**, 36(12): 2379–2387.

11. Kim JH, Koros WJ, Paul DR. Physical aging of thin 6FDA-based polyimide membranes containing carboxyl acid groups. Part II. Optical properties. *Polymer* **2006**, 47(9): 3104–3111.

12. Koh YP, Simon SL. Structural relaxation of stacked ultrathin polystyrene films. *Journal of Polymer Science Part B: Polymer Physics* **2008**, 46(24): 2741–2753.

13. Pye JE, Rohald KA, Baker EA, Roth CB. Physical Aging in Ultrathin Polystyrene Films: Evidence of a Gradient in Dynamics at the Free Surface and Its Connection

to the Glass Transition Temperature Reductions. *Macromolecules* **2010**, 43(19): 8296–8303.

14. Baker EA, Rittigstein P, Torkelson JM, Roth CB. Streamlined ellipsometry procedure for characterizing physical aging rates of thin polymer films. *Journal of Polymer Science Part B: Polymer Physics* **2009**, 47(24): 2509–2519.

15. Gray LAG, Yoon SW, Pahner WA, Davidheiser JE, Roth CB. Importance of Quench Conditions on the Subsequent Physical Aging Rate of Glassy Polymer Films. *Macromolecules* **2012**, 45(3): 1701–1709.

16. Boucher VM, Cangialosi D, Alegría A, Colmenero J. Enthalpy Recovery of PMMA/Silica Nanocomposites. *Macromolecules* **2010**, 43(18): 7594–7603.

17. Boucher VM, Cangialosi D, Alegría A, Colmenero J, Pastoriza-Santos I, Liz-Marzan LM. Physical aging of polystyrene/gold nanocomposites and its relation to the calorimetric Tg depression. *Soft Matter* **2011**, 7(7): 3607.

18. Baker RW. Future directions of membrane gas separation technology. *Ind. Eng. Chem. Res* **2002**, 41(6): 1393–1411.

19. Rittigstein P, Torkelson JM. Polymer-nanoparticle interfacial interactions in polymer nanocomposites: confinement effects on glass transition temperature and suppression of physical aging. *Journal of Polymer Science Part B: Polymer Physics* **2006**, 44(20): 2935–2943.

20. Huang Y, Paul DR. Effect of Film Thickness on the Gas-Permeation Characteristics of Glassy Polymer Membranes. *Industrial & Engineering Chemistry Research* **2007**, 46(8): 2342–2347.

21. Huang Y, Paul DR. Effect of molecular weight and temperature on physical aging of thin glassy poly(2,6-dimethyl-1,4-phenylene oxide) films. *Journal of Polymer Science Part B: Polymer Physics* **2007**, 45(12): 1390–1398.

22. Rowe BW, Pas SJ, Hill AJ, Suzuki R, Freeman BD, Paul DR. A variable energy positron annihilation lifetime spectroscopy study of physical aging in thin glassy polymer films. *Polymer* **2009**, 50(25): 6149–6156.

23. Rezac ME, Pfromm PH, Costello LM, Koros WJ. Aging of thin polyimide-ceramic and polycarbonate-ceramic composite membranes. *Industrial & Engineering Chemistry Research* **1993**, 32(9): 1921–1926.

24. Pfromm PH, Koros WJ. Accelerated physical aging of thin glassy polymer films. *Polymeric Materials Science and Engineering* **1994**, 71 401–402.

25. Kim JH, Jang J, Zin W-C. Estimation of the Thickness Dependence of the Glass Transition Temperature in Various Thin Polymer Films. *Langmuir* **2000**, 16(9): 4064–4067.

26. Ellison CJ, Torkelson JM. The distribution of glass-transition temperatures in nanoscopically confined glass formers. *Nature Materials* **2003**, 2(10): 695–700.

27. Forrest JA, Dalnoki-Veress K, Stevens JR, Dutcher JR. Effect of free surfaces on the glass transition temperature of thin polymer films. *Physical Review Letters* **1996**, 77(10): 2002–2005.

28. Forrest JA, Dalnoki-Veress K. The glass transition in thin polymer films. *Advances in Colloid and Interface Science* **2001**, 94(1-3): 167–195.

29. Priestley RD, Ellison CJ, Broadbelt LJ, Torkelson JM. Structural relaxation of polymer glasses at surfaces, interfaces, and in between. *Science* **2005**, 309(5733): 456–9.

30. Ellison CJ, Kim SD, Hall DB, Torkelson JM. Confinement and processing effects on glass transition temperature and physical aging in ultrathin polymer films: novel fluorescence measurements. *The European Physical Journal E - Soft Matter* **2002**, 8(2): 155–66.

31. Kawana S, Jones RAL. Effect of physical ageing in thin glassy polymer films. *The European Physical Journal E - Soft Matter* **2003**, 10(3): 223–30.

32. Cangialosi D, Wübbenhorst M, Groenewold J, Mendes E, Picken SJ. Diffusion mechanism for physical aging of polycarbonate far below the glass transition temperature studied by means of dielectric spectroscopy. *Journal of Non-Crystalline Solids* **2005**, 351(33-36): 2605–2610.

33. Priestley RD, Broadbelt LJ, Torkelson JM. Physical Aging of Ultrathin Polymer Films above and below the Bulk Glass Transition Temperature: Effects of Attractive vs Neutral Polymer−Substrate Interactions Measured by Fluorescence. *Macromolecules* **2005**, 38(3): 654–657.

Chapter 2: Background

2.1 PHYSICAL AGING AND THE GLASSY STATE

When an amorphous polymer is above its glass transition temperature (T_g), the timescales for molecular relaxation are much smaller than typical experimental timescales (i.e., the imposed heating or cooling rate), and the material can readily achieve an equilibrium state. If the polymer sample is continuously cooled, however, the timescales for structural relaxation become larger until eventually exceeding the experimental timescales, resulting in a material that is no longer in equilibrium. The temperature around which this crossover of timescales occurs is known as the glass transition temperature.[1] Although it is not a true thermodynamic transition, it resembles a second-order transition and is usually reported as a single temperature despite its dependence on kinetic factors. The non-equilibrium nature of the glassy state is common to all amorphous substances, not just polymer glasses, and is manifested by material properties, such as volume (V) and enthalpy (H), which are in excess of equilibrium values.[2] Over time, a glassy material will progress toward an equilibrium state, and the excess properties will decrease. Thus, the temperature alone is not sufficient for describing the state of a glassy polymer; its properties are also dependent on the constantly-evolving structural state of the material, which is often characterized by the fictive temperature (T_f) or the displacement from equilibrium (δ).[1]

Figure 2.1 provides an illustration of T_g, T_f, δ, and the evolution of excess properties towards equilibrium at a given aging temperature (T_a). The plots of volume and enthalpy are qualitatively similar, so both variables are included on the ordinate in Figure 2.1.

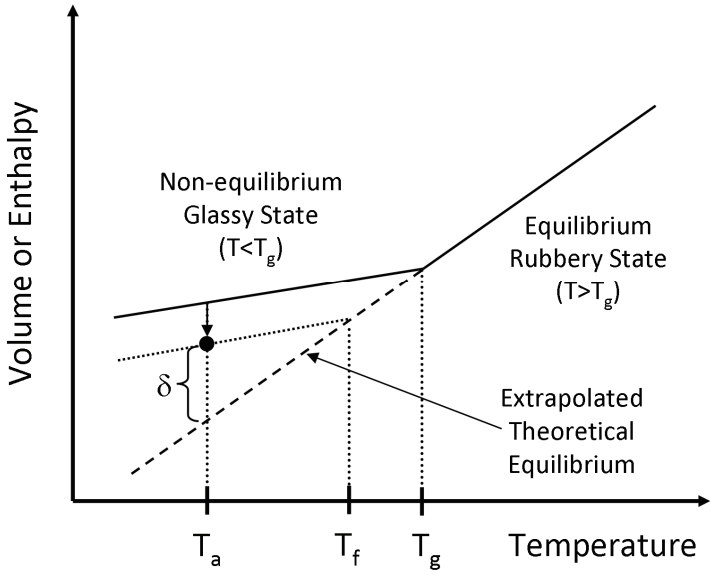

Figure 2.1: Schematic diagram of volume or enthalpy versus temperature for a glass-forming polymer.

"Physical aging" is a term often used to describe these relaxation phenomena, and it can be defined as the change in any property over time due only to structural relaxations in a glassy material that is progressing towards equilibrium, absent any influence from the surroundings (e.g., no temperature changes and no applied stresses).[1] The physical aging process results in the densification of the polymer and thus a decrease of its free volume. It is different from chemical aging, weathering, and other such phenomena in that it is thermoreversible and does not involve any chemical changes (e.g., oxidation or chain scission).[1,2] Thermoreversability means that the aging effects can be erased by heating the material above its T_g for a sufficient period of time, which allows the material to achieve an equilibrium state. This is very important from an experimental point of view, since it provides a method of "resetting" the aging clock to an effective "zero time" and is thus a reliable way of ensuring that any experiments performed are meaningful and repeatable.

Because many properties change as the material undergoes physical aging, understanding and accounting for physical aging is critical for any application that uses glassy polymers. There are a variety of methods that have been used to track aging, including differential scanning calorimetry (DSC),[3–12] gas permeability measurement,[13–25] dilatometry,[26–28] creep response measurement,[2,5,29] dielectric spectroscopy,[30–33] fluorescence techniques,[34–42] positron annihilation spectroscopy (PALS),[25,33,43,44] and ellipsometry.[20,23,45–48] Physical aging in bulk polymer systems has been studied for many years using these techniques and others, but much of the recent literature has focused on aging in polymers subject to confinement.

2.2 POLYMERS IN CONFINEMENT

Polymers that are confined in one or more dimension, such as thin films or nanocomposites, are of tremendous practical interest in a variety of applications. For example, gas separation membranes utilize a thin, selective polymer layer to perform a variety of important industrial separations, such as the recovery of hydrogen from ammonia purge gas streams or the removal of CO_2 from natural gas.[49] Thus, a great deal of attention has been focused on understanding the properties and behavior of confined polymers. Confinement can have a pronounced effect on the measured glass transition. Researchers using techniques such as ellipsometry, X-ray reflectivity, Brillouin light scattering, fluorescence spectroscopy, and DSC have investigated the effect of confinement (i.e., film thickness, in many cases) on the glass transition.[42,50–57] Most of the studies involving freestanding thin films or films supported on a non-attractive substrate have found that T_g generally decreases with decreasing film thickness. Studies

of thin films supported on attractive substrates, such as PMMA on silica, have demonstrated that the T_g can increase with decreasing film thickness.[58] The attractive polymer-substrate interactions are believed to decrease molecular mobility of the near-interface material, thus increasing the measured T_g. Material near a free surface is believed to have greater mobility than the bulk polymer, which tends to depress the T_g in freestanding films or those lacking strong polymer-substrate interactions. As a film is made thinner, the near-interface material represents an increasingly greater fraction of the total and thus has a greater effect on the glass transition behavior. In some studies, however, no significant effect of film thickness on the glass transition has been observed.[58,59] In the work of Priestley et al., this finding has been attributed to a balance between the competing effects of substrate-polymer interactions (which tend to increase T_g) and greater free surface mobility (which tends to decrease the T_g).[58] Tress et al. suggest that sample preparation techniques are crucially important and that the observations of T_g changes by other researchers are the result of artifacts of preparation, such as residual solvent that remains in the film even after annealing above the T_g of the sample.[59] The glass transition and glassy dynamics of confined polymers continue to be important and challenging areas of research, with many questions yet to be answered.

2.3 KINETICS OF PHYSICAL AGING AND STRUCTURAL RELAXATION IN GLASSES

The kinetics of the aging process in polymers depends on the driving force provided by the existence of excess properties (i.e., the magnitude of the departure from equilibrium, shown as δ in Figure 2.1) and the local segmental mobility, which depends on the structure of the material. Both of these factors also depend on temperature. As the

driving force decreases during aging, the segmental mobility also decreases as the material becomes denser. Consequently, the aging process is non-linear and self-retarding.[2] Because the aging process slows as it progresses, aging phenomena usually persist over very long timescales. For bulk polymers at normal service temperatures (i.e., well below T_g), physical aging often occurs throughout the lifetime of the material.[2]

Early studies of inorganic glasses by Tool helped establish that a relaxation time that depended only on temperature was not sufficient for describing the kinetics of structural relaxation.[60,61] Kovacs pioneering work in poly(vinyl acetate) (PVAc) and PS demonstrated many of the features of structural relaxation in glassy polymers, including its non-linearity, which results in the asymmetry of approach to equilibrium for temperature jumps of equal magnitude (i.e., equal departures from equilibrium) but opposite sign, and the so-called memory effect, which arises from the existence of a distribution of relaxation times rather than a single relaxation time.[26,62] Models of aging behavior are generally of the mathematical form shown below.

$$\frac{d\delta}{dt} = -\frac{\delta}{\tau(t,T)} \tag{2.1}$$

In equation 2.1, δ represents the difference between the instantaneous value of some property (e.g., volume, enthalpy, fictive temperature) and its equilibrium value, and τ is a relaxation time that depends on both temperature and aging time.

The fictive temperature concept is often used in phenomenological models of structural relaxation and physical aging, such as the Tool-Narayanaswamy-Moynihan (TNM) model, to capture the dependence of the relaxation time on the instantaneous structural state of the polymer.[61,63,64] In the TNM model, the entire thermal history is modeled, and the change in fictive temperature (T_f) can be calculated as shown in the equation below.[65]

$$T_f = T_0 + \sum_i \Delta T_i \left\{ 1 - \exp\left[-\left(\int_0^t \frac{dt'}{\tau} \right)^{\beta} \right] \right\} \tag{2.2}$$

In equation 2.2, T_0 is the initial temperature ($T_0 > T_g$), ΔT_i is the *i*-th temperature step, β is the non-exponentiality parameter, and τ is the relaxation time. The relaxation time, τ, is given by the equation below.

$$\tau = A \exp\left[\frac{x\Delta h^*}{RT} + \frac{(1-x)\Delta h^*}{RT_f} \right] \tag{2.3}$$

In the above equation, A is a constant, x is the nonlinearity parameter (which defines the relative contributions of temperature and structure to the relaxation time), Δh^* is the apparent activation enthalpy, T is the temperature and R is the universal gas constant. The TNM model is often used in DSC and dilatometry experiments, and it is able to describe the key features of relaxation in glasses.[65,66] However, the model parameters sometimes depend on the thermal history, and it is often difficult to ascribe physical meaning to these parameters.[67] Additionally, in order to model DSC data, a sufficient amount of data for the equilibrium region (i.e., above T_g) must be available so that an equation describing the heat capacity of the equilibrium state as a function of temperature can be determined. For aging temperatures far below T_g, the model fitting is often much poorer than it is in the near-T_g regime.[68]

2.4 GAS PERMEATION IN POLYMER MEMBRANES

The permeation of gases through non-porous polymer membranes (i.e., films) occurs *via* a solution-diffusion mechanism, whereby gas dissolves into the membrane at

its upstream (i.e., higher-pressure) face, diffuses through the membrane, and desorbs at the downstream (i.e., lower-pressure) face.[69,70] A permeability coefficient for gas A (P_A) can be defined as the flux of gas A (N_A) normalized by the imposed partial pressure gradient ($\Delta p_A/\ell$), as shown in the equation below.

$$P_A = \frac{N_A \ell}{\Delta p_A} \tag{2.4}$$

In this equation, ℓ represents the membrane thickness, and Δp_A represents the difference in partial pressure between the upstream and downstream face of the membrane. For common experimental conditions (i.e., using a single gas and imposing a much higher partial pressure at the upstream face than at the downstream face), Fick's first law can be used to show that the permeability coefficient, P, depends on the product of the diffusivity of the gas in the polymer (D) and the solubility coefficient at the upstream face (S).

$$P = DS \tag{2.5}$$

The permeability thus depends on both a thermodynamic factor (the equilibrium partioning coefficient, S) and a kinetic factor (D). The diffusivity of a gas in a polymer generally depends on the molecular size of the gas, with smaller gases (i.e., H_2 and He) typically having higher diffusion coefficients. Solubility generally depends on the gas condensability, which is often described in terms of the critical temperature (T_c), normal boiling point (T_b), or the Lennard-Jones potential well depth (ε/k), and thus more condensable gases (which are typically larger) tend to have higher solubility coefficients.

Gas permeability coefficients usually correlate well with the free volume of the polymer.[71,72] The following equation is often used to describe the dependence of gas permeability on fractional free volume (FFV).

$$P = A\exp\left[-B/FFV\right] \tag{2.6}$$

In this equation, A and B are gas-dependent constants. This correlation has been used by Park and Paul to develop an improved group contribution method for FFV estimation, based solely on the polymer structure, that allows for better prediction of gas permeability in glassy polymers than previous methods.[72]

The ideal selectivity ($\alpha_{A/B}$) of a polymer is defined as the ratio of pure-gas permeability coefficients for gas *A* and gas *B* (where gas A is generally the more permeable gas, so that $\alpha_{A/B}$ is greater than unity).

$$\alpha_{A/B} = \frac{P_A}{P_B} = \left(\frac{D_A}{D_B}\right)\left(\frac{S_A}{S_B}\right) \tag{2.7}$$

As shown in equation 2.7, the permselectivity can be written as the product of the diffusivity selectivity (D_A/D_B) and the solubility selectivity (S_A/S_B). As a general rule, glassy polymers like polysulfone[73] tend to be more size-sieving (i.e., diffusion-selective) than rubbery polymers. Rubbery polymers like poly(dimethylsiloxane) typically have weak size-sieving ability, and thus their overall selectivities are controlled primarily by their solubility selectivities.[74,75]

2.5 GAS PERMEATION AGING STUDIES OF THIN FILMS

Gas molecules serve as exquisitely sensitive probes for monitoring changes in the free volume of a polymer. As a polymer ages, its free volume decreases, and a decrease in the pure-gas permeability coefficients and an increase in selectivity is generally observed. A significant portion of the literature on aging of confined polymers has

focused on aging in glassy materials that are of interest as gas separation materials, such as polysulfone (PSF) and various polyimides (notably Matrimid).[13,15–19,22,24,76–82] Typically, the polymers of interest have T_gs greater than 150 °C (often much higher).[13,17,24,78] These studies are normally conducted at near-ambient temperatures (35 °C, most often), and gas permeability is measured over the course of weeks or months. Researchers using gas permeation techniques have generally observed accelerated or enhanced physical aging with decreasing film thickness. The thickness at which noticeable modifications in the aging behavior begin has been observed to be on the order of a few microns, which is much greater than the thickness typically associated with the onset of T_g depression in thin films (by roughly an order of magnitude or more, for many polymers).[56,57]

In the early 1990's, studies of time-dependent gas transport behavior in glassy polymers by Rezac et al. and Pfromm et al. revealed that the aging behavior of thin films ($\ell < 1$ μm) can be accelerated relative to that of thicker bulk films.[13–16] Later work by McCaig et al. on a glassy polyarylate also observed that physical aging in thin films is more rapid than it is in bulk films.[24] Huang and Paul performed systematic aging studies of freestanding films of polysulfone (PSF), Matrimid, and poly(2,6-dimethyl-1,4-phenylene oxide) using gas permeability tracking and ellipsometry and found that the aging of films less than 1 μm in thickness is more rapid than that of bulk films, strongly thickness-dependent, and dependent on the chemical structure of the polymer.[17–19,21,45,46] The lower limit of film thickness in their studies was roughly 400 nm, which is still above the regime where the glass transition temperature changes significantly with thickness. Figure 2.2 presents their oxygen permeability data for a series of polysulfone films with different thicknesses that were aged at 35°C.

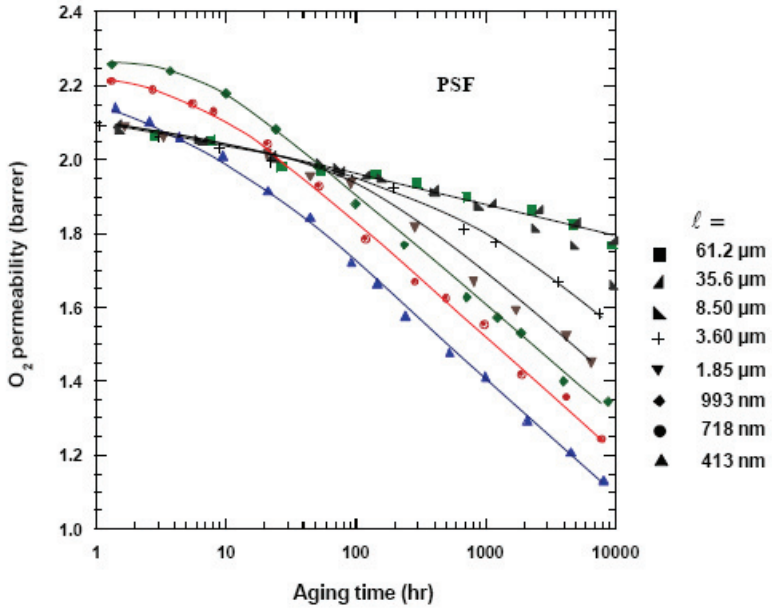

Figure 2.2: Oxygen permeability data for freestanding PSF films aged at 35 °C.[17]

They observed qualitatively similar behavior for other probe gases; however, less-permeable gases (such as N_2 and CH_4) typically exhibit a larger decrease in permeability relative to the initial measured values, giving rise to moderate increases in permselectivity over time. Their ellipsometric studies of physical aging also showed accelerated aging for thin films.[45,46] Huang et al. and McCaig et al. suggested a diffusive mechanism for free volume loss, in which free volume elements can diffuse to film surfaces and escape, rendering the film more dense. This mechanism, in conjunction with a bulk "lattice contraction" mechanism that is independent of film thickness, was used to rationalize the observations of thickness-dependent aging in thin films and the lack of thickness dependence in bulk films. In a study of the temperature dependence of aging as assessed by gas permeability, Huang and Paul observed that the difference between the aging rates of 400 nm and 3.6 µm PSF films was greater for films aged at 35 °C than for films aged at 45 °C or 55 °C.[19] Increasing the temperature increased the

aging rate at each thickness but decreased the sensitivity of aging rate to film thickness. For the thinnest films considered (400 nm), the difference in the aging rates at the three temperatures considered was small. A study of PPO films aged at different temperatures showed similar results.[20]

Rowe et al. extended studies of PSF and Matrimid to films as thin as 18 nm.[22] A PDMS coating technique was used to eliminate convective flow of gas through pinhole defects, thus enabling the study of these ultrathin films. Within experimental uncertainty, the PDMS coating did not affect the aging behavior of the coated film. As film thickness was decreased incrementally from 465 nm to 20 nm, the initial permeability values were lower and the initial selectivities were higher. For a 20 nm PSF film, the initial oxygen permeability was approximately 30-40% less than that of a bulk or 465 nm PSF film, indicating that the thinner film had already achieved a denser, lower-free volume state by the time the first measurement could be made. These findings were attributed to rapid aging that occurred during the first hour of aging time (which is experimentally inaccessible using these techniques). Rapid aging during the first hour (and perhaps rapid structural relaxation that occurs during cooling to the aging temperature from above T_g) also resulted in slightly lower aging rates for the thinnest films when compared to the thicker films studied. The properties of the ultrathin films strongly deviated from those of bulk films, and these deviations were said to be consistent with the ideas of enhanced mobility of near-surface material and T_g depression in the thinnest films.[22]

Cui et al. studied the aging behavior of 6FDA-based polyimides using gas permeability measurement and observed dramatic differences between the behavior of bulk films and films of ~1000 nm or less.[81] The oxygen permeabilities of the thin films after 1000 hr of aging were approximately an order of magnitude less than the initial

values, while a 41 μm bulk film was found to undergo only a 10-15% reduction in permeability over the time period.

In general, gas permeation aging studies have observed that by the time the films reach 100 hours of aging time, thinner films typically show most of the following characteristics relative to thicker ones: lower absolute permeability values, higher selectivities, faster rates of permeability decline, and slighter greater rates of increase in selectivity.[17,21,22] In some cases, the rate of permeability decline may not continue to increase with decreasing thickness. For example, the thinnest films studied by Rowe et al. (20 nm PSF and 18 nm Matrimid) show a slower rate of permeability decline than some of the thicker films, but they have absolute permeability values that are significantly lower.[22] This finding indicates that, for the thinnest films, which would be expected to have depressed T_gs, rapid aging occurring in the first hour may result in a highly "aged" film that has a reduced driving force for physical aging and thus a slower rate of permeability decline. In summary, the consensus among researchers using gas permeability to track physical aging is that aging in unsupported thin films is thickness-dependent and accelerated relative to bulk.

2.6 CALORIMETRIC AGING STUDIES OF CONFINED GLASSES

Historically, DSC has been widely used to study the physical aging and dynamic structural relaxation (i.e., relaxation that occurs during cooling or heating while the polymer is below T_g) of glassy materials. Early studies by Petrie in the 1970s helped establish DSC as a viable and useful technique for studying physical aging in polymer glasses.[11,12] Much recent work pertaining to physical aging and enthalpy relaxation has

focused on aging in confined geometries such as polymer thin films,[65] molecular glass-formers confined in nanopores,[9] and nanocomposites.[83–87] Brief summaries of some of these studies are provided below.

Koh and Simon studied the aging of stacked ultrathin PS films using DSC.[65] They observed that the T_g broadened and decreased with decreasing film thickness. An aging rate was defined as the rate of change in the fictive temperature (T_f) with respect to the logarithm of time ($-dT_f/d \log t_a$). When aged at the same distance from T_g, bulk and ultrathin films (62 nm) showed similar aging rates, but the time required to reach equilibrium was slightly greater for the 62 nm films than it was for bulk. When aged at the same temperature, however, the ultrathin films had reduced aging rates compared to bulk yet required a shorter time to reach equilibrium. They note that their results suggest the possibility that at aging temperatures that are more than 15 °C lower than T_g (i.e., $T_g - T_a > 15$ °C), the ultrathin films may begin to show greater aging rates and shorter equilibration times than bulk when aged at equivalent distances from T_g. Using the equilibration time as the criteria for comparing the aging responses of the various films, the ultrathin films were said to undergo accelerated aging. The DSC thermograms for the thin films also showed a reduced height in the heat capacity overshoot peak and a broader glass transition relative to those observed in bulk films. Modeling efforts indicated that the thinner films had a broader distribution of relaxation times than the corresponding bulk films.[65]

Simon et al. used DSC to study the physical aging of ortho-terphenyl (o-TP) confined in a nanoporous matrix.[9] The confined o-TP exhibited accelerated aging relative to bulk, and the equilibrium state reached by the confined glasses was different from that of the bulk material. Simon et al. were able to model the aging behavior by accounting for isochoric glass formation (i.e., the o-TP "sticks" to the walls of the

nanopores and cannot undergo volume changes, thus leading to tensile stresses in the confined o-TP glass).

Boucher et al. studied enthalpy recovery in poly(methyl methacrylate) (PMMA)/silica nanocomposites using DSC.[85] Addition of silica nanoparticles did not affect T_g. Physical aging of the nanocomposites was accelerated relative to that of bulk PMMA when aged at 80 °C (i.e., T_g – 43 °C). Higher ratios of silica particle surface area to PMMA volume correlated with more rapid physical aging. A recent paper from Cangialosi et al. considered both PMMA-silica and PS-silica nanocomposites and observed accelerated aging in both systems.[84] A decoupling between the segmental mobility (as determined by broadband dielectric spectroscopy) and both the calorimetric T_g and physical aging rate was observed. A model based on the diffusion of free volume holes to the silica/polymer interface was used to rationalize their observations. Boucher et al. also studied the physical aging and glass transition of PS/gold nanocomposites by DSC.[83] When aged at the same temperature, samples with greater amounts of gold nanoparticles (i.e., a greater degree of confinement) reached equilibrium faster than a bulk PS sample. The finding that a decreased amount of time is required for PS/gold nanocomposite samples to reach equilibrium is similar to the observation of Koh and Simon discussed previously. A more recent DSC study by Boucher et al. found that even PS films with thicknesses in the range of hundreds of nanometers demonstrated accelerated aging (as judged by the time required to reach equilibrium) when aged at 358 K or 369 K.[88]

Flory et al. investigated the enthalpy relaxation and T_g of nanocomposites of PMMA and both unmodified and amino-functionalized single-wall carbon nanotubes (SWNT).[87] The T_g of unmodified SWNT nanocomposites was the same as that of pure PMMA, while the amino-functionalized nanocomposites showed a T_g increase of ~17 °C.

The physical aging of both nanocomposite systems was reduced relative to that of neat PMMA when aged at the same distance from T_g, as judged by their approach to a constant recovered enthalpy value.

A study by Langhe et al. explored physical aging of PS layers in multilayered films of PS and polycarbonate (PC) using DSC.[89] The PS/PC films had PS layer thicknesses ranging from 50 to 500 nm. The T_g of the PS layers in these films was independent of layer thickness and essentially the same as that of bulk PS. Isothermal aging studies at 80 °C showed that aging rate decreased as layer thickness decreased. A film with 50 nm PS layers had an aging rate 50% lower than that of bulk PS. The fraction of interphase material (i.e., material surrounding the PS/PC layer interface containing both PS and PC), which increases as layer thickness decreases, was inversely correlated with aging rate. The increased T_g of the interphase material was hypothesized to lead to longer relaxation times, thus reducing the aging rate. It was also suggested that the interphase material could impose mechanical constraints on PS layer relaxation that become more important as the interphase fraction increases. The enthalpy relaxation occurring during cooling these films at different rates was also studied, but the enthalpy recovered upon reheating the sample after cooling did not depend on layer thickness and was similar to that of bulk PS.

DSC studies of physical aging in confined glassy polymers, which are usually conducted at temperatures near the T_g of the polymer being studied, have often observed accelerated aging in confinement,[9,65,83–85,88] though some studies have observed decreases in the aging rate with confinement.[87,89] Generally, however, these studies have found that confinement has a pronounced effect on aging behavior.

2.7 AGING STUDIES OF CONFINED POLYMERS USING OTHER TECHNIQUES

In addition to gas permeation measurement and DSC, many other techniques have been used to study physical aging in confined polymer systems. The most common of these include ellipsometry,[23,45,47,48,90] fluorescence spectroscopy,[34,35,42,91] and dielectric spectroscopy.[33,91–96] Summaries of some of these studies are provided below.

Kawana and Jones studied the physical aging of polystyrene (PS) films via ellipsometry by measuring the overshoot in thermal expansivity versus temperature of films aged for 7 days at 80 °C.[47] The characteristic temperature of the relaxation peak was independent of film thickness, but the peak height decreased with decreasing film thickness. They also observed that physical aging occurred in 18 nm films but could not be detected in 10 nm films. Their findings were attributed to the existence of a liquid-like surface layer on the order of 10 nm.

Ellison et al. used fluorescence spectroscopy to study the aging behavior of thin films of poly(isobutyl methacrylate) supported on fused quartz and found no significant dependence of aging rate on film thickness at aging temperatures of 298 K and 323 K.[42] The lack of thickness dependence was attributed to a possible balance between the competing effects of T_g enhancement (which would increase the quantity T_g-T_a and, based on their studies of the effect of temperature on aging rate, tend to increase the aging rate) and the proportionately greater polymer-substrate interactions in the thinner films (which would tend to decrease the aging rate).

A study by Priestley et al. using fluorescence observed physical aging 7 K above the bulk T_g for a chromophore-labeled 20 nm PMMA film on a silica substrate, yet no aging was observed for a 500 nm PMMA film aged at the same temperature.[34] The 500 nm film exhibited an increase in aging rate with decreasing aging temperature, while the

20 nm film exhibited a decreasing aging rate with decreasing aging temperature; additionally, the absolute magnitude of the aging rate in the 20 nm film was much lower than in the 500 nm film at all temperatures considered. The reduced aging rate in the ultrathin films was attributed to the attractive polymer-substrate interactions (which increase T_g and become proportionately greater as a film is made thinner), and it was suggested that the increase in aging rate with increasing temperature could be due to thermal energy overcoming some of these interactions and thereby enhancing the structural relaxation in the ultrathin sample at elevated temperatures. Later work by Priestley et al. on supported PMMA films revealed a distribution of aging rates across the thickness of the film, with virtually no relaxation near the PMMA-substrate interface, bulk-like aging in the interior of the film, and a 50% decrease in aging rate at the free surface of the film.[35] The change in relaxation rates was found to propagate over 100 nm into the film, a length scale that is greater than that over which T_g is altered by surfaces and interfacial interactions. Priestley et al. also studied the physical aging of PS supported on a non-attractive silica substrate by measuring changes in the peak fluorescence intensity of chromophore-doped PS films.[34] When aged at 32 °C ($T_{g,bulk}$ − 71 °C), the aging response of a 20 nm film was similar to that of a 500 nm film. However, when aged at 93 °C ($T_{g,bulk}$ – 10 °C), the 20 nm film showed no aging while the 500 nm film aged more rapidly than it did at 32 °C. The absence of aging in the 20 nm film aged at 93 °C was said to arise from T_g depression, which caused the 20 nm film to be above its T_g and in equilibrium at 93 °C.

Pye et al. used an ellipsometry procedure developed in their laboratories[23] to study aging in thin PS films and observed that a ~30 nm film aged at a slower rate than a ~2400 nm film at all temperatures considered.[90] The difference between the aging rates of the two PS films depended on the aging temperature. For the aging temperatures they

considered, there was generally a larger difference between the aging rates of thicker and thinner films when the aging temperature was a greater distance from T_g. The difference in aging rates did not correspond merely to a shift in the aging rates to lower temperatures due to T_g depression in the ~30 nm film, which they found to be consistent with the idea of a gradient in dynamics across the film.

Rowe et al. characterized the aging behavior of PSF films using variable-energy PALS.[44] The results indicated that free volume decreased throughout the film during physical aging, as expected. A 450 nm film was observed to undergo accelerated aging when compared to a bulk sample, which is in agreement with previous studies of PSF films that used gas permeation techniques.[17] Additionally, Rowe et al. observed reduced ortho-positronium lifetimes at lower implantation energies, suggesting the existence of smaller free volume elements in the near-surface region of the film (within the first 50 nm). In contrast, variable-energy PALS studies of PS films by Cao et al. and Algers et al. showed an increase in o-Ps lifetime at low implantation energies.[97,98] Rowe et al. suggested that the near-surface regions of PSF films age more rapidly than bulk and that the enhanced mobility offered by a free surface allows that region of the film to reach a lower free volume state more quickly than bulk. Using established correlations, the o-Ps lifetime was used to calculate the fractional free volume (FFV), and the FFV was then used to calculate the oxygen permeability. The permeability values calculated from the PALS aging data (with no adjustable parameters) were then compared to data gathered independently using gas permeability measurements over time. For films of 50 nm, 125 nm, and ~450 nm, there was remarkably good agreement between the two sets of data.[44]

There has been discussion in the literature about the possibility of fundamental differences in the aging of stiffer-backbone polymers like PSF or Matrimid and that of a polymer like PS, which has a more flexible backbone.[23,99,100] Gray et al. used

ellipsometry to compare the aging behavior of PS and PSF films.[99] They measured the change in thickness of PS and PSF films quenched from above T_g in either a supported or freestanding state and then held at a given aging temperature (65 °C for PS, 100 °C for PSF). For both PS and PSF, 400 nm and 1000 nm films that were supported during the quench showed essentially identical aging behavior. The physical aging of PS films quenched while supported was then compared to that of films quenched in a freestanding state (i.e., mimicking the annealing procedure used in many of the gas permeation aging studies). They observed that 1260 nm and 600 nm films quenched in a freestanding state aged more slowly than supported-quenched films of similar thickness, despite undergoing much more rapid cooling through T_g. Upon reheating the freestanding-quenched films above T_g and then cooling in a supported state, the subsequent aging behavior was nearly identical to that of a film originally quenched in a supported state. The difference in aging rates between supported-quenched and freestanding-quenched films was much less in the 600 nm film than in the 1260 nm film. The aging rates of freestanding-quenched PS films exhibited noticeable thickness dependence at these length scales. This finding differs from what was observed in supported films, which did not show any thickness dependence in their study and were observed previously to have thickness-independent aging rates until becoming thinner than 100 nm.[90] They suggest that different quench conditions (i.e., freestanding vs. supported) would lead to different types of stresses in the glassy film, which would in turn affect the aging rate. They further argue that the biaxial stress in supported-quenched films would be independent of thickness, while the uniaxial stress in freestanding-quenched films held by a wire frame would depend on thickness.[99]

The studies of physical aging in confined polymer films using the techniques described in this section have found that the aging behavior depends strongly on the aging temperature, interfacial characteristics (i.e., polymer-substrate interactions or the

presence of free surfaces), and, in many cases, the film thickness. These studies have usually been performed on substrate-supported films, and typically the length scales associated with aging behavior changes (relative to bulk) occur are smaller than those observed in gas permeation studies.

2.8 MULTILAYER CO-EXTRUSION

Multilayer co-extrusion is a polymer processing operation in which two or more polymers are used to produce films with distinct layers. Some commercial products that use multilayered films include brightness-enhancing filters for electronic screens, films for window glass reinforcement, air bladders used in shoes, and iridescent film used in ribbons and gift wrap.[101] This technology is often used to produce films with properties that are more desirable than could be achieved using a single polymer. For example, a polymer that is a good oxygen barrier can be co-extruded with a polymer that is a good water barrier to produce a film for packaging applications that possesses the beneficial attributes of both component polymers. This technology is often very useful when one component is expensive or susceptible to degradation or attack by gases or vapors in the environment (e.g., humidity or oxygen), as it allows for the more expensive or more sensitive polymer to be laminated between what are typically less expensive protective layers. Recent studies of multilayered films have found that these materials show promise as barrier materials, gradient refractive index lenses, polymeric laser materials , and dielectric materials.[102–107]

2.9 REFERENCES

1. Hutchinson JM. Physical aging of polymers. *Progress in Polymer Science* **1995**, 20(4): 703–760.

2. Struik LCE. *Physical Aging in Amorphous Polymers and Other Materials*. Amsterdam, Elsevier, 1978.

3. Andreozzi L, Faetti M, Giordano M, Palazzuoli D. A calorimetric study of structural relaxation in the glassy state of a liquid-crystal polymer. *Philosophical Magazine B Physics of Condensed Matter Statistical Mechanics, Electronic, Optical and Magnetic Properties* **2002**, 82(4): 397–407.

4. Berens AR, Hodge IM. Effects of annealing and prior history on enthalpy relaxation in glassy polymers. 1. Experimental study on poly(vinyl chloride). *Macromolecules* **1982**, 15(3): 756–761.

5. Echeverria I, Su P-C, Simon SL, Plazek DJ. Physical aging of a polyetherimide: Creep and DSC measurements. *Journal of Polymer Science Part B: Polymer Physics* **1995**, 33(17): 2457–2468.

6. Hodge IM. Effects of annealing and prior history on enthalpy relaxation in glassy polymers. 4. Comparison of five polymers. *Macromolecules* **1983**, 16(6): 898–902.

7. Hodge IM, Huvard GS. Effects of annealing and prior history on enthalpy relaxation in glassy polymers. 3. Experimental and modeling studies of polystyrene. *Macromolecules* **1983**, 16(3): 371–375.

8. Li Q, Simon SL. Enthalpy recovery of polymeric glasses: is the theoretical limiting liquid line reached? *Polymer* **2006**, 47(13): 4781–4788.

9. Simon SL, Park J-Y, McKenna GB. Enthalpy recovery of a glass-forming liquid constrained in a nanoporous matrix: negative pressure effects. *The European Physical Journal E - Soft Matter* **2002**, 8(2): 209–16.

10. Andreozzi L, Faetti M, Giordano M, Palazzuoli D. Physical Aging in Side-Chain Liquid Crystal Polymers: A DSC Investigation of the Enthalpy Relaxation. *Macromolecules* **2002**, 35(24): 9049–9056.

11. Marshall AS, Petrie SEB. Rate-determining factors for enthalpy relaxation of glassy polymers. Molecular weight. *Journal of Applied Physics* **1975**, 46(10): 4223.

12. Petrie SEB. Thermal behavior of annealed organic glasses. *Journal of Polymer Science Part A-2: Polymer Physics* **1972**, 10(7): 1255–1272.

13. Rezac ME, Pfromm PH, Costello LM, Koros WJ. Aging of thin polyimide-ceramic and polycarbonate-ceramic composite membranes. *Industrial & Engineering Chemistry Research* **1993**, 32(9): 1921–1926.

14. Rezac ME. Update on the Aging of a Thin Polycarbonate-Ceramic Composite Membrane. *Industrial & Engineering Chemistry Research* **1995**, 34(9): 3170–3172.

15. Pfromm PH, Koros WJ. Accelerated physical aging of thin glassy polymer films. *Polymeric Materials Science and Engineering* **1994**, 71 401–402.

16. Pfromm PH, Koros WJ. Accelerated physical ageing of thin glassy polymer films: evidence from gas transport measurements. *Polymer* **1995**, 36(12): 2379–2387.

17. Huang Y, Paul DR. Physical aging of thin glassy polymer films monitored by gas permeability. *Polymer* **2004**, 45(25): 8377–8393.

18. Huang Y, Paul DR. Experimental methods for tracking physical aging of thin glassy polymer films by gas permeation. *Journal of Membrane Science* **2004**, 244(1-2): 167–178.

19. Huang Y, Paul DR. Effect of Temperature on Physical Aging of Thin Glassy Polymer Films. *Macromolecules* **2005**, 38(24): 10148–10154.

20. Huang Y, Paul DR. Effect of molecular weight and temperature on physical aging of thin glassy poly(2,6-dimethyl-1,4-phenylene oxide) films. *Journal of Polymer Science Part B: Polymer Physics* **2007**, 45(12): 1390–1398.

21. Huang Y, Paul DR. Effect of Film Thickness on the Gas-Permeation Characteristics of Glassy Polymer Membranes. *Industrial & Engineering Chemistry Research* **2007**, 46(8): 2342–2347.

22. Rowe BW, Freeman BD, Paul DR. Physical aging of ultrathin glassy polymer films tracked by gas permeability. *Polymer* **2009**, 50(23): 5565–5575.

23. Baker EA, Rittigstein P, Torkelson JM, Roth CB. Streamlined ellipsometry procedure for characterizing physical aging rates of thin polymer films. *Journal of Polymer Science Part B: Polymer Physics* **2009**, 47(24): 2509–2519.

24. McCaig MS, Paul DR. Effect of film thickness on the changes in gas permeability of a glassy polyarylate due to physical aging Part I. Experimental observations. *Polymer* **2000**, 41(2): 629–637.

25. Boersma A, Cangialosi D, Picken SJ. Mobility and solubility of antioxidants and oxygen in glassy polymers. Part II. Influence of physical aging on antioxidant and oxygen mobility. *Polymer Degradation and Stability* **2003**, 79(3): 427–438.

26. Kovacs A. Transition vitreuse dans les polymeres amorphes. Etude phenomenologique. *Fortschritte Der Hochpolymeren-Forschung* **1963**, 394–507.

27. Greiner R, Schwarzl FR. Volume relaxation and physical aging of amorphous polymers I. Theory of volume relaxation after single temperature jumps. *Colloid & Polymer Science* **1989**, 267(1): 39–47.

28. Bero CA, Plazek DJ. Volume-dependent rate processes in an epoxy resin. *Journal of Polymer Science Part B: Polymer Physics* **1991**, 29(1): 39–47.

29. Kuzmychov O, Koplin C, Jaeger R, Büchner H, Gopp U. Physical aging and the creep behavior of acrylic bone cements. *Journal of Biomedical Materials Research Part B: Applied Biomaterials* **2009**, 91B(2): 910–917.

30. Gopalakrishnan TR, Beiner M. Effects of quenching and physical aging on the relaxation behavior of nanophase-separated side chain polymers. *Journal of Physics Conference Series* **2006**, 40 67–75.

31. Wypych A, Duval E, Boiteux G, Ulanski J, David L, Mermet A. Effect of physical aging on nano- and macroscopic properties of poly(methyl methacrylate) glass. *Polymer* **2005**, 46(26): 12523–12531.

32. McGonigle EA, Daly JH, Jenkins SD, Liggat JJ, Pethrick RA. Influence of physical aging on the molecular motion and structural relaxation in poly (ethylene terephthalate) and related polyesters. *Macromolecules* **2000**, 33(2): 480–489.

33. Cangialosi D, Wübbenhorst M, Groenewold J, Mendes E, Schut H, Veen A van, Picken SJ. Physical aging of polycarbonate far below the glass transition temperature: Evidence for the diffusion mechanism. *Physical Review B* **2004**, 70 224213.

34. Priestley RD, Broadbelt LJ, Torkelson JM. Physical Aging of Ultrathin Polymer Films above and below the Bulk Glass Transition Temperature: Effects of Attractive vs Neutral Polymer−Substrate Interactions Measured by Fluorescence. *Macromolecules* **2005**, 38(3): 654–657.

35. Priestley RD, Ellison CJ, Broadbelt LJ, Torkelson JM. Structural relaxation of polymer glasses at surfaces, interfaces, and in between. *Science* **2005**, 309(5733): 456–9.

36. Rittigstein P, Torkelson JM. Polymer-nanoparticle interfacial interactions in polymer nanocomposites: confinement effects on glass transition temperature and suppression of physical aging. *Journal of Polymer Science Part B: Polymer Physics* **2006**, 44(20): 2935–2943.

37. Royal JS, Victor JG, Torkelson JM. Photochromic and fluorescent probe studies in glassy polymer matrices. 4. Effects of physical aging on poly(methyl methacrylate) as sensed by a size distribution of photochromic probes. *Macromolecules* **1992**, 25(2): 729–734.

38. Royal JS, Torkelson JM. Monitoring the molecular scale effects of physical aging in polymer glasses with fluorescence probes. *Macromolecules* **1990**, 23(14): 3536–3538.

39. Royal JS, Torkelson JM. Photochromic and fluorescent probe studies in glassy polymer matrices. 5. Effects of physical aging on bisphenol A polycarbonate and poly(vinyl acetate) as sensed by a size distribution of photochromic probes. *Macromolecules* **1992**, 25(18): 4792–4796.

40. Royal JS, Torkelson JM. Physical aging effects on molecular-scale polymer relaxations monitored with mobility-sensitive fluorescent molecules. *Macromolecules* **1993**, 26(20): 5331–5335.

41. Victor JG, Torkelson JM. Photochromic and fluorescent probe studies in glassy polymer matrices. 3. Effects of physical aging and molar weight on the size distribution of local free volume in polystyrene. *Macromolecules* **1988**, 21(12): 3490–3497.

42. Ellison CJ, Kim SD, Hall DB, Torkelson JM. Confinement and processing effects on glass transition temperature and physical aging in ultrathin polymer films: novel fluorescence measurements. *The European Physical Journal E - Soft Matter* **2002**, 8(2): 155–66.

43. Cangialosi D, Wübbenhorst M, Schut H, Veen A van, Picken S. Dynamics of polycarbonate far below the glass transition temperature: A positron annihilation lifetime study. *Physical Review B* **2004**, 69(13): 1–9.

44. Rowe BW, Pas SJ, Hill AJ, Suzuki R, Freeman BD, Paul DR. A variable energy positron annihilation lifetime spectroscopy study of physical aging in thin glassy polymer films. *Polymer* **2009**, 50(25): 6149–6156.

45. Huang Y, Paul DR. Physical Aging of Thin Glassy Polymer Films Monitored by Optical Properties. *Macromolecules* **2006**, 39(4): 1554–1559.

46. Huang Y, Wang X, Paul DR. Physical aging of thin glassy polymer films: Free volume interpretation. *Journal of Membrane Science* **2006**, 277(1-2): 219–229.

47. Kawana S, Jones RAL. Effect of physical ageing in thin glassy polymer films. *The European Physical Journal E - Soft Matter* **2003**, 10(3): 223–30.

48. Kim JH, Koros WJ, Paul DR. Physical aging of thin 6FDA-based polyimide membranes containing carboxyl acid groups. Part II. Optical properties. *Polymer* **2006**, 47(9): 3104–3111.

49. Bernardo P, Drioli E, Golemme G. Membrane Gas Separation: A Review/State of the Art. *Industrial & Engineering Chemistry Research* **2009**, 48(10): 4638–4663.

50. Forrest JA, Dalnoki-Veress K. The glass transition in thin polymer films. *Advances in Colloid and Interface Science* **2001**, 94(1-3): 167–195.

51. Koh YP, McKenna GB, Simon SL. Calorimetric glass transition temperature and absolute heat capacity of polystyrene ultrathin films. *Journal of Polymer Science Part B: Polymer Physics* **2006**, 44(24): 3518–3527.

52. Efremov MY, Warren JT, Olson EA, Zhang M, Kwan AT, Allen LH. Thin-Film Differential Scanning Calorimetry: A New Probe for Assignment of the Glass Transition of Ultrathin Polymer Films. *Macromolecules* **2002**, 35(5): 1481–1483.

53. Mattsson J, Forrest JA, Borjesson L. Quantifying glass transition behavior in ultrathin free-standing polymer films. *Physical Review E* **2000**, 62(4): 5187.

54. Kawana S, Jones RAL. Character of the glass transition in thin supported polymer films. *Physical Review E* **2001**, 63(2): 21501.

55. Jackson CL, McKenna GB. The glass transition of organic liquids confined to small pores. *Journal of Non-Crystalline Solids* **1991**, 131-133 221–224.

56. Ellison CJ, Torkelson JM. The distribution of glass-transition temperatures in nanoscopically confined glass formers. *Nature Materials* **2003**, 2(10): 695–700.

57. Kim JH, Jang J, Zin W-C. Estimation of the Thickness Dependence of the Glass Transition Temperature in Various Thin Polymer Films. *Langmuir* **2000**, 16(9): 4064–4067.

58. Priestley RD, Mundra MK, Barnett NJ, Broadbelt LJ, Torkelson JM. Effects of nanoscale confinement and interfaces on the glass transition temperatures of a series of poly (n-methacrylate) films. *Australian Journal of Chemistry* **2007**, 60(10): 765–771.

59. Tress M, Erber M, Mapesa EU, Huth H, Müller J, Serghei A, Schick C, Eichhorn K-J, Voit B, Kremer F. Glassy Dynamics and Glass Transition in Nanometric Thin Layers of Polystyrene. *Macromolecules* **2010**, 43(23): 9937–9944.

60. Tool AQ, Eicitlin CG. VARIATIONS CAUSED IN THE HEATING CURVES OF GLASS BY HEAT TREATMENT. *Journal of the American Ceramic Society* **1931**, 14(4): 276–308.

61. Tool AQ. RELATION BETWEEN INELASTIC DEFORMABILITY AND THERMAL EXPANSION OF GLASS IN ITS ANNEALING RANGE. *Journal of the American Ceramic Society* **1946**, 29(9): 240–253.

62. Kovacs AJ. The isothermal volume contraction of amorphous polymers. *J. Polymer Sci.* **1958**, 30(131-147):

63. Moynihan CT, Macedo PB, Montrose CJ, Gupta PK, DeBolt MA, Dill JF, Dom BE, Drake PW, Easteal AJ, Elterman PB, Moeller RP, Sasabe H, Wilder JA. Structural relaxation in vitreous materials. *Annals of the New York Academy of Sciences* **1976**, 279(The Glass Transition and the Nature of the Glassy State): 15–35.

64. Narayanaswamy OS. A Model of Structural Relaxation in Glass. *Journal of the American Ceramic Society* **1971**, 54(10): 491–498.

65. Koh YP, Simon SL. Structural relaxation of stacked ultrathin polystyrene films. *Journal of Polymer Science Part B: Polymer Physics* **2008**, 46(24): 2741–2753.

66. Svoboda R, Pustková P, Málek J. Structural relaxation of polyvinyl acetate (PVAc). *Polymer* **2008**, 49(13-14): 3176–3185.

67. Simon SL. Enthalpy Recovery of Poly(ether imide): Experiment and Model Calculations Incorporating Thermal Gradients. *Macromolecules* **1997**, 30(14): 4056–4063.

68. Hodge IM. Enthalpy relaxation and recovery in amorphous materials. *Journal of Non-Crystalline Solids* **1994**, 169(3): 211–266.

69. Wijmans J. The solution-diffusion model: a review. *Journal of Membrane Science* **1995**, 107(1-2): 1–21.

70. Matteucci S, Yampolskii Y, Freeman BD, Pinnau I. in:, Y. Yampolskii, I. Pinnau, B.D. Freeman (Eds.), Materials Science of Membranes for Gas and Vapor Separation, John Wiley & Sons, Ltd, 2006, pp. 1–49.

71. Lee WM. Selection of barrier materials from molecular structure. *Polymer Engineering and Science* **1980**, 20(1): 65–69.

72. Park JY, Paul DR. Correlation and prediction of gas permeability in glassy polymer membrane materials via a modified free volume based group contribution method. *Journal of Membrane Science* **1997**, 125(1): 23–39.

73. McHattie JS, Koros WJ, Paul DR. Gas transport properties of polysulphones: 1. Role of symmetry of methyl group placement on bisphenol rings. *Polymer* **1991**, 32(5): 840–850.

74. Merkel TC, Bondar VI, Nagai K, Freeman BD, Pinnau I. Gas sorption, diffusion, and permeation in poly(dimethylsiloxane). *Journal of Polymer Science Part B: Polymer Physics* **2000**, 38(3): 415–434.

75. Freeman BD, Pinnau I. Separation of gases using solubility-selective polymers. *Trends in Polymer Science* **1997**, 5(5): 167–173.

76. McCaig M., Paul DR, Barlow JW. Effect of film thickness on the changes in gas permeability of a glassy polyarylate due to physical aging Part II. Mathematical model. *Polymer* **2000**, 41(2): 639–648.

77. Dorkenoo KD, Pfromm PH. Experimental evidence and theoretical analysis of physical aging in thin and thick amorphous glassy polymer films. *Journal of Polymer Science Part B: Polymer Physics* **1999**, 37(16): 2239–2251.

78. Dorkenoo KD, Pfromm PH. Accelerated Physical Aging of Thin Poly[1-(trimethylsilyl)-1-propyne] Films. *Macromolecules* **2000**, 33(10): 3747–3751.

79. Rowe BW, Freeman BD, Paul DR. Influence of previous history on physical aging in thin glassy polymer films as gas separation membranes. *Polymer* **2010**, 51(16): 3784–3792.

80. Cui L, Qiu W, Paul DR, Koros WJ. Responses of 6FDA-based polyimide thin membranes to CO2 exposure and physical aging as monitored by gas permeability. *Polymer* **2011**, 52(24): 5528–5537.

81. Cui L, Qiu W, Paul DR, Koros WJ. Physical aging of 6FDA-based polyimide membranes monitored by gas permeability. *Polymer* **2011**, 52(15): 3374–3380.

82. Horn NR, Paul DR. Carbon dioxide plasticization and conditioning effects in thick vs. thin glassy polymer films. *Polymer* **2011**, 52(7): 1619–1627.

83. Boucher VM, Cangialosi D, Alegría A, Colmenero J, Pastoriza-Santos I, Liz-Marzan LM. Physical aging of polystyrene/gold nanocomposites and its relation to the calorimetric Tg depression. *Soft Matter* **2011**, 7(7): 3607.

84. Cangialosi D, Boucher VM, Alegría A, Colmenero J. Enhanced physical aging of polymer nanocomposites: The key role of the area to volume ratio. *Polymer* **2012**, 53(6): 1362–1372.

85. Boucher VM, Cangialosi D, Alegría A, Colmenero J. Enthalpy Recovery of PMMA/Silica Nanocomposites. *Macromolecules* **2010**, 43(18): 7594–7603.

86. Lu H, Nutt S. Restricted Relaxation in Polymer Nanocomposites near the Glass Transition. *Macromolecules* **2003**, 36(11): 4010–4016.

87. Flory AL, Ramanathan T, Brinson LC. Physical Aging of Single Wall Carbon Nanotube Polymer Nanocomposites: Effect of Functionalization of the Nanotube on the Enthalpy Relaxation. *Macromolecules* **2010**, 43(9): 4247–4252.

88. Boucher VM, Cangialosi D, Alegría A, Colmenero J. Enthalpy Recovery in Nanometer to Micrometer Thick Polystyrene Films. *Macromolecules* **2012**, 45(12): 5296–5306.

89. Langhe DS, Murphy TM, Shaver A, LaPorte C, Freeman BD, Paul DR, Baer E. Structural relaxation of polystyrene in nanolayer confinement. *Polymer* **2012**, 53(9): 1925–1931.

90. Pye JE, Rohald KA, Baker EA, Roth CB. Physical Aging in Ultrathin Polystyrene Films: Evidence of a Gradient in Dynamics at the Free Surface and Its Connection to the Glass Transition Temperature Reductions. *Macromolecules* **2010**, 43(19): 8296–8303.

91. Priestley RD. Evidence for the molecular-scale origin of the suppression of physical ageing in confined polymer: fluorescence and dielectric spectroscopy

studies of polymer-silica nanocomposites. *Journal of Physics: Condensed Matter* **2007**, 19(20): 205120.

92. Labahn D, Mix R, Schönhals A. Dielectric relaxation of ultrathin films of supported polysulfone. *Physical Review E* **2009**, 79(1): 1–9.

93. Fukao K, Miyamoto Y. Glass transitions and dynamics in thin polymer films: dielectric relaxation of thin films of polystyrene. *Physical Review E* **2000**, 61(2): 1743–54.

94. Fukao K, Sakamoto A. Aging phenomena in poly(methyl methacrylate) thin films: Memory and rejuvenation effects. *Physical Review E* **2005**, 71(4): 41803.

95. Cangialosi D, Wübbenhorst M, Groenewold J, Mendes E, Picken SJ. Diffusion mechanism for physical aging of polycarbonate far below the glass transition temperature studied by means of dielectric spectroscopy. *Journal of Non-Crystalline Solids* **2005**, 351(33-36): 2605–2610.

96. Boucher VM, Cangialosi D, Alegría A, Colmenero J, González-Irun J, Liz-Marzan LM. Accelerated physical aging in PMMA/silica nanocomposites. *Soft Matter* **2010**, 6(14): 3306.

97. Algers J, Suzuki R, Ohdaira T, Maurer FHJ. Characterization of free volume and density gradients of polystyrene surfaces by low-energy positron lifetime measurements. *Polymer* **2004**, 45(13): 4533–4539.

98. Cao H, Yuan J-P, Zhang R, Sundar C., Jean Y., Suzuki R, Ohdaira T, Nielsen B. Free volumes and holes near the polymer surface studied by positron annihilation. *Applied Surface Science* **1999**, 149(1-4): 116–124.

99. Gray LAG, Yoon SW, Pahner WA, Davidheiser JE, Roth CB. Importance of Quench Conditions on the Subsequent Physical Aging Rate of Glassy Polymer Films. *Macromolecules* **2012**, 45(3): 1701–1709.

100. Priestley RD. Physical aging of confined glasses. *Soft Matter* **2009**, 5(5): 919–926.

101. Schut JH. Microlayer films: New uses for hundreds of layers. *Plastics Technology* **2006**, 52(3): 54–57.

102. Jarus D, Hiltner A, Baer E. Barrier properties of polypropylene/polyamide blends produced by microlayer coextrusion. *Polymer* **2002**, 43(8): 2401–2408.

103. Jin Y, Tai H, Hiltner A, Baer E, Shirk JS. New class of bioinspired lenses with a gradient refractive index. *Journal of Applied Polymer Science* **2007**, 103(3): 1834–1841.

104. Wang H, Keum JK, Hiltner A, Baer E, Freeman B, Rozanski A, Galeski A. Confined crystallization of polyethylene oxide in nanolayer assemblies. *Science* **2009**, 323(5915): 757–60.

105. Wolak M a., Pan M-J, Wan A, Shirk JS, Mackey M, Hiltner A, Baer E, Flandin L. Dielectric response of structured multilayered polymer films fabricated by forced assembly. *Applied Physics Letters* **2008**, 92(11): 113301.

106. Mackey M, Hiltner A, Baer E, Flandin L, Wolak MA, Shirk JS. Enhanced breakdown strength of multilayered films fabricated by forced assembly microlayer coextrusion. *Journal of Physics D: Applied Physics* **2009**, 42(17): 175304.

107. Singer KD, Kazmierczak T, Lott J, Song H, Wu Y, Andrews J, Baer E, Hiltner A, Weder C. Melt-processed all-polymer distributed Bragg reflector laser. *Optics Express* **2008**, 16(14): 10358–10363.

Chapter 3: Materials and Experimental Methods

3.1 MATERIALS

Polysulfone (PSF) and polystyrene (PS) were the glassy polymers studied in this work. PSF is an important material in the gas separation membrane industry, and its aging behavior has been well-characterized *via* gas permeability tracking.[1–6] Because its gas permeation behavior has been well-studied in our laboratory, straightforward comparison between our results and those of previous studies can be made. PS, while not a commercially relevant material for gas separation membranes, is perhaps the most commonly studied polymer in the aging literature. Aging studies of PS using gas permeation techniques, however, have not been previously reported. PSF (UDEL P-3700, Solvay Advanced Polymers) was used to make films with hundreds of alternating layers of PSF and a rubbery co-layering material. The co-layering materials, supplied by Dow Chemical Co., were Engage 8100 (EO), an ethylene-1-octene copolymer containing 13 mol % octene, and Infuse 9007 (OBC), an olefin block copolymer. The multilayered films produced were used in both gas permeation and DSC aging studies. PS (Styron 685D) was used to produce thin films that were used in gas permeation aging studies. PDMS (Wacker Dehesive 944, with OL catalyst and V24 crosslinker) was used as a coating layer in the production of thin PS films. The relevant properties and chemical structures of the materials used are shown in Table 3.1 below.

Table 3.1: Bulk material properties

Polymer	Density	T_g	T_m	X_c	Tensile Modulus	P_{O_2}	P_{N_2}	α_{O_2/N_2}
Polysulfone 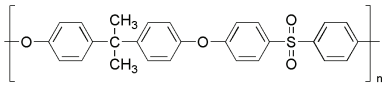	1.24	184 °C	---	---	2690	1.5	0.28	5.4
Polystyrene 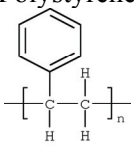	1.04	105 °C	---	---	2920	3.6	0.7	5.2
Engage 8100 (EO) 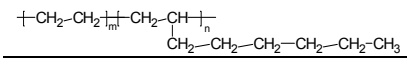	0.87	-52 °C	60 °C	15%	2.9	32	11	2.8
Infuse 9007 (OBC)	0.866	-60 °C	120 °C	8%	1.78	44	17	2.6
PDMS 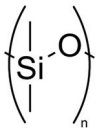	0.91	-120 °C	---	---	NR	800	400	2.0

Density values taken from manufacturer data sheets; reported in units of g/cm³.
Tensile modulus from manufacturer data sheets; reported in units of MPa (NR = Not reported).
Permeability values (at 35 °C) are reported in Barrers (Ba), where $1\ \text{Ba} = 10^{-10}\ \frac{\text{cm}^3(\text{STP})\ \text{cm}}{\text{cm}^2\ \text{s cmHg}}$.

3.2 MULTILAYER CO-EXTRUSION

An extruder at Case Western Reserve University was used to produce multilayered films used in gas transport and DSC aging studies. This type of multilayer co-extrusion technology was originally developed by Walter Schrenk and others at The Dow Chemical Company in the 1960s.[7–9] The multilayered layered film extruder is fitted

with melt metering pumps, a carefully designed feedblock, and special layer-multiplying dies that enable the production of films with alternating polymer layers (arranged ABABA..., where "A" is one polymer and "B" is another). A schematic of the extruder is shown in Figure 3.1 below.

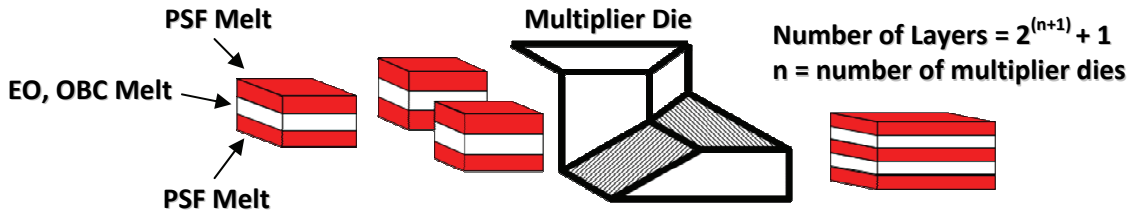

Figure 3.1: Schematic drawing of layer-multiplying co-extrusion process

Figure 3.1 shows how the extruder, when fitted with an ABA feedblock, produces films containing $2^{n+1}+1$ layers, where n is the number of layer-multiplying dies. The dies split the incoming melt stream vertically, spread the two streams separately, and then recombine the melt streams by stacking one atop the other. Thus, with each successive die, the number of layers is essentially doubled (whether or not an exact doubling occurs depends on the feedblock). A surface layer can also be applied to the multilayered film structure prior to the exit die. In many cases, the inclusion of surface or "skin" layers improves film quality, although these layers are not strictly necessary. The PSF/EO films were prepared with sacrificial EO skin layers (to be removed prior to study), while the PSF/OBC films did not have skin layers.

In this work, the films studied contained 129, 257, or 513 total layers. The layer thickness can be changed in three ways: changing the number of multiplier dies, adjusting the ratio of polymer A to polymer B in the feed, or changing the overall feed rate. In the production of PSF/EO films, the feed ratio was changed to produce different PSF layer

thicknesses, while the total number of layers was held constant at 257. For PSF/OBC films, the feed ratio was kept constant at 1:1, and the number of multiplier dies and overall feed rate was adjusted to produce different PSF layer thicknesses in films with 129, 257, or 513 layers. Figure 3.2 shows a representative AFM image of a 257-layer PSF/OBC film.

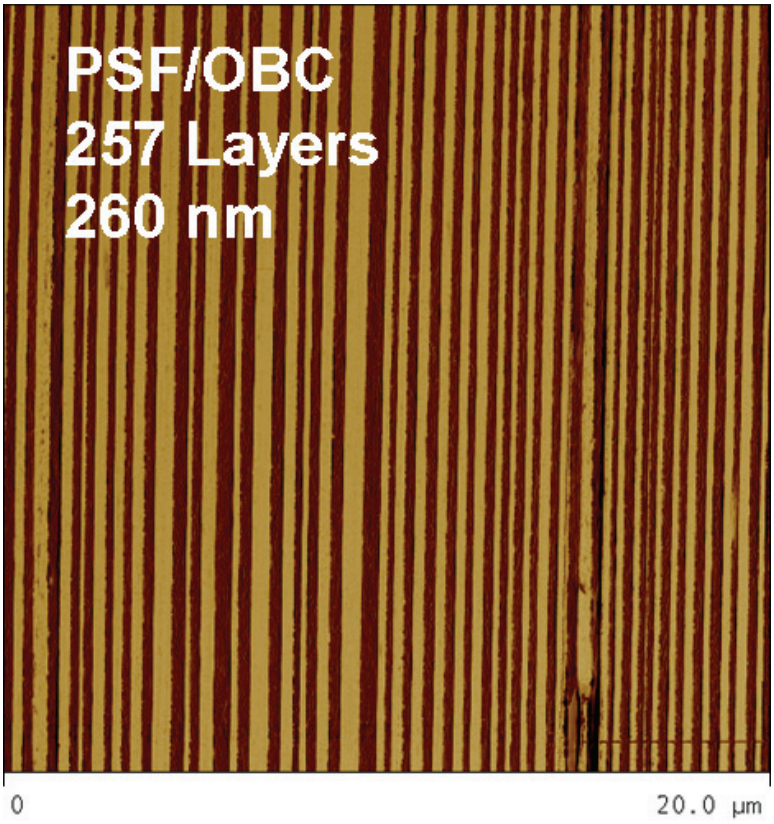

Figure 3.2: AFM image (tapping mode) of 257-layer PSF/OBC film produced by melt co-extrusion. Target PSF layer thickness was 290 nm, and the measured thickness was 260 ± 40 nm. The lighter colored regions are the PSF layers.

3.3 FILM PREPARATION FROM SOLUTION

3.3.1 Solution Casting

Thick films (ℓ > 25 μm) were prepared by casting from solution onto a glass or silicon substrate. Methylene chloride (dichloromethane) was used as the solvent, as it is quite volatile (T_b ~ 40 °C) and has a history of successful use in our labs for casting thick films. For films prepared on glass plates or silicon wafers, a metal casting ring was used to contain the polymer solution, and a glass cover plate was placed atop the casting ring to retard solvent evaporation. Petri dishes with very flat bottoms (Fine® brand) were also used to prepare thick films. After the polymer solutions were poured onto the substrate, they were allowed to dry for 5-7 days in a fume hood to ensure ample time for solvent evaporation before being removed. After removal from the substrate, the film was placed in a vacuum oven (typically at ambient temperature) to dry for a minimum one day before aging tests or other characterization steps were performed.

3.3.2 Spin Coating

3.3.2.1 Preparation of Solutions

Polymer solutions for spin coating were first prepared by mixing solvent with a known amount of polymer in a 20 mL scintillation vial. A Teflon-coated magnetic stir bar was used to agitate the solutions until the polymer was fully dissolved (typically overnight). Toluene was used as the solvent in the preparation of PS solutions. The solvents generally used for spin coating are less volatile than those used for solution casting, since evaporation that is too rapid would prevent the deposition of uniform, high-quality coated films. Prior to spin-coating, the solutions were successively filtered

through Teflon syringe filters with pore sizes of 0.45 μm, 0.2 μm, and 0.1 μm. In some cases, the solutions were unable to pass through the 0.1 μm filter, so these solutions were filtered twice through a 0.2 μm filter.

3.3.2.2 Spin Coating Conditions

Thin films ($\ell < 1$ μm) were prepared using a spin coater housed in a Class 100 clean room. Approximately 3-5 mL of polymer solution was deposited from a sterile dropper onto a silicon wafer (5" diameter) and then spun for 1 minute. The spinning speed ranged from 500-1000 rpm. In order to achieve different film thicknesses, the solution concentration or spinning speed was varied. Thickness characterization of spin-coated films was carried out after coating using either ellipsometry or profilometry (see section 3.4).

3.3.2.3 PDMS Coating of Thin Films

After measuring the thickness of the glassy layer atop the silicon wafer (using ellipsometry), a layer of PDMS was spun atop the previously-deposited glassy layer. The PDMS layer, which is highly permeable to gases, prevents pinhole defects from rendering a thin film unusable by blocking convective flow through such defects. The mass transfer resistance of the PDMS layer, which is typically small, can be accounted for using a series resistance model. Use of this coating layer greatly improves the chances that a thin film will be able to be used for aging studies. The target thickness of this PDMS layer was 5 μm. After deposition of the PDMS solution, the wafer was placed under vacuum at room temperature in a vacuum oven to facilitate removal of any air bubbles in the PDMS. The PDMS was then crosslinked by heating the wafer to 100 °C for 30-40 minutes in a temperature-controlled oven. After crosslinking, the thickness of the PDMS layer was measured using a profilometer.

3.3.2.4 Lifting Thin Films

Before permeation tests can be performed on thin films, the films must be removed from the surface of the wafer. First, a razor blade was used to score the film in such a way that the resulting film pieces (roughly 1" x 1.25") would be appropriately sized for subsequent permeation testing. De-ionized water was then used to float the film onto the surface of the water. The score lines allow the water to get between the film and substrate, and as the water wets the wafer surface and underside of the film, the film is separated from the wafer and floats atop the surface of the water. The floated film pieces are lifted from the water using a thin, rectangular wire frame. The lifted films are hung in a container (typically a glass beaker) and then stored under vacuum at room temperature for at least 1 day prior to beginning an aging study.

3.3.2.5 Cleaning of Silicon Wafers

Wafers used for spin-coating can be reused if they are properly cleaned. To be considered clean, the wafers should be free of polymer residue and other particles (e.g., dust or fibers) that would prevent the deposition of a uniform polymer film. After lifting the thin films from the wafer using water, cleaning was performed by successively rinsing the wafers with acetone, isopropyl alcohol (IPA), and de-ionized water. If necessary, a swab or wipe was used in conjunction with solvent to remove remnants of the film still adhering to the wafer. After rinsing, the wafers were blown dry with compressed air. The acetone and IPA facilitate the removal of organic residues on the wafer surface without damaging the native oxide layer.

3.4 THICKNESS CHARACTERIZATION

Three techniques were used to measure film thickness in this work. For thick films (i.e., 25 μm or greater), a handheld micrometer (B.C. Ames, Framingham, MA) was used. For the thin films prepared via spin-coating, a J.A. Woolam variable-angle spectroscopic ellipsometer (VASE) and/or a Dektak 6M profilometer were used.

Ellipsometry is a technique that shines light of a known polarization onto a sample at a prescribed angle of incidence. A change in polarization occurs when the light is reflected from the sample, and these changes are related to the optical properties and thickness of the sample. The thickness measurements in this work were performed using incidence angles of 65°, 70°, and 75°. Using the software program WVASE32, the data for wavelengths ranging from 400 nm to 1000 nm were fit to a model of the polymer-substrate system (i.e., the spin-coated polymer film on a silicon wafer). The model assumes that there is a 2 nm silicon oxide layer on the wafer surface, and the polymer film is modeled as a Cauchy layer, in which the refractive index of the polymer can be described by Equation 3.1,

$$n = A + \frac{B}{\lambda^2} + \frac{C}{\lambda^4} \tag{3.1}$$

where λ is the wavelength of light, and A, B, and C are best-fit constants. Thickness measurements made using ellipsometry are non-destructive, accurate, and easy to perform. However, the practical upper limit of film thickness that can be accurately and easily measured using this technique is typically around 1000-1500 nm.

Profilometry is also useful for measuring the thickness of thin films, and it does not suffer from the same thickness limitations as ellipsometry. For these measurements, a small cut is made in the polymer film such that the wafer surface is exposed. The

profilometer drags a stylus across the film and measures the displacement of the stylus tip. The difference in height between the film and the exposed wafer surface gives the film thickness. In this work, profilometry was used to measure the thickness of PDMS coating layers applied to PS films and, in some cases, to provide an initial thickness guess for fitting ellipsometry data.

3.5 SAMPLE PREPARATION FOR PERMEATION TESTS

Polymer film samples were prepared for permeation testing by mounting them between two discs of aluminum tape. The tape discs were punched from aluminum tape using a rubber mallet and a cutting die that was similar in size to the permeation cell sample holder. In order to permit gas permeation through the polymer films, circular holes of a known diameter were cut from the tape discs using a cutting die.

Bulk films (i.e., films with thicknesses on the order of 25 μm or greater) were mounted directly onto the pre-cut tape discs. For aging studies, the films were annealed above the T_g of the glassy material of interest before mounting. Annealing above T_g erases the prior thermal history of the glassy material and provides a well-defined starting point for aging studies. For PSF-containing films, the samples were annealed at 195 °C for ~15 minutes, while PS films were annealed for ~20 minutes at 120 °C. For measurements of the bulk gas permeability coefficients of rubbery or as-cast films, no annealing step was performed. The thin films considered in this study are fragile, and special care must be taken in preparing them for permeation testing. A porous ceramic disc was used to support the film and prevent tearing upon exposing the upstream side to

pressurized gas. Figure 3.3 shows an exploded cross-sectional view of a mounted sample.

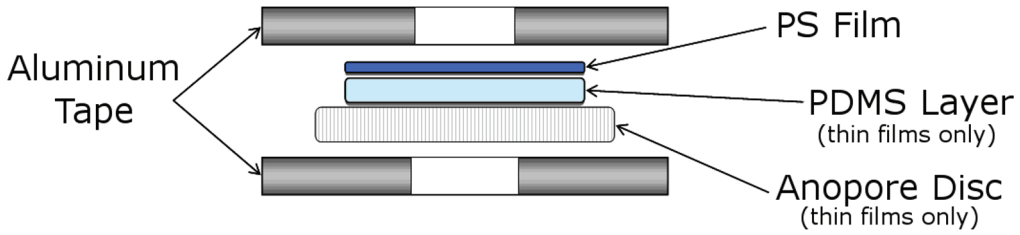

Figure 3.3: Illustration of film masking for permeation testing

3.6 GAS PERMEABILITY MEASUREMENT

The gas permeability coefficients of the polymer films considered in this work were measured using a constant-volume, variable pressure permeation cell. One important advantage of this type of system over others is that it allows the pure gas permeabilities of a variety of gases to be measured, as it relies solely on pressure measurements rather than gas-specific detectors. A drawing of the apparatus is shown in Figure 3.4. In this type of system, a film masked with aluminum tape is placed into the permeation cell sample holder, which divides the system into upstream and downstream sides. Prior to permeation testing, the system is evacuated using a vacuum pump that is attached to a cold trap (filled with liquid nitrogen) to prevent pump oil from entering the permeation system. Upon exposing the upstream side of the film to gas at a known pressure, gas begins to permeate through the film and pass into the downstream side of the system. A pressure transducer allows the gas pressure in the downstream side of the system to be measured over time. Using the ideal gas law and the relevant system

parameters (i.e., temperature, downstream volume, and exposed film area), the gas flux through the film can be calculated.

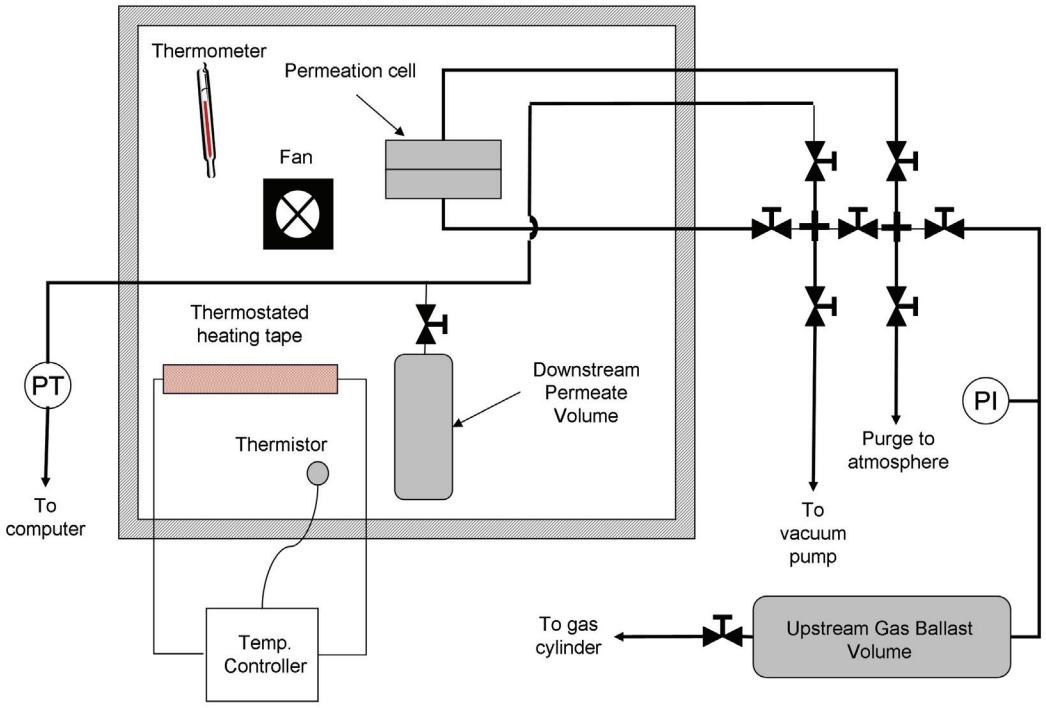

Figure 3.4: Schematic drawing of constant-volume, variable-pressure permeation cell used to measure pure gas permeability coefficients

The sample holder and most of the downstream tubing is located inside an insulated box maintained at 35 °C. The large upstream gas ballast volume ensures that the upstream pressure does not change over the course of the experiment, and the experiments are performed so that the downstream pressure never exceeds 10 torr (typically, it does not exceed 4 torr). Thus, the pressure difference across the film is essentially constant over the course of the experiment (e.g., for a 2 atm upstream pressure, the maximum change in Δp would be on the order of 0.5%). Unless otherwise

indicated, all permeation experiments were performed at an upstream pressure of roughly 30 psia (~2 atm).

3.7 DIFFERENTIAL SCANNING CALORIMETRY (DSC)

In this work, a PerkinElmer DSC 6000 equipped with an Intracooler SP cooling device was used to characterize the aging behavior and glass transition temperatures of bulk and multilayered films. DSC is a technique used to characterize the glass transition, melting, and crystallization of polymeric materials. DSC can be used to determine the temperatures at which these transitions occur, the changes in energy that occur during melting or crystallization, and the change in heat capacity that occurs at the glass transition. The DSC temperature calibration is performed using the melting temperatures indium, tin, and zinc. These metals all have well-defined melting points and are commonly used as DSC calibration standards. The heat flow calibration is performed using indium, which is commonly used for this purpose and has a well-known heat of fusion (28.45 J/g). The validity of the calibration was checked periodically (typically once a week) using indium to ensure that the instrument remained properly calibrated.

Physical aging can be quantified using DSC by determining the enthalpy that is recovered when an aged sample is heated through T_g. In order to do this, two scans must be performed: one for the sample after aging, and another for the same sample with no aging (i.e., a reference scan). Typically, the unaged reference scan is performed immediately after the scan of the "aged" sample. By subtracting unaged scan from the aged scan and then integrating the resultant curve, the recovered enthalpy can be calculated. Figure 3.5(a) shows a typical DSC temperature program used in aging

studies, and Figure 3.5(b) shows how recovered enthalpy is calculated from the DSC thermograms.

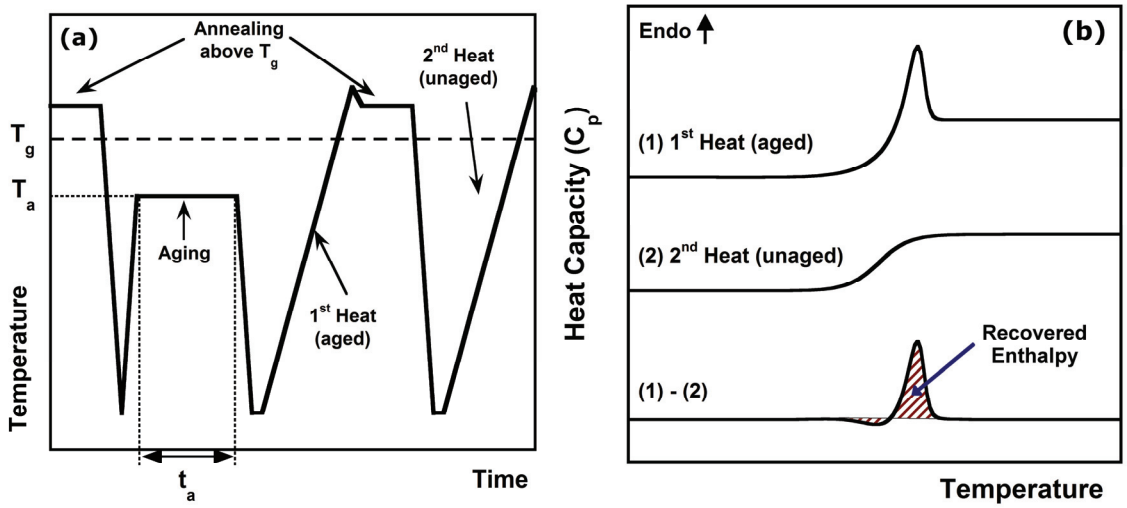

Figure 3.5: (a) Typical temperature program for DSC studies (b) Calculation of recovered enthalpy from DSC heating scans.

As is done in gas permeation aging experiments, an annealing step (at T ~ T_g+10 °C) is performed before the aging step in order to erase the prior thermal history and provide a well-defined "zero time" for the DSC aging studies.

3.8 ATOMIC FORCE MICROSCOPY

Atomic force microscopy (AFM) was used to determine the actual layer thickness of the PSF layers in multilayered films. This work was performed by our collaborators at Case Western Reserve University (CWRU). The AFM used was a Digital Instruments Nanoscope IIIa operated in tapping mode. The average PSF layer thickness was

calculated from an AFM image by counting the number of layers in part of the sample, measuring the thickness of each individual layer, and then calculating the mean. The average layer thickness measured was typically within 10% of the target thickness calculated prior to the extrusion run. The standard deviation in layer thickness was typically 15-20% of the average value. AFM images confirmed that the films used in this work are composed of continuous, well-formed layers.

3.9 ELEMENTAL ANALYSIS

Elemental analysis was performed to determine the mass percentage of PSF in layered samples. The elemental analysis results were used to normalize both the DSC thermograms and the recovered enthalpy data for layered films. This procedure allows for meaningful comparisons to be made between bulk and layered films that contain different amounts of PSF. Galbraith Laboratories (Knoxville, TN) performed elemental analysis for sulfur (S), which is present in PSF but not in the co-layering materials. The repeat unit of PSF is known, so it is possible to calculate the theoretical mass fraction of sulfur in a sample of pure PSF ($\omega_{S,PSF} = 0.0725$). Using this value and the measured values from elemental analysis samples, the mass fraction of PSF in a multilayered PSF film ($\omega_{PSF,sample}$) can be calculated as follows:

$$\omega_{PSF,sample} = \frac{\omega_{S,sample}}{\omega_{S,PSF}} \tag{3.2}$$

Elemental analysis was performed on multiple samples of bulk PSF, PSF/EO, and PSF/OBC films, and the average values were used in calculations. The samples for

elemental analysis were all taken from the center of the film roll, which is also where samples for both DSC and permeability aging studies were taken.

3.10 REFERENCES

1. Huang Y, Paul DR. Physical aging of thin glassy polymer films monitored by gas permeability. *Polymer* **2004**, 45(25): 8377-8393.

2. Rowe BW, Freeman BD, Paul DR. Physical aging of ultrathin glassy polymer films tracked by gas permeability. *Polymer* **2009**, 50(23): 5565-5575.

3. Huang Y, Paul DR. Effect of Film Thickness on the Gas-Permeation Characteristics of Glassy Polymer Membranes. *Industrial & Engineering Chemistry Research* **2007**, 46(8): 2342-2347.

4. Huang Y, Paul DR. Experimental methods for tracking physical aging of thin glassy polymer films by gas permeation. *Journal of Membrane Science* **2004**, 244(1-2): 167-178.

5. Huang Y, Paul DR. Effect of Temperature on Physical Aging of Thin Glassy Polymer Films. *Macromolecules* **2005**, 38(24): 10148-10154.

6. Rowe BW, Freeman BD, Paul DR. Influence of previous history on physical aging in thin glassy polymer films as gas separation membranes. *Polymer* **2010**, 51(16): 3784-3792.

7. Schrenk W, Chisholm D, Cleereman K, Alfrey Jr. T. Method of Preparing Multilayer Plastic Articles, U.S. Patent Number 3565985, 1971.

8. Schrenk W, Chisholm D, Cleereman K, Alfrey Jr. T. Multilayer Iridescent Plastic Articles, U.S. Patent Number 3576707, 1971.

9. Schrenk W, Chisholm D, Cleereman K, Alfrey Jr. T. Multilayer Plastic Articles, U.S. Patent Number 3647612, 1972.

Chapter 4: Characterization of Engage 8100 and As-extruded Multilayered Polysulfone/Engage 8100 Films

4.1 SUMMARY

In order to compare the gas permeation aging behavior of polysulfone layers in multilayered films with that of previously studied thin films, the contribution of the rubbery co-layering material must be eliminated. This is accomplished by using a series resistance model to extract the PSF permeability from permeability measurements on multilayered films. Thus, it is necessary to know the permeability of the rubbery co-layering material and the volume fraction of each polymer in the layered films. The co-layering material used in the first set of films was an ethylene-1-octene copolymer called Engage 8100 (EO). Literature data of measured gas permeability coefficients were not available for the EO material. Experimental difficulties in measuring the EO permeability were initially encountered, making it difficult to know if our permeability measurements were accurate. In order to confirm that our measurements were reasonable, comparisons were made between the properties of our EO material and those of related materials. Engage 8100 was first compared with natural rubber (thought to be a completely amorphous analog to polyethylene with respect to gas diffusion) and two types of polyethylene that had different crystallinity. Property comparisons were also made between Engage 8100 and other ethylene-α-olefin copolymers. These comparisons confirmed that our measurements of Engage 8100 followed the trends established by previous researchers. The favorable comparisons demonstrated that we could use our measured permeability values in the series model calculations with confidence. The permeability values for pure EO and pure PSF were also used in fitting the series model to permeability measurements of as-extruded PSF/EO films. The model matched the experimental data reasonably well, although at PSF volume fractions of 0.5 and lower, the model slightly over-predicted the O_2 and N_2 permeabilities. The measured O_2/N_2

selectivities at these same compositions were slightly higher than those predicted by the model. These measurements provided confirmation that the series model would be useful for extracting the permeability of PSF layers from gas permeability measurements of multilayered films.

4.2 INTRODUCTION AND MOTIVATION

The multilayered films studied in this work contain glassy polysulfone (PSF) and a rubbery co-layering material. In order to compare the gas permeation aging behavior of the polysulfone layers with that of previously studied thin, freestanding films, the contribution of the rubbery co-layering material must be eliminated. This is accomplished by using a series resistance model for the multilayered films:

$$\frac{1}{P_{layered}} = \frac{\varphi_{PSF}}{P_{PSF}} + \frac{\varphi_X}{P_X} \tag{4.1}$$

where φ_i is the volume fraction of component *i* (PSF or rubbery co-layering material), P_{PSF} is the permeability of the PSF layers (the quantity of interest), P_X is the permeability of the co-layering material (a constant), and $P_{layered}$ is the composite film permeability (the measured quantity). The permeability of the PSF layers (P_{PSF}) can be easily calculated by re-arranging Eq. 4.1 into the following equation.

$$P_{PSF} = \varphi_{PSF}\left(\frac{1}{P_{layered}} - \frac{\varphi_X}{P_X}\right)^{-1} \tag{4.2}$$

Data regarding the gas permeability of EO were not available in the literature, and many difficulties in measuring the EO permeability were encountered during the initial

phase of this work. It was therefore difficult to know whether or not our EO permeability measurements were accurate. In order to verify our results, comparisons of permeability and selectivity values were made between our EO material and certain types of polyethylene and polyethylene analogs having different amounts of crystallinity. Additionally, the permeability, melting temperature, and crystallinity of Engage 8100 were compared to other ethylene copolymers that have different types and amounts of comonomer.

4.3 THERMAL CHARACTERIZATION OF ENGAGE 8100 (EO)

DSC scans were performed on the EO material. Figure 4.1 shows a DSC thermogram for the EO material.

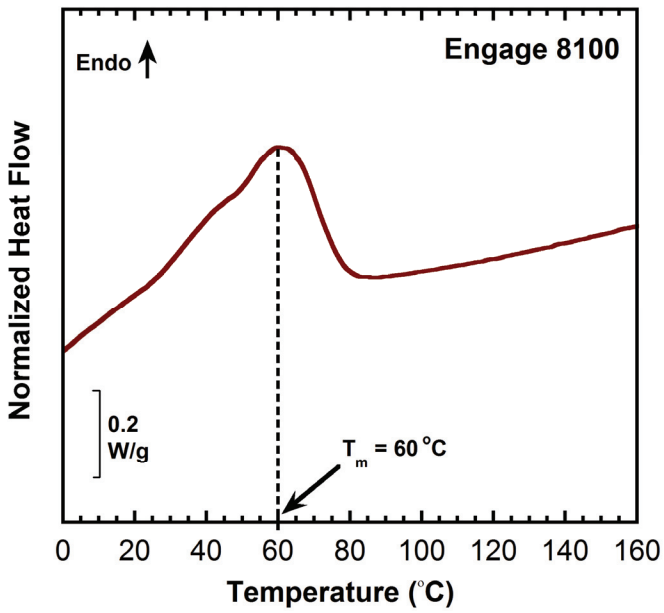

Figure 4.1: DSC thermogram (2nd heating, 10 °C/min) for Engage 8100.

The thermogram for the EO material exhibits a broad melting endotherm that peaks at 60 °C. The temperature at which this peak occurs is reported as the melting temperature, and the measured value is identical to the melting temperature reported on the supplier datasheet for Engage 8100. The crystalline content of the EO material, assuming a heat of fusion of 290 J/g (the value for polyethylene), was calculated as 15%. A DMTA scan was also performed to measure the storage and loss modulus of the EO material (1 Hz, 2 °C/min, 0.07% strain). The peak in the tan delta curve, which typically reported as the glass transition of the material, occurs at -39 °C. The T_g reported in the supplier data sheet is -52 °C. Relatively large differences (10-25 °C) in T_g between calorimetric techniques like DSC and mechanical tests like DMTA are frequently observed, with DMTA tests typically giving higher values of T_g than DSC at typical frequencies and heating rates used for the respective measurements.[1] Figure 4.2 shows the storage modulus (E'), loss modulus (E''), and tan δ curves for Engage 8100 obtained *via* DMTA. At the temperatures of interest for aging studies by gas permeability (35 °C), the EO material is in the rubbery state and should not impose a significant mechanical constraint on volume relaxation in the PSF layers of multilayered PSF/EO films.

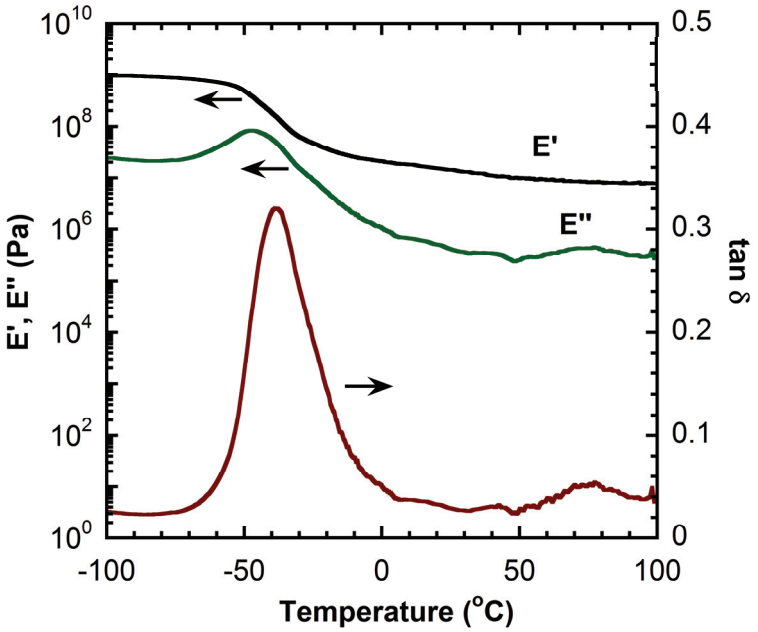

Figure 4.2: DMTA results for Engage 8100. Storage modulus (E') and loss modulus (E'') are plotted on a logarithmic scale, and tan δ is plotted on a linear scale.

4.4 COMPARISON OF EO MATERIAL TO POLYETHYLENE

Michaels and Bixler studied the permeation properties of polyethylene (PE) samples having different degrees of crystallinity.[2] In their study, they also considered the permeation measurements made by van Amerongen for natural rubber,[3] with the assumption that natural rubber is a completely amorphous analog for polyethylene (with respect to diffusion). Michaels and Bixler calculated the amorphous content of a polymer sample (φ_α) from the sample density using the equation below, assuming a two-phase mixture of crystalline and amorphous regions having densities of 0.9970 g/cm³ (ρ_c) and 0.8540 g/cm³ (ρ_α), respectively.

$$\varphi_\alpha = \frac{\rho_{sample} - \rho_c}{\rho_\alpha - \rho_c} \tag{4.3}$$

In order to determine if our measurements of EO permeability were reasonable, a comparison was made between the properties of EO and the polymers studied by Michaels, Bixler, and van Amerongen. Using the density of the EO material (0.87 g/cm³), the calculated fraction of amorphous content was 0.89. The He, O_2, and N_2 permeabilities of EO were measured at 35 °C and compared with the previously mentioned data. Figure 4.3 shows a comparison of the (a) permeability and (b) selectivity data for the EO material, two types of PE (Alathon 14 and Hydropol), and natural rubber.

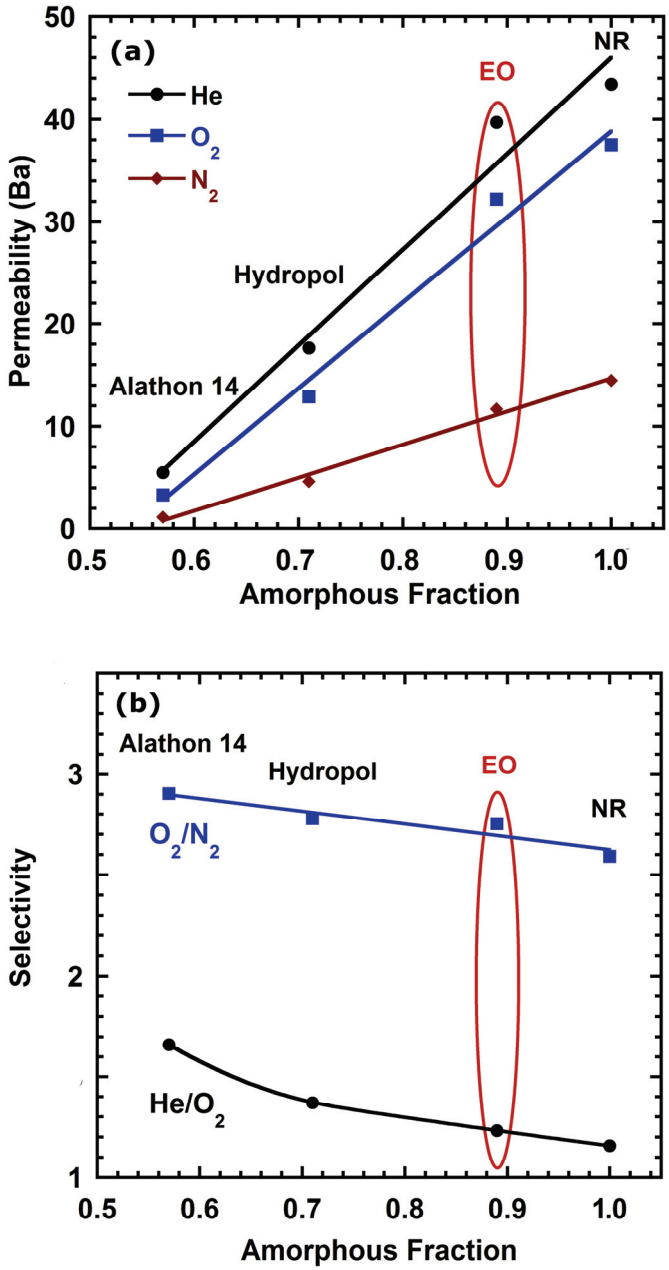

Figure 4.3: (a) Permeability of Engage 8100 (EO) at 35 °C compared to different grades of polyethylene (Alathon 14 & Hydropol) and natural rubber (NR) as a function of amorphous fraction. (b) O_2/N_2 and He/O_2 selectivity values for the polymers shown in (a) versus amorphous fraction. Lines are shown to guide the eye.

The measured permeability coefficients and selectivities for EO were found to be reasonable when compared to data for similar polymers gathered from the literature. These results helped to establish that our EO permeability measurements could be used in the series model equation to extract the permeability of the PSF layers.

4.5 COMPARISON OF EO MATERIAL TO OTHER ETHYLENE COPOLYMERS

Comparisons between the properties of Engage 8100 and those of other copolymers of ethylene and α-olefins were also made. Laguna et al. studied the properties of ethylene copolymers synthesized with metallocene catalysts that contained 1-hexene, 1-octene, or 1-dodecene as the comonomer.[4] The materials they studied covered a broad range of comonomer content and crystallinity. Figure 4.4 shows the fraction of crystalline material (calculated from polymer density) as a function of the comonomer content, and Figure 4.5 shows the measured melting points versus comonomer content. Our values for Engage 8100 have been added to the data of Laguna et al. for comparison. Both the crystalline fraction and melting point of Engage 8100 follow the trends established by the work of Laguna et al. In this work, the primary property of interest is the gas permeability of the EO material, as this quantity will be used in series model calculations to determine the PSF layer permeability. Based on the crystallinity and melting point data (cf., Figs. 4.4 and 4.5), it is reasonable to expect that the permeability would also follow the trends established by these other ethylene copolymers. Figure 4.6 shows the oxygen permeability of PE, the various ethylene-α-olefin copolymers studied by Laguna et al., and our EO material versus the volume fraction of amorphous material in the samples. The Engage 8100 material used in this

work has the highest O_2 permeability of the samples considered, which was expected because of its high amorphous content (i.e., low crystallinity). Based on the trends established by Laguna et al.,[4] the O_2 permeability measured for our EO material appears to be reasonable.

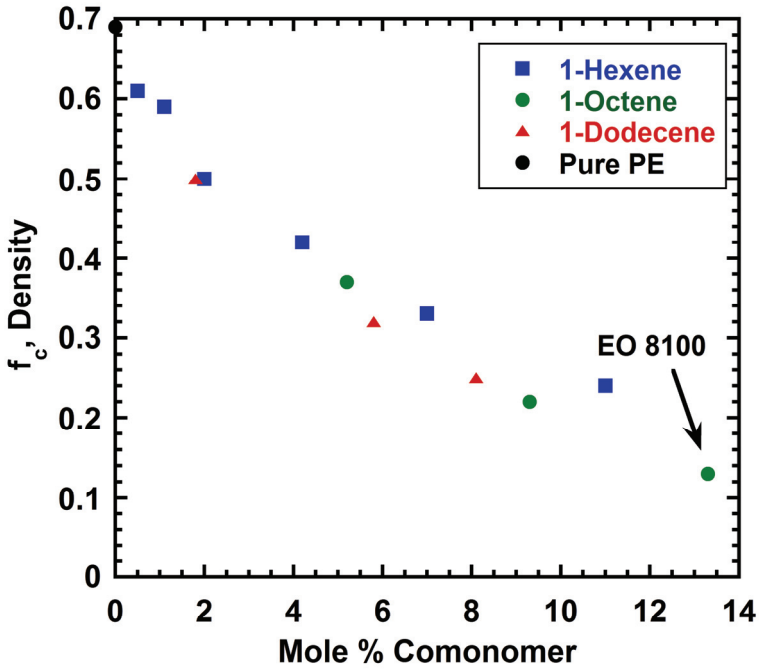

Figure 4.4: Fraction of crystalline material (using density values and an equation analogous to Eq. 4.3) for polyethylene and various ethylene copolymers as a function of comonomer content.

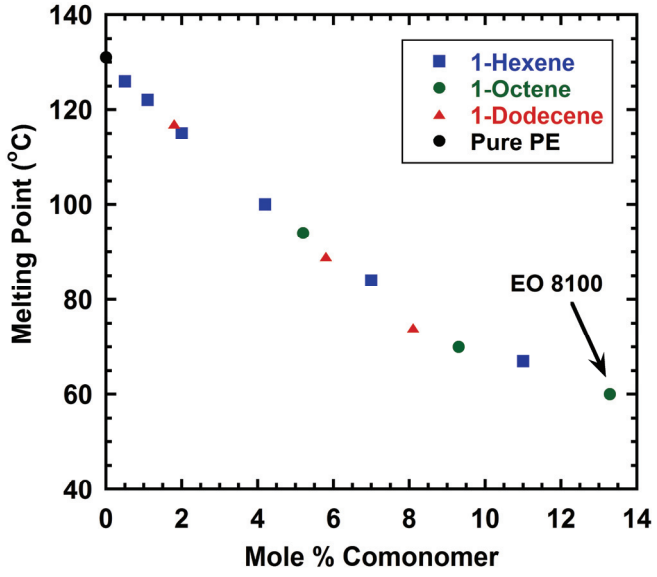

Figure 4.5: Melting point of polyethylene and various ethylene copolymers measured using DSC as a function of comonomer content.

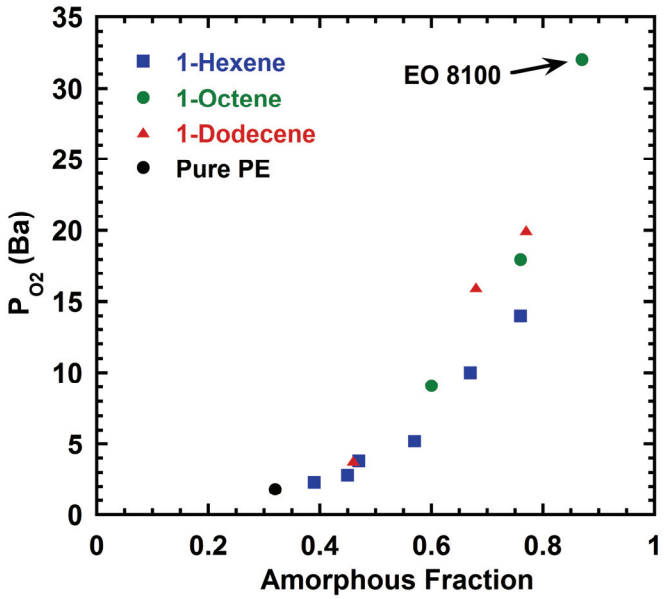

Figure 4.6: Oxygen permeability at 35 °C for polyethylene and various ethylene copolymers as a function of amorphous fraction

4.6 PERMEABILITY MEASUREMENTS ON AS-EXTRUDED PSF/EO FILMS

The series resistance model (Eq. 4.1) should be able to predict the composite permeability of multilayered PSF/EO films if the volumetric composition and bulk permeability values for PSF and EO are known. Inherent in these predictions is the assumption that the permeabilities of PSF and EO do not differ significantly from the bulk values when confined in thin layers. In order to confirm the accuracy of our measured values for the bulk EO permeability and the validity of using the series model for these multilayered films, permeability measurements were made on as-extruded PSF/EO films. The PSF/EO films all had 257 layers and nominal PSF volume fractions ranging from 0.2 to 0.9 (in increments of 0.1). The measured gas permeabilities of bulk "control" films of pure PSF and pure EO were used as inputs to the model. The O_2, N_2, and He permeability of each film was measured at 35 °C. Figure 4.7 compares experimental data with the series model predictions for (a) permeability and (b) O_2/N_2 selectivity. In general, the model predicts the layered film permeability reasonably well. At values of $\varphi_{PSF} < 0.5$, the model slightly over-predicts the layered film permeability values for all gases. The measured O_2/N_2 selectivity values for $\varphi_{PSF} < 0.5$ are slightly greater than the predicted values. Because the measured O_2 and N_2 permeability values were lower than the model predictions, and based on the well-known permeability-selectivity tradeoff, this finding was not unexpected. In order to more easily assess how well the series model fits the data for each permeation species, the fits for individual gases can be examined. Eq. 4.1 suggests that a plot of 1/P vs. φ_{PSF} should be linear. Figure 4.8(a-c) shows the series model fits for the inverse permeability of (a) O_2, (b) N_2, and (c) He versus the volume fraction of PSF, with lines drawn that connect the data points for bulk PSF and bulk EO.

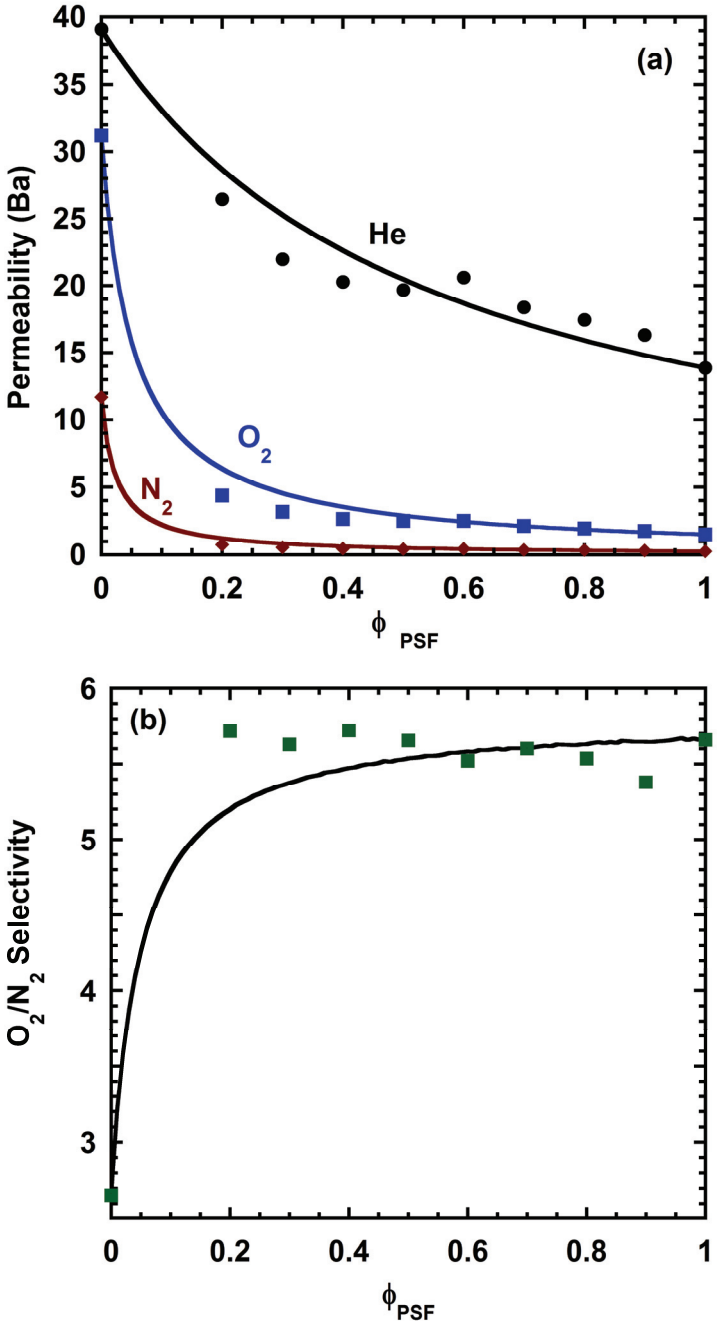

Figure 4.7: (a) O_2, N_2, and He permeability and (b) O_2/N_2 selectivity at 35 °C for bulk PSF, bulk EO, and multilayered PSF/EO films of various compositions. Solid lines give the series model predictions based on the pure PSF and EO film measurements (i.e., models fits are constrained by the intercepts at $\varphi = 0$ and $\varphi = 1$).

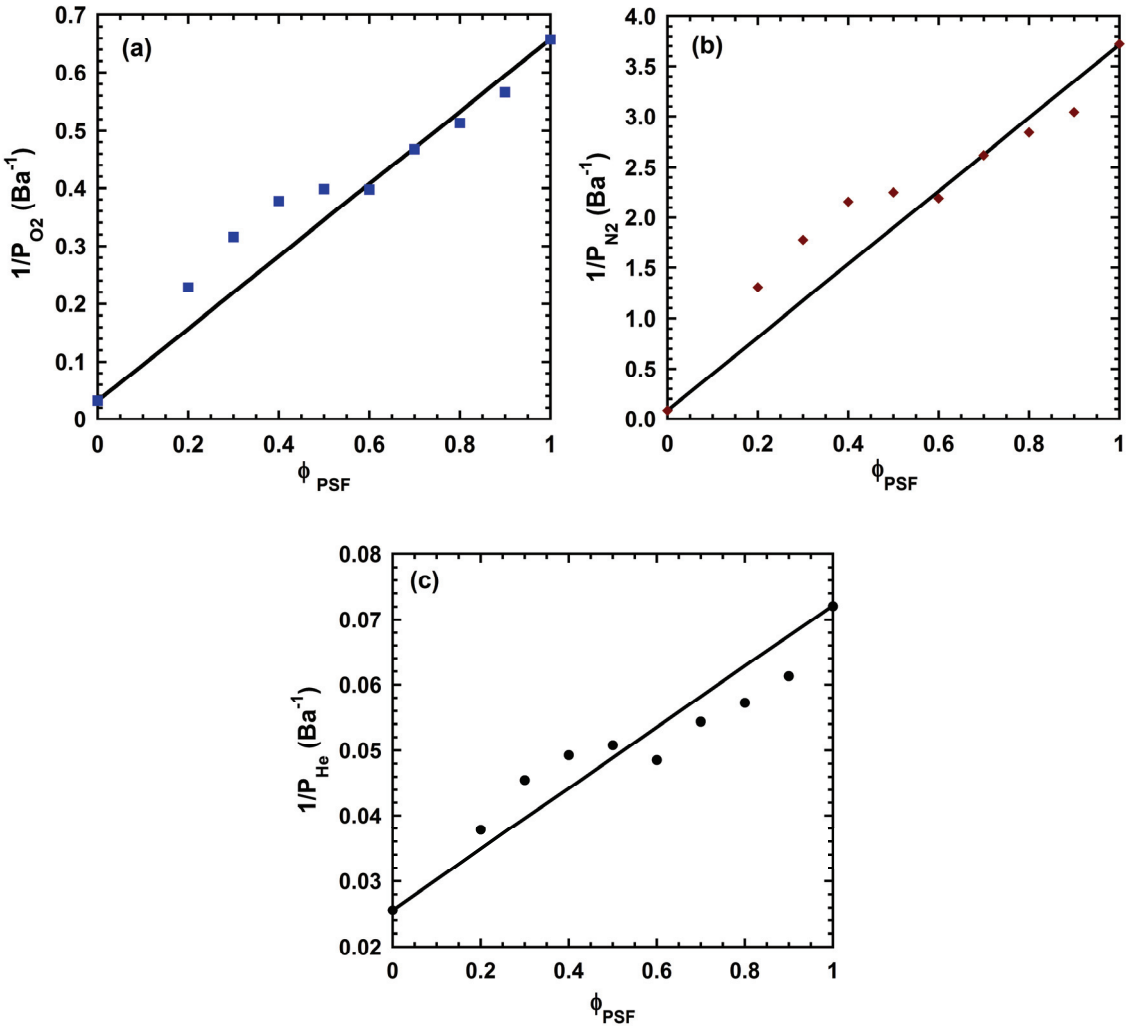

Figure 4.8: Plots of series model predictions for (a) O_2 permeability (b) N_2 permeability (c) He permeability. Lines are drawn through the data points for pure EO and pure PSF.

Plotting the data in the manner of Figure 4.8 allows for easier comparison over the entire range of compositions, especially for O_2 and N_2. PSF and EO have O_2 and N_2 permeabilities that are considerably different (a factor of ~20 for O_2 permeability and ~40 for N_2 permeability), with PSF being the less permeable polymer. Since the PSF layers primarily control the mass transfer through the layered films, linear plots of the type

shown in Figure 4.8 are typically easier to interpret than the hyperbolic curves shown in Figure 4.7. In Figure 4.8(a-c), it is easier to see that the model predicts permeability values higher than the measured values for $\varphi_{PSF} < 0.5$. The agreement between the model and the experimental data for O_2 and N_2 is generally better for values of $\varphi_{PSF} \geq 0.5$.

Some potential reasons for the discrepancies between the model and experimental data can be suggested. As the PSF content of a film is decreased, the sensitivity of the layered film permeability to small changes in the PSF content increases. The plots shown in Figs. 4.7 and 4.8 are based on the nominal (i.e., target) volume fraction of PSF in the layered samples. This value is determined from the feed rates of PSF and EO to the extruder. During the final step of the extrusion process, the film passes through a coat-hanger die and is spread to its final width. The EO material, which has a lower viscosity than PSF at the extrusion temperature, has a tendency to flow toward the film edges and accumulate there. Thus, the edges of the film roll have more rubbery material than the center. Elemental analysis of PSF/EO films confirmed that the PSF content in the center of the film can be greater than the nominal composition and that the relative error in volume fraction is greater in samples with lower PSF content. For example, the films with a nominal $\varphi_{PSF} = 0.5$ that were tested had an average PSF content by mass of 67.8%, which corresponds to $\varphi_{PSF} = 0.6$ (~20% higher than the nominal composition). The films with a nominal $\varphi_{PSF} = 0.2$ had an average PSF content by mass of 33.7%, which corresponds to $\varphi_{PSF} = 0.26$ (~30% higher than the nominal composition). The composite film permeability is more sensitive to small changes in the PSF content when the PSF content is low, which can be shown by differentiating the Eq. 4.1 (holding constant the component permeabilities) and solving for the quantity $dP/d\varphi$. Thus, at lower values of φ_{PSF}, error in the actual volumetric composition has a greater effect on the deviation of the experimentally measured permeability values from the model predictions than it does

at higher values of φ_{PSF}. Due to the lower permeability of PSF compared to EO, the enrichment of PSF in the center of the films during film formation is expected to lead to lower measured permeability values for the layered films, especially at lower PSF content, which is in agreement with our experimental observations.

4.7 CONCLUSIONS

Comparisons were made between the properties of the ethylene-1-octene copolymer used in our studies (Engage 8100) and other materials. Because we initially experienced difficulty in measuring the gas permeability of EO, we wanted to verify the accuracy of our results and demonstrate that the measured values could be used in the series model equation to extract the PSF layer permeability from permeation measurements of layered films. In one case, the gas permeation properties of two grades of polyethylene and natural rubber (a hypothesized analog to polyethylene with respect to diffusion) were compared with our EO material. In the other case, pure polyethylene and various ethylene-1-olefin copolymers were compared with EO. Both sets of comparisons showed that the properties of our EO material followed the trends established by previous researchers. Thus, the EO permeability values we measured were deemed reasonable, allowing us to use them to calculate the permeability of PSF layers during aging experiments. Uncertainty in the volume fraction of PSF in layered films can lead to errors in the PSF permeability values, so it is suggested that normalized comparisons of aging data (i.e., looking at the relative rate of permeability decline) could be useful in comparing the aging behavior of multilayered and bulk films. Reasonably good

agreement was seen between series model predictions and experimental permeability values in as-extruded PSF/EO films.

4.8 REFERENCES

1. Lee C-H, Park J-J. The Properties of DSC and DMA for Epoxy Nano-and-Micro Mixture Composites. *Transactions on Electrical and Electronic Materials* **2010**, 11(2): 69–72.

2. Michaels AS, Bixler HJ. Flow of gases through polyethylene. *Journal of Polymer Science* **1961**, 50(154): 413–439.

3. Amerongen GJ van. The Permeability of Different Rubbers to Gases and Its Relation to Diffusivity and Solubility. *Journal of Applied Physics* **1946**, 17(11): 972.

4. Laguna MF, Cerrada ML, Benavente R, Perez E, Quijada R. Permeation measurements in ethylene-1-hexene, ethylene-1-octene, and ethylene-1-dodecene copolymers synthesized with metallocene catalysts. *Journal of Polymer Science Part B: Polymer Physics* **2003**, 41(18): 2174–2184.

Chapter 5: Physical Aging of Layered Glassy Polymer Films via Gas Permeability Tracking

---

This chapter has been adapted with permission from an article published in Polymer (Murphy TM, Langhe DS, Ponting M, Baer E, Freeman BD, Paul DR. Physical aging of layered glassy polymer films *via* gas permeability tracking. *Polymer* **2011**, 52(26): 6117-6125). Ponting and Langhe helped with production of layered films, AFM characterization, and editing of the manuscript. Baer, Freeman, and Paul served as research supervisors and assisted with editing of the paper. All writing and experimental work was performed by the author.

5.1 SUMMARY

The physical aging of polymers in confined environments has been an area of intense study in recent times. The rate of physical aging in thin films of many polymers used in gas separation membranes is dependent on film thickness and accelerated relative to bulk. In this study, the physical aging of polymer films with alternating glassy polysulfone (PSF) and rubbery polyolefin layers (either Engage 8100, an ethylene-octene copolymer (EO) or Infuse 9007, an olefin block copolymer (OBC)) was monitored by measuring the gas permeability of O_2 and N_2 as a function of aging time at 35 °C. The alternating layer structures were formed by melt co-extrusion. The polysulfone layers have thicknesses ranging from 185-400 nm, and the overall thicknesses of the films are on the order of 80-120 μm. The aging of freestanding thin films of polysulfone is rapid and exhibits a clear thickness dependence, whereas aging of multilayered films was observed to be similar to bulk and showed no dependence on layer thickness. After 1000 hr of aging, a 400 nm freestanding PSF film decreased in O_2 permeability by 35%, whereas on average the bulk and multilayered films only experienced a decline of 10-15%. A slight increase in O_2/N_2 selectivity in the multilayered films was observed over the course of aging.

5.2 RESULTS AND DISCUSSION

5.2.1 Permeability calculations

To facilitate comparison between films of different compositions, layer thicknesses, and overall thicknesses, it is useful to calculate the permeability of the PSF layers alone. This allows for a direct comparison between layered and bulk films, and it also enables comparison between the films considered in this study and the freestanding thin films studied by other researchers. The permeability of bulk EO and OBC films were measured at various times, and no changes in permeability with time were observed. Because the co-layering materials are well above their T_g values, the properties of those layers will not undergo changes due to physical aging (e.g., McCaig measured the permeability of rubbery poly(dimethylsiloxane) (PDMS) over time and did not observe any physical aging).[1] The series resistance model shown below was used to calculate the permeability of the PSF layers:

$$\frac{1}{P_{layered}} = \frac{\varphi_{PSF}}{P_{PSF}} + \frac{\varphi_X}{P_X} \tag{5.1}$$

In the above equation, the volume fractions of PSF and the co-layering material (EO or OBC) are represented by φ_{PSF} and φ_x, respectively; because the film is composed of only two polymers, φ_{PSF} and φ_x sum to unity. The PSF and co-layering material permeability values are represented by P_{PSF} and P_x, respectively, while the permeability of the composite layered film is $P_{layered}$. Knowing the volume fraction of PSF and the permeability of the co-layering material enables calculation of the PSF layer permeability from measurements of the composite film permeability.

The calculation of layer permeability is subject to uncertainties in its inputs that affect the calculated result. For a film of PSF and EO with a nominal PSF volume fraction of 0.50, an uncertainty in the volume fraction of ±0.05 leads to uncertainty in the permeability value that is roughly ±10% of the value calculated using the nominal volume fraction (for films with lower PSF content, the effect on permeability is magnified). For example, the composite permeability of a 50/50 PSF/EO film is 2.7 Barrer (Ba), and the PSF layer permeability is calculated as 1.41 Ba using the nominal volume fraction of 0.5. If the film actually contains PSF at a volume fraction of 0.45, the calculated permeability should be 1.27 Ba; if the volume fraction were 0.55, the calculated permeability would be 1.54 Ba. Thus, uncertainties in the volume fraction can lead to noticeable over- or under-reporting of the proper absolute permeability value. Therefore, it is often useful to normalize permeability data to more easily compare the rate of permeability decline between different films, which may have significantly different absolute permeability values. The normalization procedure used here involves fitting a line to the linear portion of the calculated PSF layer permeability versus log(time) data, extrapolating the line back to an aging time of 1 hr, and then using the permeability value at t = 1 hr to normalize all other points in the data series. This procedure allows for straightforward comparison of the permeability decline and rate of aging and in bulk, multilayered, and thin films. Most of the discussion related to the figures presented here will focus on the PSF layer permeability and the normalized PSF layer permeability.

5.2.2 Gas permeability and aging in multilayered and bulk films

Table 5.1 provides information on the layered films whose aging behavior was monitored via gas permeability tracking. Two bulk PSF films, which were prepared during the extrusion runs that produced multilayered PSF/EO and PSF/OBC films, were also studied. The thicknesses of the two bulk films were 79 μm and 80 μm.

Table 5.1: Composition and layer thickness data for layered films studied.

	Co-Layering Material	Nominal PSF Content (vol. %)	Number of Layers	PSF Layer Thickness (nm)	Overall Thickness (μm)
1	EO	60	257	400	98
2	EO	50	257	320	86
3	EO	30	257	190	81
4	OBC	50	257	260	126
5	OBC	50	513	185	84

Note: Details regarding the structure and properties of PSF, EO, and OBC are given in Chapter 3.

Figures 5.1, 5.2, and 5.3 present the time dependence of composite oxygen permeability for bulk PSF, PSF/EO, and PSF/OBC films, respectively. The results for the bulk "control" films of PSF produced during the PSF/EO and PSF/OBC extrusion runs are included in the respective plots for the multilayered systems. Figure 5.1 allows direct comparison of the results for the two bulk films studied here with a film studied by Huang et al.[2] While the two extruded films show nearly perfect agreement, demonstrating good reproducibility, the solution-cast film from Huang et al. shows a higher absolute permeability. The rate of permeability decline, however, appears similar in all bulk films. There are possible explanations for the differences in absolute permeability. The film studied by Huang et al. was prepared *via* solution casting, while the films studied here were produced *via* extrusion. McHattie et al. observed that sample preparation technique (*i.e.*, extrusion vs. solution casting) can significantly affect the

measured permeability of PSF films, with extruded films always showing a lower permeability than cast films.[3] Additionally, the grade of PSF used in Huang's studies (Udel P-3500 NT LCD) is different from the grade used here (Udel P-3700), although many of the properties expected to affect permeability and aging behavior (*e.g.*, T_g and density) are the same for these two grades.

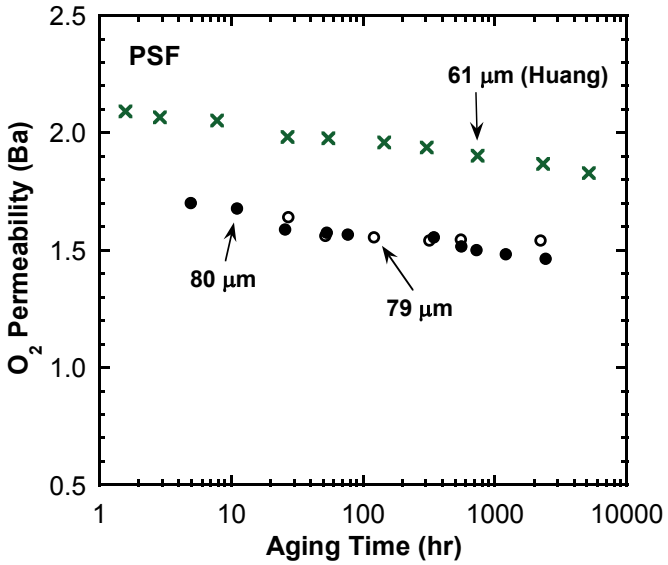

Figure 5.1: Aging as monitored by oxygen permeability for thick (> 50 μm) freestanding bulk PSF films at 35 °C. The data of Huang et al. are from the literature.[2]

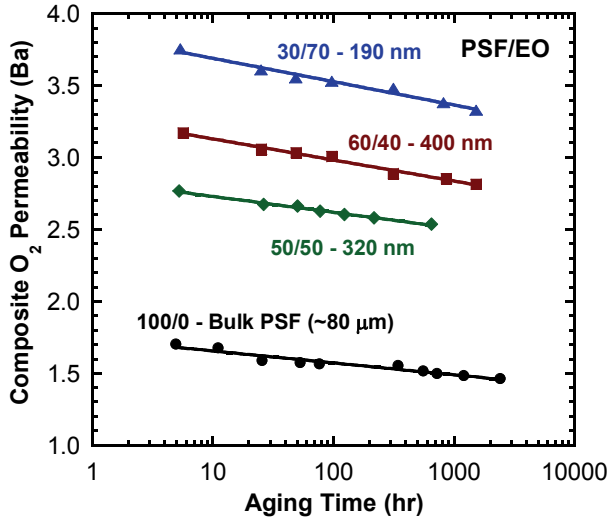

Figure 5.2: Composite layered film oxygen permeability data for PSF/EO films aged at 35 °C. Data for bulk PSF film produced during PSF/EO extrusion run also included. All PSF/EO films contain 257 layers, and the thickness values given for layered films are those of the PSF layers. Lines are shown to guide the eye.

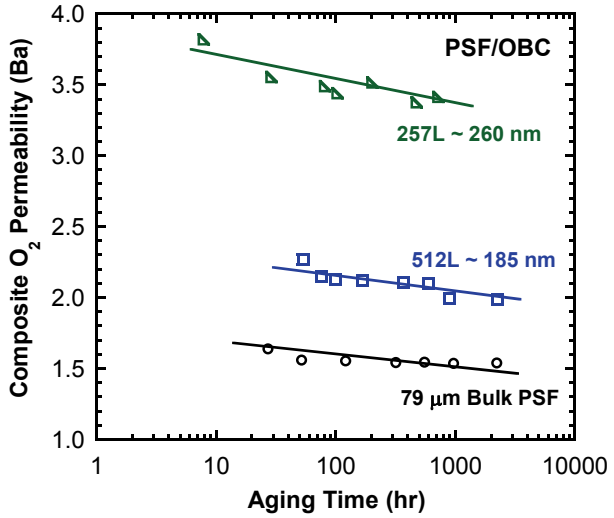

Figure 5.3: Oxygen permeability of composite layered PSF/OBC films (257L = 257 layers; 512L = 512 layers). Data for bulk PSF film produced during PSF/OBC extrusion run also included. All PSF/OBC films have a nominal PSF content of 50% by volume, and the thickness values given for layered films are those of the PSF layers. Lines are shown to guide the eye.

The composite permeability includes the contribution of the rubbery co-layering material, so the composite permeability values for the layered films are expected to be higher than bulk values. This expectation is borne out in Figures 5.2 and 5.3. For our purposes, it is more relevant and interesting to consider the calculated PSF layer permeability determined using Equation 1. Figures 5.4 and 5.5 show the calculated PSF layer permeability for PSF/EO and PSF/OBC films, respectively. When examined individually, there appears to be a trend of higher permeability with increasing layer thickness for a given multilayered system (although the bulk permeability curves are below those for the most permeable layered film in both cases). When PSF/EO and PSF/OBC data are combined, however, this trend does not hold, so it is difficult to interpret the data any further. Additionally, the sensitivity of the calculated PSF layer permeability to the volume fraction of PSF (discussed previously in section 5.2.1) suggests that some caution be exercised when interpreting the meaning of the absolute permeability values. Within a given figure (for Figures 5.1-5.5), the decline in permeability appears to be similar for all films. Normalizing and then combining all the data makes it easier to compare the relative permeability decline in all the films considered.

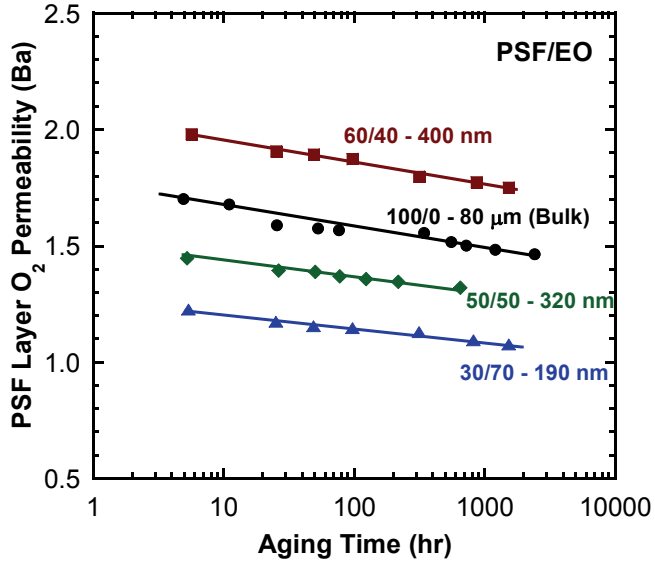

Figure 5.4: Calculated PSF layer oxygen permeability data for PSF/EO layered films and bulk PSF film aged at 35 °C. Lines are shown to guide the eye.

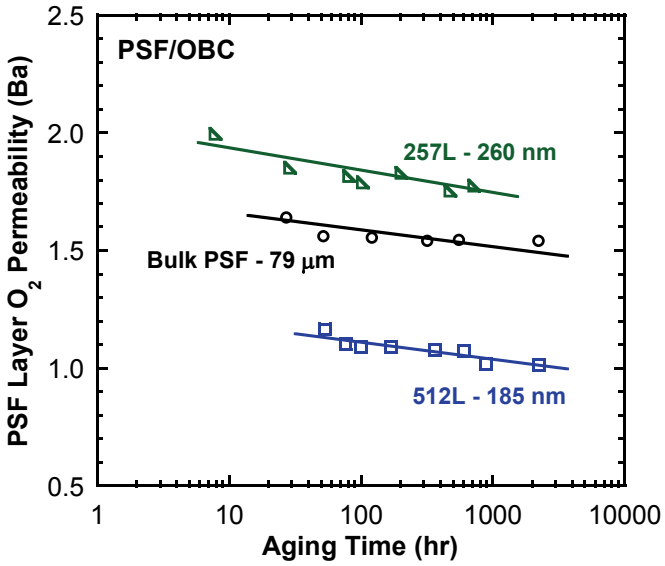

Figure 5.5: Calculated PSF layer oxygen permeability for PSF/OBC films and bulk PSF film aged at 35 °C. Lines are shown to guide the eye.

Figure 5.6 presents the normalized O_2 permeability data for PSF/EO, PSF/OBC, and bulk films, as well as a curve for a 400 nm PSF film studied by Huang et al.[2] All bulk and layered film data essentially collapse onto a single line, indicating that the rate of permeability decline in these films is similar. The 400 nm PSF film (whose overall thickness is at the upper end of the range of layer thicknesses considered here) undergoes much more rapid aging than any of the bulk or multilayered films. At 1000 hr of aging time, the 400 nm freestanding PSF film has decreased in permeability by 35%, whereas on average the bulk and multilayered films have only experienced a decline of 10-15%.

As polymer free volume decreases during physical aging, the permeability of larger gas molecules declines more rapidly than that of smaller ones.[2] Thus, the relative permeability decline of N_2 will be greater than that of O_2 (since N_2 is the larger molecule), and an increase in O_2/N_2 selectivity will be observed as the polymer ages. Figure 5.7 shows the O_2/N_2 pure gas selectivity data for the films studied.

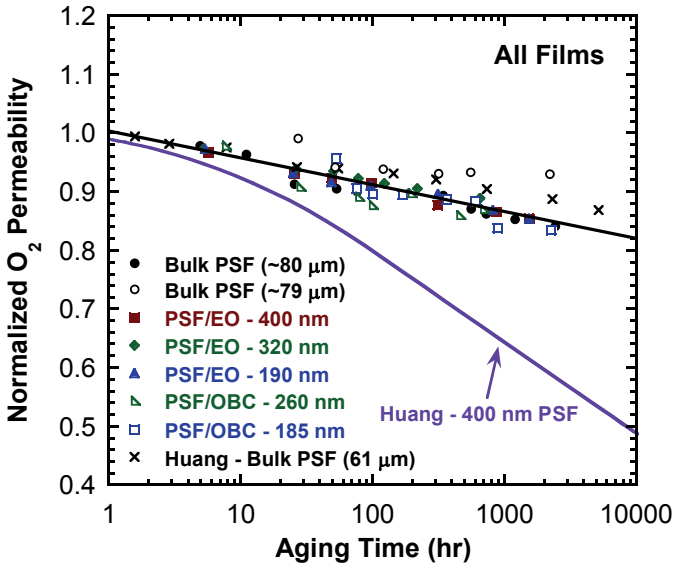

Figure 5.6: Normalized oxygen permeability aging data for all films studied. Aging curves from Huang et al.[2] for a 400 nm freestanding PSF film and a 61 µm bulk film are taken from the literature and shown for comparison. The thickness values given for layered films are those of the PSF layers.

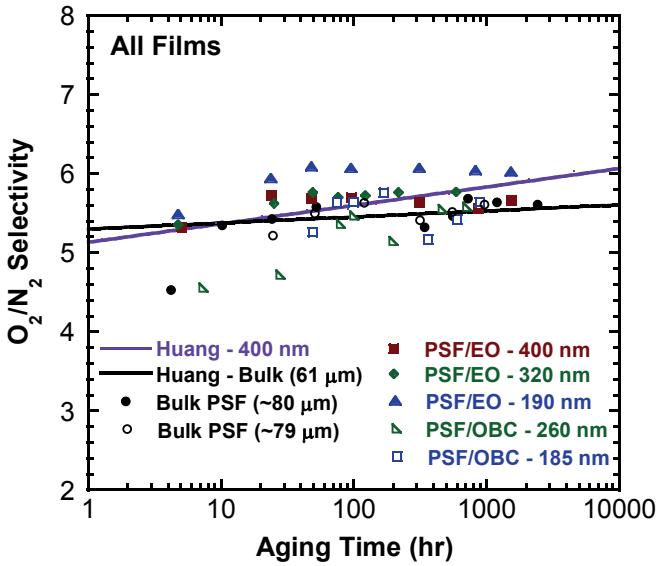

Figure 5.7: Influence of physical aging on O_2/N_2 pure gas selectivity in PSF films. Solid lines are results from Huang et al.[2] for a 400 nm freestanding PSF film and a 61 μm bulk film. The thickness values given for layered films are those of the PSF layers.

As expected, the selectivity increases slightly as physical aging progresses for all films. The increase for the 400 nm freestanding thin film is slightly greater than that of bulk films, although the difference in the rate of selectivity increase is much less prominent than the differences in permeability decline observed for freestanding versus bulk films. The similarity in magnitude and rate of increase of selectivity in all films indicates that the N_2 permeability data should tell essentially the same story as the O_2 data. This is indeed the case, so plots of N_2 permeability are not shown for the sake of clarity and brevity.

Some potential reasons why the multilayered films age in a manner similar to bulk films can be identified. Enhanced mobility of polymer chains near free surfaces has been proposed as an explanation for decreased T_g and accelerated aging in thin polymer

films.[4–6] It should be noted, however, that some studies of thin polymer films *via* dielectric spectroscopy do not observe significant changes in molecular mobility or T_g down to film thicknesses of 10 nm or less.[7–9] Sepúlveda et al.[10] studied aging in ultrathin films of toluene, a molecular glass former, and demonstrated that surface atoms are able to attain low-energy configurations more efficiently the those in the bulk, which leads to accelerated aging in thinner films. For thin, freestanding polymer films, a larger percentage of the sample is composed of near-surface material than for bulk films; thus, it is reasonable to expect a reduced T_g and a possible acceleration of physical aging in such films compared to bulk (depending on the aging temperature and the material's T_g). For the multilayered films studied here, there are many polymer-polymer interfaces ($2n$-2 for a film with PSF layers at the surfaces of the film, where n is the number of PSF layers) and few free surfaces (two), so the fraction of material near a free surface is more similar to that of a bulk film than a freestanding thin film. Thus, accelerated aging due to the enhanced free surface mobility associated with freestanding PSF films may not be observed in multilayered films.

The presence of the rubbery layers in these multilayered films could also impose a mechanical constraint on volume contraction that is absent in the case of freestanding films. In designing this study, relatively soft, low-modulus materials were chosen as co-layering materials for PSF to minimize this effect.

Another hypothesis that has been invoked to explain rapid aging in confined films is that free volume in the polymer can "diffuse" to free surfaces where it is then eliminated.[1,11–15] Because the timescale for diffusion is proportional to the square of the film thickness, thinner films would have smaller diffusive timescales and thus age more rapidly than thicker samples. In the layered films considered here, if the free volume

cannot "diffuse" across the layer interface and be eliminated, the aging behavior observed would not be accelerated relative to bulk.

Another possibility is that during extrusion, which takes place at 290-300 °C, there are chemical reactions at the layer interfaces that introduce connectivity across the interface, thereby reducing the mobility of the near-interface polymer chains and leading to bulk-like aging behavior. One observation that lends credence to this notion is the fact that peeling the EO "skin layer" off of the PSF/EO films proved much more difficult than expected. In some cases, peeling the EO layer resulted in layer delamination and an uneven surface (only films with uniform surfaces were used for aging studies). It seems intuitively reasonable to suspect that chain connectivity across a layer interface would cause difficulty in removing the EO skin layer and could render the material near an interface less mobile than it would be otherwise. Researchers using a PDMS coating technique to eliminate pinhole defects in glassy thin films found that the presence of a relatively thick PDMS layer on one surface of the thin film does not seem to change the aging behavior of the thin film within experimental uncertainty.[4,16] This technique involves spin-coating the PDMS atop the already-deposited thin film at room temperature and then curing it at temperatures below the T_g of the underlying glassy film. This experimental protocol should lead to well-defined PSF and PDMS layers with very little (if any) connectivity at the interface, which is one possible difference between the layered films discussed here and PDMS-coated thin films studied previously by others. Also, because the process of glass formation (which occurs upon removing a sample from the annealing oven and cooling through T_g) is different for freestanding and multilayered films, dissimilar aging behavior may be observed, as glassy materials are known to be highly history-dependent. Further investigation is required to pinpoint the reasons for

bulk-like aging behavior observed in multilayered films and to determine whether other glassy materials behave similarly.

5.2.3 Aging rate comparison

A measure of aging rate, r_i, from permeability data can be defined as follows:

$$r_i = -\frac{\partial \log P_i}{\partial \log t} \tag{5.2}$$

where the subscript *i* refers to the gas species of interest. Figure 13 presents the calculated aging rates from O_2 permeability data as function of layer or film thickness for thin (i.e., ~400-4,000 nm) and bulk PSF films studied by Huang et al.[2] and the bulk and layered films considered in this study.

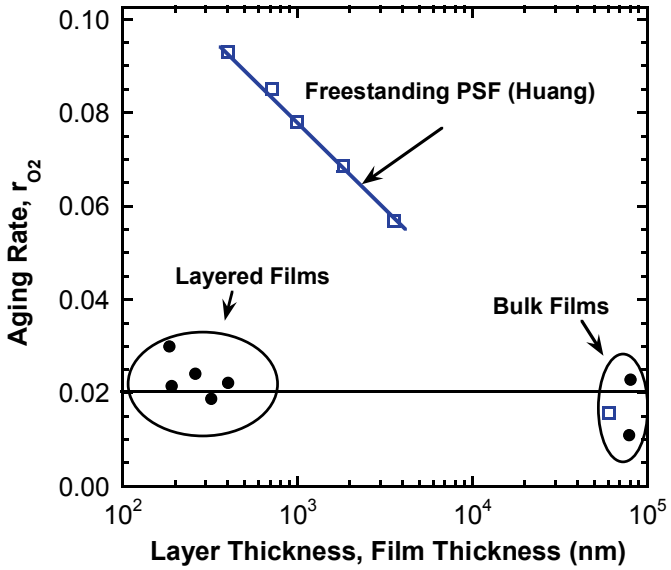

Figure 5.8: Aging rates from oxygen permeability data for bulk, multilayered, and thin PSF films at 35 °C. Horizontal line shows average aging rate for all bulk and layered films. Data from Huang et al.[2] are given by the unfilled square symbols (□).

The aging rates in freestanding thin films show a strong dependence on thickness, and aging rates for each of these films, which range from roughly 0.05 to 0.1, are higher than for any bulk or multilayered film. The multilayered films do not show any noticeable dependence of aging rate on layer thickness, and aging rates in these films are essentially equal to those of bulk films. The aging rates for layered and bulk films are clustered around an average value of 0.02, implying that the films age in a similar manner. This result is significant, because it suggests that different types of confinement can affect property changes due to aging in different ways. There are potential benefits of having materials that are confined yet do not undergo rapid property changes. For example, some of the potential applications for extruded multilayered films involve optical applications where stability of relevant properties is important, such as gradient refractive index (GRIN) lenses[17] and polymer lasers.[18]

5.2.4 Comparison to the permeability-selectivity upper bound

Polymeric membrane materials typically exhibit a tradeoff between permeability and selectivity, a concept first described empirically by Robeson as the "upper bound".[19,20] The theoretical framework for upper bound behavior was developed years later by Freeman,[21] and further study of the influence of temperature on the upper bound was recently published by Rowe et al.[22] As a polymer undergoes physical aging, its permeability decreases while its selectivity increases. Figure 14 is an upper bound plot for O_2 and N_2 containing data for PSF/EO and PSF/OBC layered films as well as for bulk and 400 nm PSF films studied by Huang et al.[2]

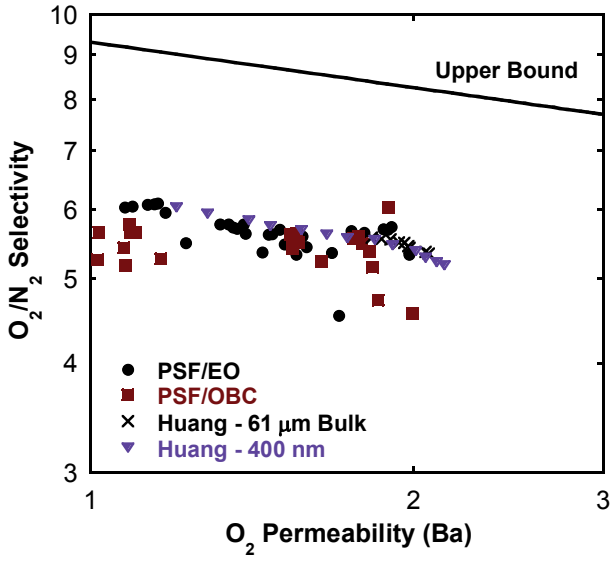

Figure 5.9: Influence of physical aging on the tradeoff between permeability and selectivity and comparison with the upper bound.[19] Data from Huang et al.[2] are taken from the literature and shown for comparison.

For all films shown, physical aging generally results in movement that is roughly parallel to the upper bound line. This trend is consistent with observations by Rowe et al., who found that PSF and Matrimid both experience property changes due to aging that cause movement parallel to the upper bound.[4]

5.3 CONCLUSIONS

The physical aging of layered and bulk PSF films at 35 °C was studied by measuring gas permeability over time. These layered films age in a manner similar to that of bulk films, as demonstrated by the similarity amongst the rates of permeability decline for these two types of films. Freestanding thin films of PSF (*i.e.*, those studied by Huang et al.[2] and Rowe et al.,[4] with overall thicknesses similar to the layer thicknesses of

PSF/EO and PSF/OBC films) undergo more rapid aging than the films considered in this study. The thin PSF films studied by Huang et al. show a strong dependence of aging rate on film thickness, and the absolute magnitudes of the aging rates are higher for all thin films than they are for any bulk or layered film. Multilayered PSF/EO and PSF/OBC films show no dependence of aging rate on layer thickness, and the aging rates for the multilayered films are similar to those of bulk PSF films. In this study, the choice of confining polymer (EO or OBC) does not appear to affect the rate of aging. From this work, it appears that the effect of film thickness on physical aging stems from free surfaces and not merely thickness per se. When plotted on an "upper bound" plot, permeability and selectivity changes due to aging cause movement parallel to the upper bound for bulk, multilayered, and freestanding thin films, which is consistent with past findings. The bulk-like aging behavior observed for multilayered films stands in sharp contrast to that of freestanding thin films, indicating that surfaces and interfaces play an important role during physical aging.

5.4 REFERENCES

1. McCaig MS, Paul DR. Effect of film thickness on the changes in gas permeability of a glassy polyarylate due to physical aging Part I. Experimental observations. *Polymer* **2000**, 41(2): 629-637.

2. Huang Y, Paul DR. Physical aging of thin glassy polymer films monitored by gas permeability. *Polymer* **2004**, 45(25): 8377-8393.

3. McHattie JS, Koros WJ, Paul DR. Gas transport properties of polysulphones: 1. Role of symmetry of methyl group placement on bisphenol rings. *Polymer* **1991**, 32(5): 840-850.

4. Rowe BW, Freeman BD, Paul DR. Physical aging of ultrathin glassy polymer films tracked by gas permeability. *Polymer* **2009**, 50(23): 5565-5575.

5. Kawana S, Jones RAL. Effect of physical ageing in thin glassy polymer films. *The European Physical Journal E - Soft Matter* **2003**, 10(3): 223-30.

6. Rowe BW, Pas SJ, Hill AJ, Suzuki R, Freeman BD, Paul DR. A variable energy positron annihilation lifetime spectroscopy study of physical aging in thin glassy polymer films. *Polymer* **2009**, 50(25): 6149-6156.

7. Labahn D, Mix R, Schönhals A. Dielectric relaxation of ultrathin films of supported polysulfone. *Physical Review E* **2009**, 79(1): 1-9.

8. Serghei A, Huth H, Schick C, Kremer F. Glassy Dynamics in Thin Polymer Layers Having a Free Upper Interface. *Macromolecules* **2008**, 41(10): 3636-3639.

9. Tress M, Erber M, Mapesa EU, Huth H, Müller J, Serghei A, Schick C, Eichhorn K-J, Voit B, Kremer F. Glassy Dynamics and Glass Transition in Nanometric Thin Layers of Polystyrene. *Macromolecules* **2010**, 43(23): 9937-9944.

10. Sepúlveda A, Leon-Gutierrez E, Gonzalez-Silveira M, Rodríguez-Tinoco C, Clavaguera-Mora M, Rodríguez-Viejo J. Accelerated Aging in Ultrathin Films of a Molecular Glass Former. *Physical Review Letters* **2011**, 107(2): 1-4.

11. Huang Y, Wang X, Paul DR. Physical aging of thin glassy polymer films: Free volume interpretation. *Journal of Membrane Science* **2006**, 277(1-2): 219-229.

12. McCaig M., Paul DR, Barlow JW. Effect of film thickness on the changes in gas permeability of a glassy polyarylate due to physical aging Part II. Mathematical model. *Polymer* **2000**, 41(2): 639-648.

13. Cangialosi D, Wübbenhorst M, Groenewold J, Mendes E, Picken SJ. Diffusion mechanism for physical aging of polycarbonate far below the glass transition temperature studied by means of dielectric spectroscopy. *Journal of Non-Crystalline Solids* **2005**, 351(33-36): 2605-2610.

14. Cangialosi D, Wübbenhorst M, Groenewold J, Mendes E, Schut H, Veen A van, Picken SJ. Physical aging of polycarbonate far below the glass transition temperature: Evidence for the diffusion mechanism. *Physical Review B* **2004**, 70 224213.

15. Boucher VM, Cangialosi D, Alegría A, Colmenero J. Enthalpy Recovery of PMMA/Silica Nanocomposites. *Macromolecules* **2010**, 43(18): 7594-7603.

16. Cui L, Qiu W, Paul DR, Koros WJ. Physical aging of 6FDA-based polyimide membranes monitored by gas permeability. *Polymer* **2011**, 52(15): 3374-3380.

17. Jin Y, Tai H, Hiltner A, Baer E, Shirk JS. New class of bioinspired lenses with a gradient refractive index. *Journal of Applied Polymer Science* **2007**, 103(3): 1834-1841.

18. Singer KD, Kazmierczak T, Lott J, Song H, Wu Y, Andrews J, Baer E, Hiltner A, Weder C. Melt-processed all-polymer distributed Bragg reflector laser. *Optics Express* **2008**, 16(14): 10358–10363.

19. Robeson LM. Correlation of separation factor versus permeability for polymeric membranes. *Journal of Membrane Science* **1991**, 62(2): 165-185.

20. Robeson LM. The upper bound revisited. *Journal of Membrane Science* **2008**, 320(1-2): 390-400.

21. Freeman BD. Basis of Permeability/Selectivity Tradeoff Relations in Polymeric Gas Separation Membranes. *Macromolecules* **1999**, 32(2): 375-380.

22. Rowe BW, Robeson LM, Freeman BD, Paul DR. Influence of temperature on the upper bound: Theoretical considerations and comparison with experimental results. *Journal of Membrane Science* **2010**, 360(1-2): 58-69.

Chapter 6: DSC Studies of Physical Aging and Structural Relaxation in Layered Glassy Polymer Films

This chapter has been adapted with permission from an article published in Polymer (Murphy TM, Langhe DS, Ponting M, Baer E, Freeman BD, Paul DR. Enthalpy recovery and structural relaxation in layered glassy polymer films. *Polymer* **2012**, 53(18): 4002-4009). Ponting and Langhe helped with production of layered films and editing of the manuscript. Baer, Freeman, and Paul served as research supervisors and also assisted with editing of the paper. All writing and experimental work was performed by the author.

6.1 SUMMARY

Recent studies of physical aging in confined polymer glasses have revealed that aging behavior in confinement often differs from bulk behavior. This study used differential scanning calorimetry (DSC) to characterize physical aging and structural relaxation in both bulk polysulfone (PSF) films and co-extruded multilayered films of PSF and Infuse 9007, an olefin block copolymer (OBC). The layered films had 129, 257, and 513 layers and average PSF layer thicknesses of 640 nm, 260 nm, and 185 nm, respectively. The films were aged isothermally at 170 °C in the DSC, and the recovered enthalpy upon reheating was measured at various aging times ranging from 5 to 600 minutes. The films with 640 nm and 260 nm PSF layers had aging rates very similar to that of bulk PSF, while the film with 185 nm PSF layers had an aging rate slightly greater than the bulk value. The cooling rate dependence of the limiting fictive temperature (T_f') in multilayered and bulk PSF samples was also characterized. Values of T_f' were similar for all films at each cooling rate. The results of this work are in general agreement with our previous gas permeation aging study of multilayered PSF films aged at 35 °C, in which the effect of layer thickness on aging behavior was minimal. This stands in contrast to studies with thin, freestanding PSF films, which exhibit accelerated aging relative to bulk and have aging rates that depend strongly on film thickness.

6.2 RESULTS AND DISCUSSION

6.2.1 Recovered enthalpy in layered and bulk films aged isothermally at 170 °C

Because enthalpy decreases as a polymer undergoes physical aging, differential scanning calorimetry (DSC) can be used to track the aging process. Upon reheating an aged film through its T_g, the enthalpy lost during aging is recovered. The enthalpy that is recovered upon reheating an aged sample through T_g is manifested by an overshoot in the DSC thermogram (see curve 1 in Figure 6.1) and can be quantified using equation 6.1.

$$\Delta H(T_a, t_a) = \int_{T_0<T_g}^{T_1>T_g} \left(C_p^{aged}(T_a, t_a, T) - C_p^{ref}(T) \right) dT \tag{6.1}$$

In equation 6.1, T_0 and T_1 are temperatures below and above the T_g, respectively. C_p^{aged} is given by the DSC thermogram of the aged sample, and C_p^{ref} is given by the DSC thermogram for the second heating scan (i.e., "unaged"), which is performed immediately after annealing above T_g and then cooling to the starting scan temperature. Figure 6.1 illustrates the procedure used to calculate the recovered enthalpy.

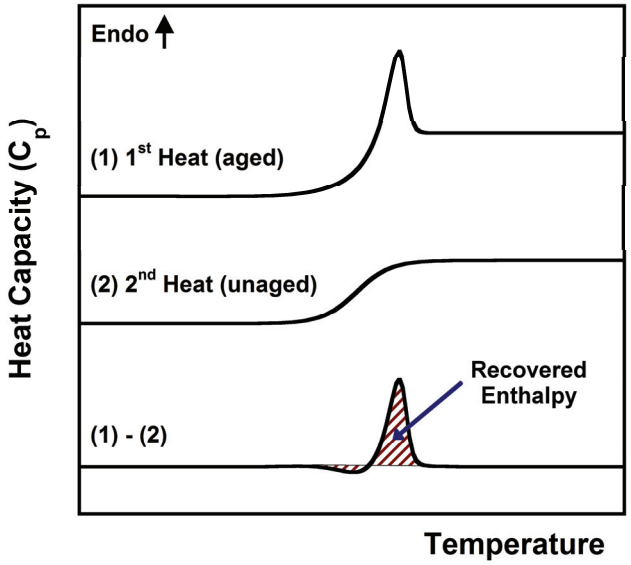

Figure 6.1: Quantification of ΔH from DSC thermograms. Recovered enthalpy is calculated from the thermograms using the DSC software.

These calculations are performed using the PerkinElmer Pyris DSC software supplied with the instrument. To compare the recovered enthalpy values of the layered and bulk films, the values calculated with the DSC software must be normalized by the mass fraction of PSF (ω_{PSF}) in each sample using equation 6.2.

$$\Delta H_{PSF} = \frac{\Delta H_{layered,total}}{\omega_{PSF}} \tag{6.2}$$

By normalizing the recovered enthalpy values so that they have units of J/(g PSF), meaningful comparisons can be made between the aging responses of bulk and layered samples. Figure 6.2(a-d) shows the normalized heat capacity curves for bulk PSF and layered PSF/OBC samples aged between 5 and 600 minutes. In Figure 6.2(a-d), longer aging times lead to greater peak heights, as expected. In the figures for this chapter, the 129-layer film is referred to as "129L", the 257-layer film as "257L", and the 513-layer films as "513L". Normalization of the DSC curves is done to facilitate comparison

between samples with different PSF content and different sample mass. The normalized heat capacity, C_p^N is calculated as follows:

$$C_p^N = \frac{C_p(T) - C_{pg}(T)}{\Delta C_p(T)} \tag{6.3}$$

In equation 6.3, $C_p(T)$ is the heat capacity given by the DSC scan, $C_{pg}(T)$ is the extrapolated glassy heat capacity, and $\Delta C_p(T)$ represents the difference between the extrapolated equilibrium liquid and glassy heat capacities at a given temperature. When defined this way, the value of C_p^N is 0 in the glassy region and equal to 1 in the equilibrium state above T_g.

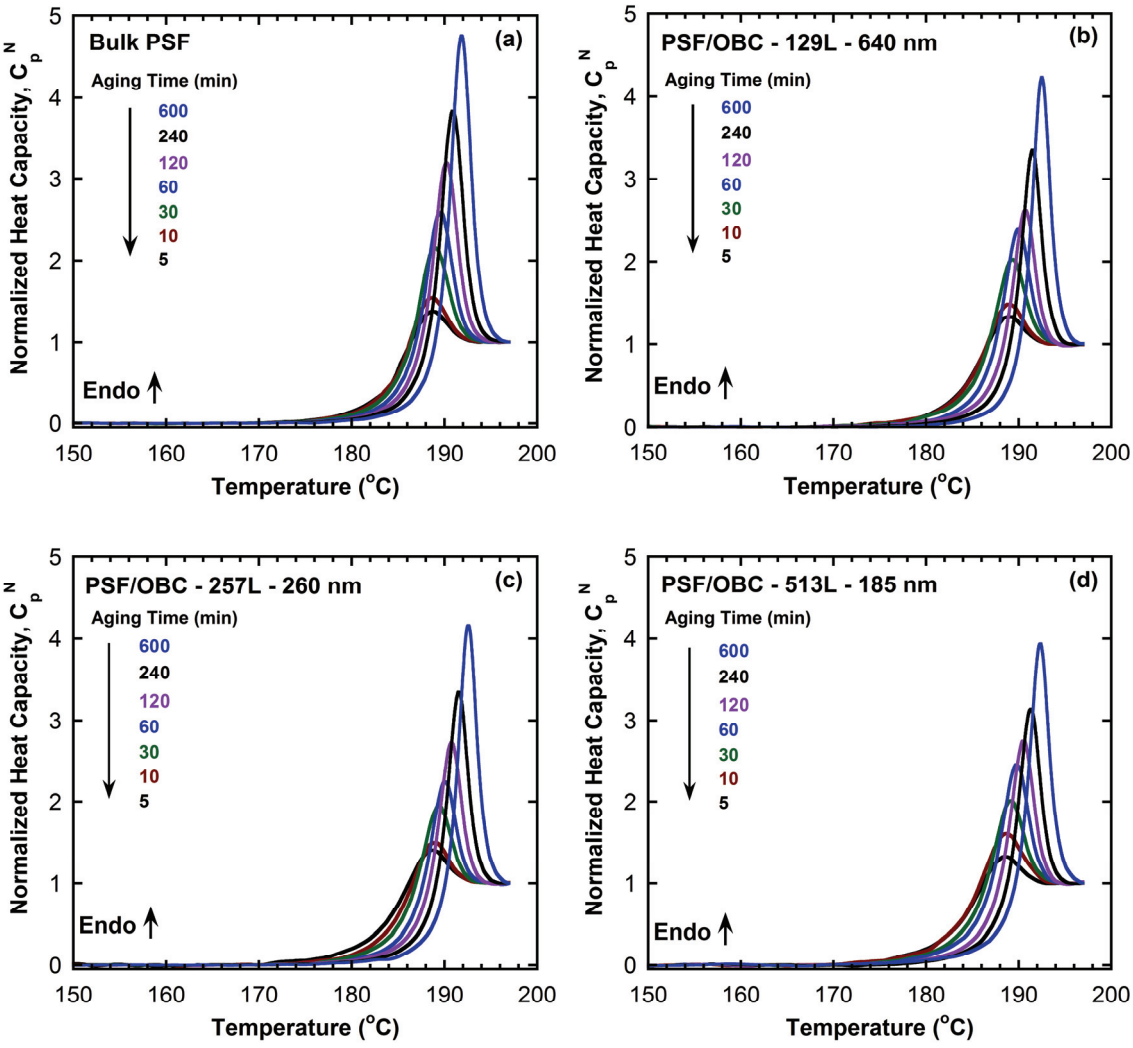

Figure 6.2: Normalized heat capacity curves as a function of aging time for bulk PSF and multilayered PSF/OBC films aged at 170 °C. (a) Bulk PSF (b) 129-layer PSF/OBC (~640 nm PSF layers) (c) 257-layer PSF/OBC (~260 nm PSF layers) (d) 513-layer PSF/OBC (~185 nm PSF layers).

The normalized heat capacity curves for all samples are qualitatively similar, although the maximum value of C_p^N is greatest in the bulk sample. The calculation of C_p^N requires extrapolating a line representing the equilibrium state heat capacity, and because of the upper limit on temperature that is imposed to avoid possible layer breakup, this results in less data being available for the temperature regime above T_g. Thus, some uncertainty in the peak values of C_p^N is expected, especially for films aged for longer periods of time. Extrapolation of the equilibrium heat capacity line is not necessary for the calculation of recovered enthalpy. In their studies of stacked ultrathin polystyrene films, Koh and Simon observed that a 62 nm film showed a reduced peak value of C_p^N and a noticeably broader glass transition than a bulk film when the samples were aged 5 degrees below T_g.[1] In this work, no apparent broadening of the glass transition was observed. Figure 6.3 shows the calculated recovered enthalpy values as a function of aging time at 170 °C for the bulk and layered PSF samples.

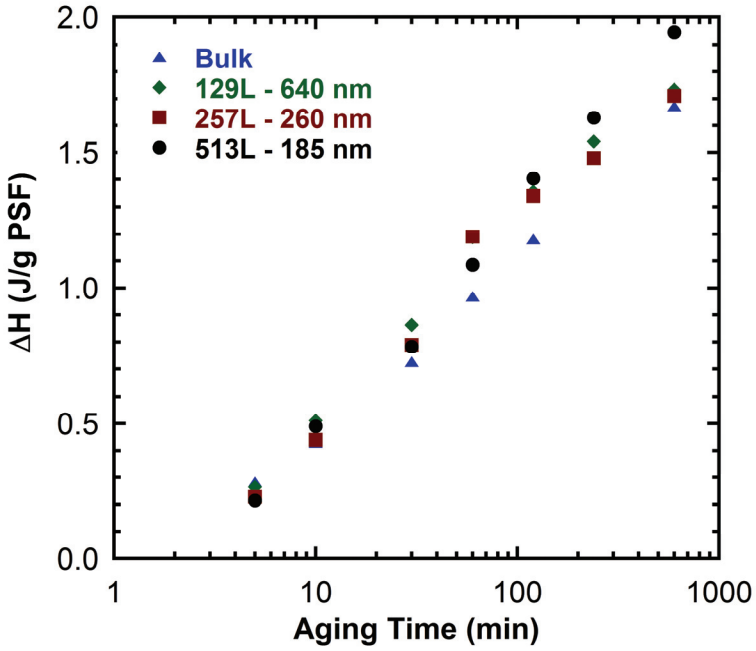

Figure 6.3: Recovered enthalpy for bulk PSF and layered PSF/OBC films as a function of aging time at 170 °C. Recovered enthalpy values were calculated as shown in Figure 6.1 and then divided by the mass fraction of PSF in the sample (determined via elemental analysis).

The calculated recovered enthalpy values at a given aging time and the rates of increase over time appear to be similar for the bulk and layered samples. To quantify the rates of increase, an aging rate for isothermal enthalpy relaxation can be defined as follows:[2]

$$r_{\Delta H} = \frac{d\Delta H}{d\log t} \tag{6.4}$$

When defined as such, the aging rate is simply the slope of the best-fit lines for the linear regions of the data sets shown in Figure 6.3. A plot of the calculated aging rates as a function of layer thickness is shown in Figure 6.4. The error bars in Figure 6.4

represent the uncertainties in the slopes of the linear regression equations from Figure 6.3.

The 129-layer film (640 nm PSF layers) and the 257-layer film (260 nm PSF layers) have aging rates of 0.76 and 0.78 J/g per decade, respectively, which are similar to the bulk value of 0.75 J/g per decade. The calculated aging rate for a 513-layer film with ~185 nm PSF layers is 0.85 J/g per decade. Unfortunately, difficulties in extruding films with very thin continuous layers prevent us from studying PSF/OBC films with PSF layers that are significantly less than ~185 nm in thickness and assessing whether the apparent increase in aging rate with decreasing layer thickness continues as the PSF layers are made progressively thinner.

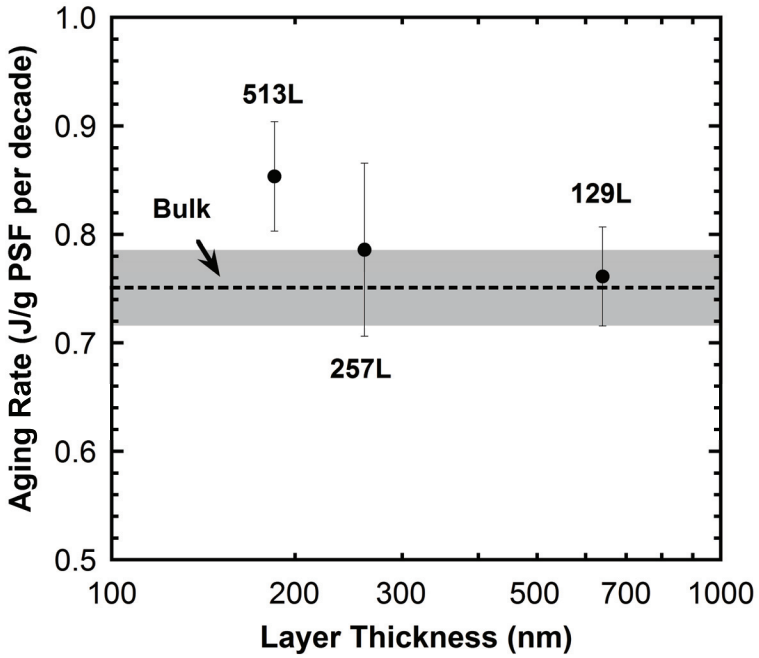

Figure 6.4: Aging rates for bulk PSF and layered PSF/OBC films aged at 170 °C. The bulk value is shown as a dashed line. Errors bars are the uncertainties from fitting the recovered enthalpy data, and the uncertainty range for the bulk sample is indicated by the gray shaded area.

Our previous DSC studies with layered films of PSF and an ethylene-1-octene copolymer (EO) aged at 170 °C revealed that for a film with ~180 nm PSF layers, the aging rate (as defined above) was 0.72 J/g per decade, which is similar to the bulk value of 0.75 J/g per decade reported here. More information about these studies and how they compare with the present work can be found in Appendix A. Based on the qualitative similarity between the DSC thermograms for the layered films, the similarity of the recovered enthalpy values for the layered and bulk films, and the findings of previous studies with PSF/EO films, we hesitate to assert that the aging of the 513-layer PSF/OBC film is truly accelerated relative to bulk. The PSF/OBC films are extruded at temperatures that allow for melt-state equilibration between PSF and OBC, resulting in well-adhered layers. The similarity between the aging of bulk and layered PSF films suggests that the nature of the interface has an important effect on aging behavior.

In a recent study by Langhe et al. of physical aging in multilayered PS/PC films using DSC, the aging rate in the PS layers systematically decreased with decreasing PS layer thickness when aged isothermally at 80 °C [2]. The decrease in aging rate was approximately linear with the logarithm of layer thickness. The differences in aging rate seen here (PSF layers aged at T_g - 16 °C) are less than those observed in the study by Langhe et al. (PS layers aged at T_g - 24 °C), and we did not observe a decrease in aging rate with decreasing layer thickness. Aside from the difference in both materials studied and aging temperature relative to T_g, another important difference between this work and the study of PS/PC layered films is that during aging of the PS layers, the confining PC layers are well below their T_g (PC T_g ~ 145 °C), whereas here the PSF layers are aged while the confining OBC layers are well above their T_g (OBC T_g ~ -60 °C). Thus, the PS layers in PS/PC films are confined by rigid, glassy PC ("hard" confinement), while the

PSF layers in PSF/OBC films are confined by the rubbery, lower-modulus OBC material ("soft" confinement).

6.2.2 Calculation of T_f' and apparent activation enthalpy

The limiting fictive temperature of a glassy sample was calculated by the Pyris DSC software using the equal areas method of Moynihan.[3,4] A graphical illustration of this method is shown in Figure 6.5.

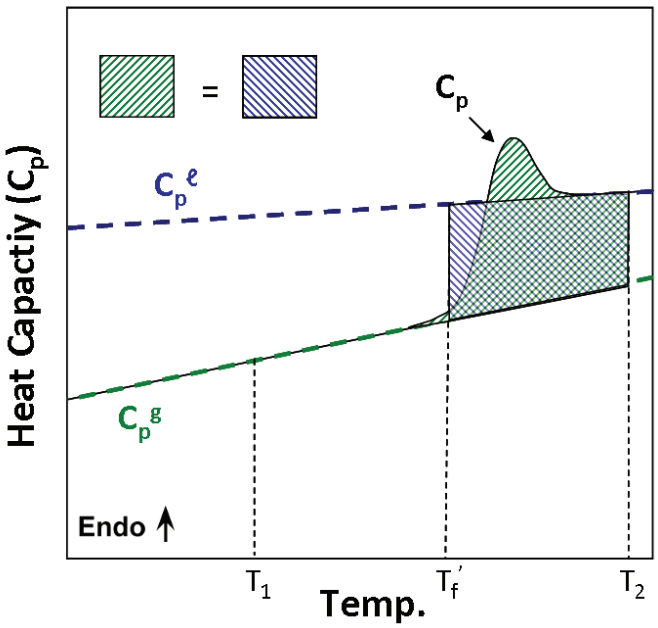

Figure 6.5: Graphical explanation of the equal areas method for calculating the limiting fictive temperature from DSC thermograms (Eq. 6.5).

Two temperatures, T_1 and T_2, which are below and above the transition region, respectively, are chosen. The heat capacity lines for the equilibrium liquid (C_p^{ℓ}) and glass (C_p^{g}) are extrapolated from the DSC thermogram for C_p, and T_f' is the value which satisfies the following equation:

$$\int_{T_1}^{T_2}(C_p - C_p^g)dT = \int_{T_f'}^{T_2}(C_p^\ell - C_p^g)dT \tag{6.5}$$

The Pyris DSC software is able to perform this calculation when supplied with T_1, T_2, and the extrapolated heat capacity lines. By measuring T_f' as a function of cooling rate (q), $\Delta h^*/R$ can be calculated using Eq. 6.6.[5] The $\Delta h^*/R$ parameter is used in phenomenological models of aging and structural relaxation in glasses (e.g., the Tool-Narayanaswamy-Moynihan [TNM] model), and its magnitude provides a quantitative measure of the sensitivity of the glass transition to changes in experimental timescale for a given material.

$$-\frac{\partial \ln|q|}{\partial\left(1/T_f'\right)} = \frac{\Delta h^*}{R} \tag{6.6}$$

Figure 6.6(a-d) shows the normalized heat capacity curves for bulk and layered PSF samples cooled at various rates and then reheated at 10 °C/min. Figure 6.7 presents data for cooling rate versus $1000/T_f$' that was used to determine $\Delta h^*/R$ for the layered and bulk PSF samples. A plot of the calculated $\Delta h^*/R$ values is shown in Figure 6.8.

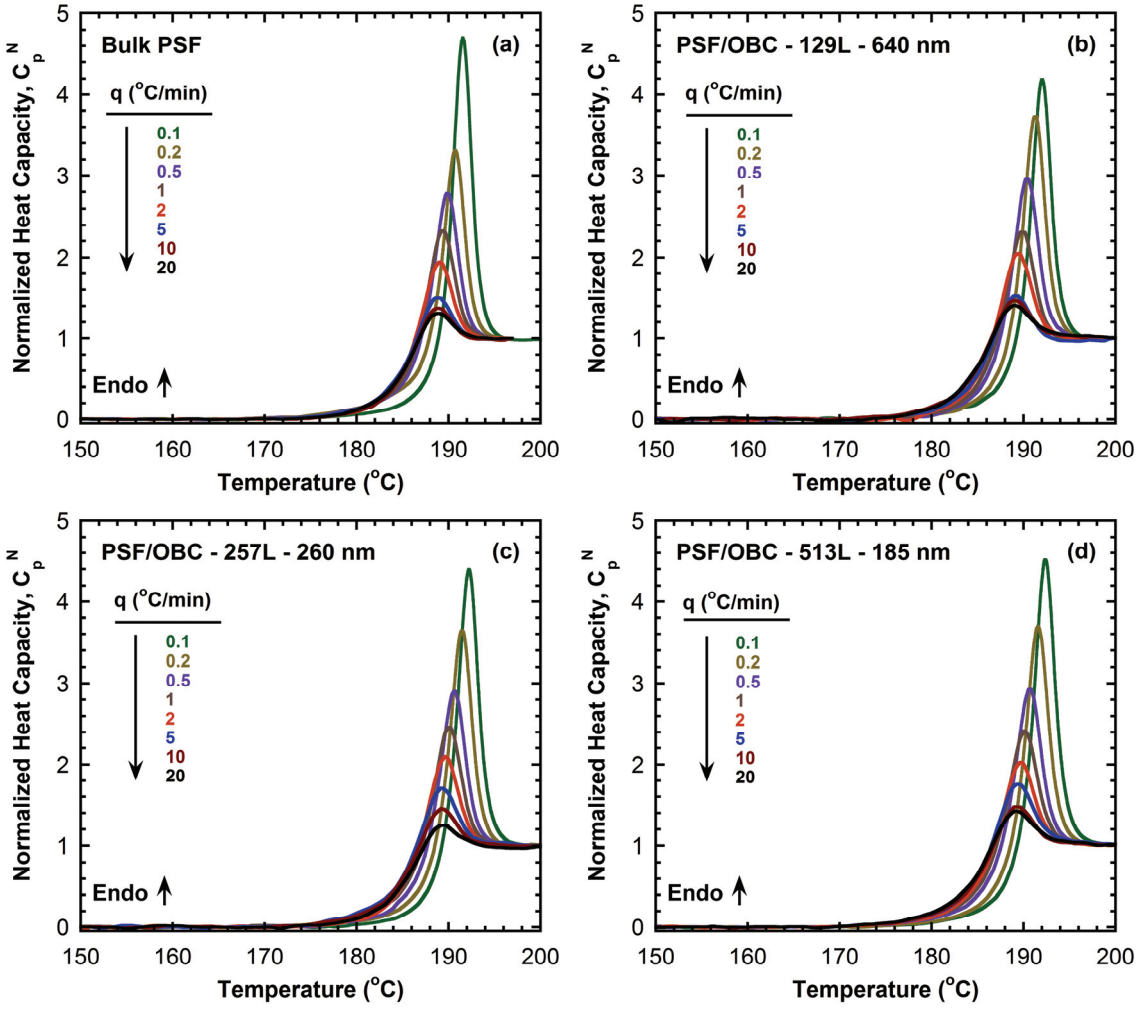

Figure 6.6: Normalized heat capacity curves as a function of cooling for bulk PSF and multilayered PSF/OBC films (a) Bulk PSF (b) 129-layer PSF/OBC (~640 nm PSF layers) (c) 257-layer PSF/OBC (~260 nm PSF layers) (d) 513-layer PSF/OBC (~185 nm PSF layers).

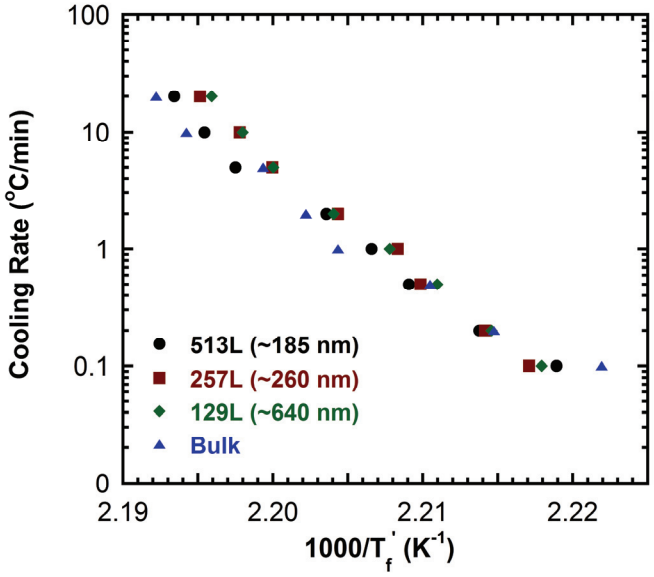

Figure 6.7: Cooling rate dependence of the limiting fictive temperature (T_f') for bulk PSF and layered PSF/OBC films. PSF layer thickness is given in parentheses.

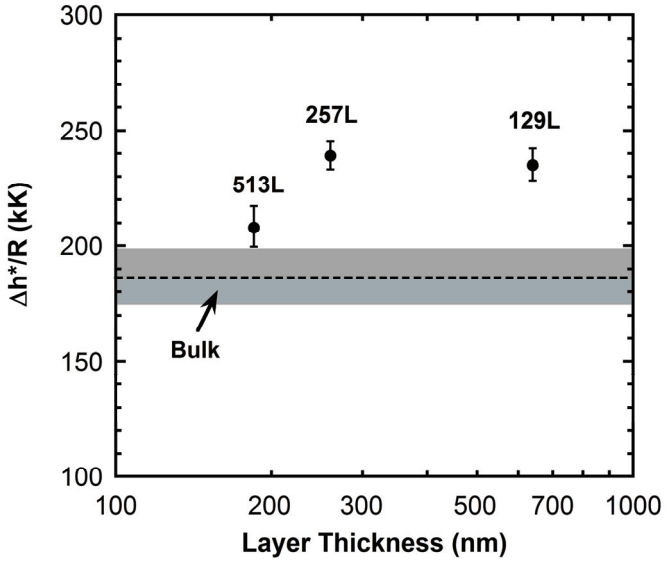

Figure 6.8: Values of $\Delta h^*/R$ versus layer thickness for bulk PSF and layered PSF/OBC films. Values of $\Delta h^*/R$ were obtained using Eq. 6.6 and the data shown in Figure 6.7. The error bars shown are the uncertainties from fitting the data of Figure 6.7.

The value of $\Delta h^*/R$ for the bulk PSF sample was 181 kiloKelvin (kK). The $\Delta h^*/R$ values of layered samples were higher than those of bulk PSF. The calculated values of $\Delta h^*/R$ did not exhibit any systematic dependence on layer thickness. In contrast, Koh and Simon observed that $\Delta h^*/R$ values decreased systematically with decreasing thickness in polystyrene films.[1] In their study, lower values of T_f' (relative to bulk) were also observed for the thinner PS films, although this was primarily due to the thinner films having reduced T_g values. Langhe et al. studied the effect of cooling rate on recovered enthalpy in both bulk PS and layered PS/PC films.[2] In their study, the amount of enthalpy recovered upon reheating through the PS T_g was similar for all films and did not depend on layer thickness. A plot of T_f' versus the logarithm of cooling rate is shown in Figure 6.9. The absolute values of the fictive temperatures are within 1 °C for all samples at each cooling rate. Consequently, the amount of relaxation occurring during cooling is quite similar for all samples considered, which is largely in agreement with the findings of Langhe et al. in which no discernable impact of layer thickness on recovered enthalpy was observed for samples cooled at different rates.

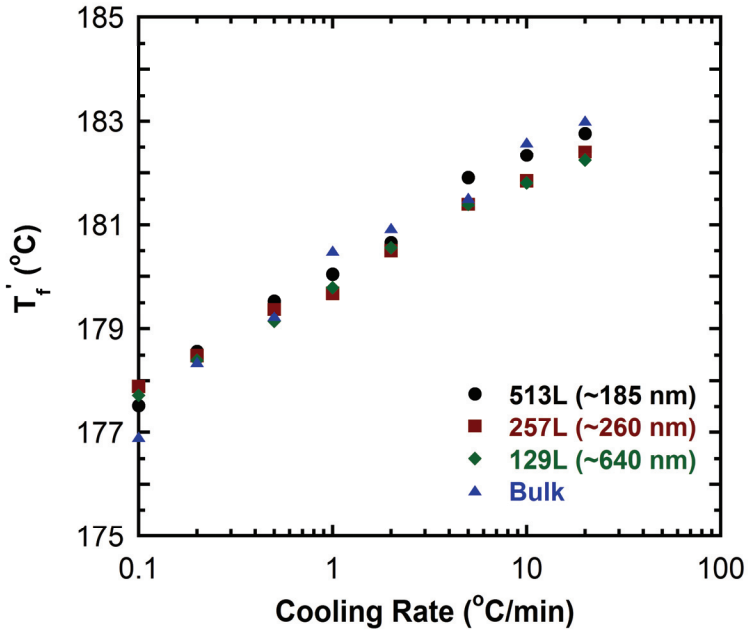

Figure 6.9: Limiting fictive temperature (T_f') as a function of cooling rate for bulk PSF and layered PSF/OBC films.

6.3 CONCLUSIONS

Isothermal aging studies at 170 °C and cooling rate studies were performed on bulk PSF and multilayered PSF/OBC samples. The aging of thin PSF layers confined in these multilayered structures is largely similar to aging in bulk PSF for films for samples having PSF layer thicknesses of ~640 nm and ~260 nm. The film with 185 nm thick PSF layers showed a slightly higher aging rate than that of bulk PSF. Difficulties in preparing layered films with PSF layers thinner than ~185 nm prevented us from determining if the higher aging rate observed in the 513-layer film was truly due to decreasing film thickness. Cooling rate studies on layered PSF/OBC and bulk PSF films were also performed by varying the cooling rate through T_g and then measuring the limiting fictive

temperature (T_f') of the samples upon reheating. T_f' was similar (within 1 °C) among all samples at each cooling rate. The results of the DSC studies presented here generally support the conclusions of our previous gas permeation aging studies of PSF/OBC and PSF/EO films aged at 35 °C, in which the aging rate was found to be independent of layer thickness and similar to the aging rate of bulk PSF. Freestanding thin films of PSF that have been previously studied using gas permeability tracking by Huang et al. show highly accelerated aging relative to bulk and a strong dependence of aging rate on film thickness.[6,7] The absence of a strong thickness dependence of the aging rates in multilayered PSF films when studied by DSC at temperatures close to T_g (170 °C) or by gas permeability tracking at temperatures far from T_g (35 °C)[8] tends to support the idea that accelerated aging in freestanding thin films relates to the presence of free or highly-mobile surfaces (i.e., surfaces or interfaces not in contact with, not adhering to, or only weakly interacting with a substrate). The multilayered films considered here and in our previous work are composed of PSF layers in intimate contact with rubbery confining layers and thus lack the large fraction of near-surface material that is present in freestanding films.

6.4 REFERENCES

1. Koh YP, Simon SL. Structural relaxation of stacked ultrathin polystyrene films. *Journal of Polymer Science Part B: Polymer Physics* **2008**, 46(24): 2741–2753.

2. Langhe DS, Murphy TM, Shaver A, LaPorte C, Freeman BD, Paul DR, Baer E. Structural relaxation of polystyrene in nanolayer confinement. *Polymer* **2012**, 53(9): 1925–1931.

3. Moynihan CT, Easteal AJ, DeBolt MA, Tucker J. Dependence of the Fictive Temperature of Glass on Cooling Rate. *Journal of the American Ceramic Society* **1976**, 59(1-2): 12–16.

4. Debolt MA, Easteal AJ, Macedo PB, Moynihan CT. Analysis of Structural Relaxation in Glass Using Rate Heating Data. *Journal of the American Ceramic Society* **1976**, 59(1-2): 16–21.

5. Moynihan CT, Macedo PB, Montrose CJ, Gupta PK, DeBolt MA, Dill JF, Dom BE, Drake PW, Easteal AJ, Elterman PB, Moeller RP, Sasabe H, Wilder JA. Structural relaxation in vitreous materials. *Annals of the New York Academy of Sciences* **1976**, 279(The Glass Transition and the Nature of the Glassy State): 15–35.

6. Huang Y, Paul DR. Physical aging of thin glassy polymer films monitored by gas permeability. *Polymer* **2004**, 45(25): 8377–8393.

7. Huang Y, Paul DR. Effect of Film Thickness on the Gas-Permeation Characteristics of Glassy Polymer Membranes. *Industrial & Engineering Chemistry Research* **2007**, 46(8): 2342–2347.

8. Murphy TM, Langhe DS, Ponting M, Baer E, Freeman BD, Paul DR. Physical aging of layered glassy polymer films via gas permeability tracking. *Polymer* **2011**, 52(26): 6117–6125.

Chapter 7: Physical Aging of Polystyrene Films Tracked by Gas Permeability

7.1 SUMMARY

Most studies using gas permeation to characterize physical aging in thin polymer films have focused on polymers of interest as membrane materials, such as polysulfone (PSF) and Matrimid. Many other physical aging studies, using techniques other than gas permeation, focus on polystyrene (PS). In this work, physical aging in bulk PS films and PDMS-coated thin PS films was studied using well-established gas permeation techniques. The ~400 nm PS films aged slightly faster than bulk PS. However, the difference between rates of aging in thin and thick films was much less than that reported in polysulfone (PSF) and Matrimid films of similar thicknesses. The ~800 nm films aged in a manner generally similar to bulk PS. Comparison of the normalized oxygen permeability of ~400 nm films of PS, PSF, and Matrimid revealed that a ~400 nm PS film experiences a slower decline in relative permeability than does a PSF or Matrimid film. Unlike what has been observed previously in studies of PSF and Matrimid films, PS films do not appear to show aging behavior that is strongly dependent on film thickness or highly accelerated relative to bulk. Because it would be difficult to use the results of PS aging studies to predict the aging behavior of typical gas separation polymers, we suggest that PS is not a good model for the aging behavior of commercially useful gas separation membrane materials.

7.2 RESULTS AND DISCUSSION

7.2.1 Calculation of PS Permeability

A detailed discussion of the methodology used to prepare and measure the thin PS films discussed in this chapter is provided in Appendix B, which also describes many of the difficulties encountered during the initial phases of this work.

Gas permeability measurements were made on PS-PDMS composite films after annealing the film at 120 °C for 20 minutes (to reset the thermal history of the film). However, it is the permeability of the PS layer alone that is of interest. The permeability of the PS layer can be calculated from measurements of PS-PDMS composite films using a model based on mass transfer resistances in series, which is shown in Eq. 7.1.

$$\frac{\ell_{composite}}{P_{composite}} = \frac{\ell_{PS}}{P_{PS}} + \frac{\ell_{PDMS}}{P_{PDMS}} \tag{7.1}$$

where ℓ_{PS} is the thickness of the PS film, ℓ_{PDMS} is the thickness of the PDMS coating layer, P_{PS} is the permeability of the PS film, and P_{PDMS} is the permeability of the PDMS layer. The total film thickness (i.e., the sum of the PS and PDMS layer thicknesses) is given by $\ell_{composite}$, and $P_{composite}$ is the permeability of the two-layer composite film. McCaig and Paul have demonstrated that the PDMS permeability (and hence the mass transfer resistance) does not change with time.[1] This method of calculation has been used in other aging studies,[2–4] and it is based on work by Henis and Tripodi.[5] In this work, the resistance of the PDMS layer was always less than ~6% of the resistance of the PS layer. Previous studies have found that the presence of the PDMS layer does not have a substantial effect on the aging behavior of PSF or a 6FDA-based polyimide.[2,4] The development

7.2.2 Gas permeability and aging in PS films

Figure 7.1a presents oxygen permeability as a function of aging time for bulk films of PS, PSF, and Matrimid. Bulk films of both grades of PS (PS900k and Styron 685D) are shown, along with data for PSF and Matrimid from Huang et al.[6] The absolute oxygen permeability of PS900k is roughly 10% higher than that of Styron 685D. The two types of PS are made by different processes (i.e., anionic polymerization for PS 900k versus free-radical polymerization for Styron 685D) and have different average molecular weights and molecular weight distributions. Additionally, the commercial material may contain oligomers and/or additives not present in PS900k. Thus, small differences in the permeability values of bulk films of PS900k and Styron 685D are not unexpected. Both grades of PS appear to age similarly, and the bulk PS films, like those of other materials, experience a steady drop in permeability over time. The oxygen permeabilities of two films of Styron 685D show good agreement with one another. Thus, for the sake of clarity, the remaining figures show only one set of data for bulk Styron 685D. Figure 7.1b shows the data of Figure 7.1a normalized by the permeability value at an aging time of 1 hr. Figure 7.1b shows that bulk PS films exhibit a more rapid relative decline in oxygen permeability than bulk PSF films do. The relative oxygen permeability decline of PS is similar to that of Matrimid, though perhaps slightly faster.

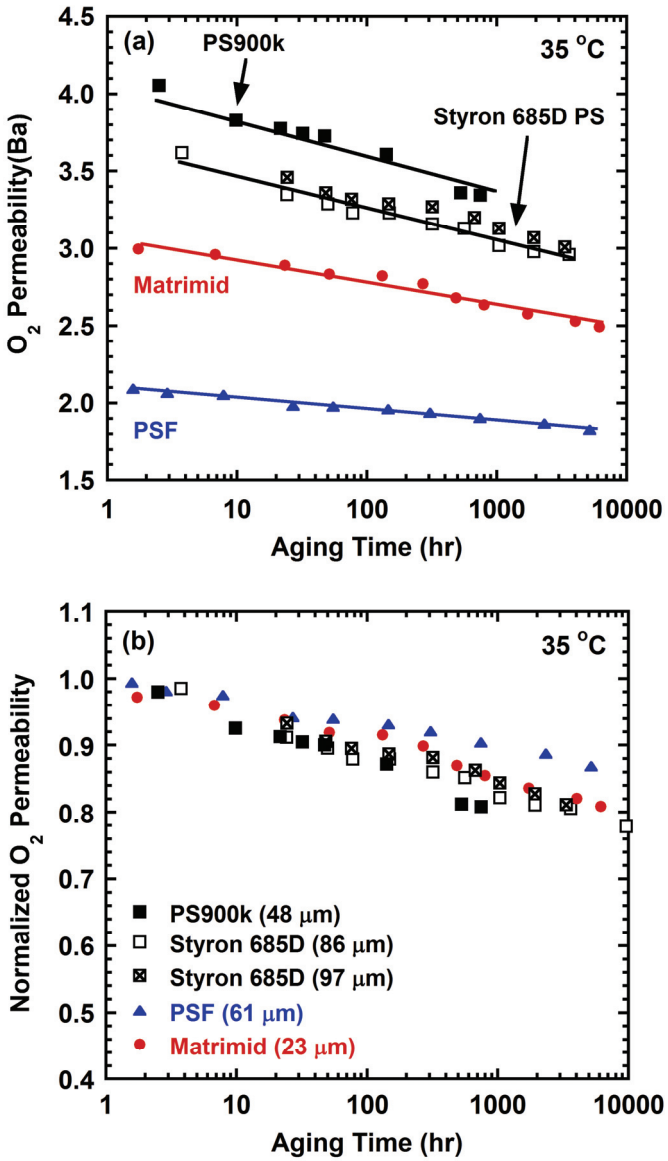

Figure 7.1: (a) Oxygen permeability as a function of aging time for bulk films of PS, Matrimid, and PSF. Data for two bulk Styron 685D films are shown. Matrimid and PSF data are from Huang.[6] Lines are provided to guide the eye. (b) Normalized oxygen permeability for bulk films as a function of aging time. Data are normalized by the permeability at 1 hour of aging time (determined by extrapolation).

Figure 7.2 shows the (a) oxygen and (b) nitrogen permeability as a function of aging time for thin and bulk PS films. For thin films (i.e., $\ell_{PS} < 1000$ nm), two samples of each thickness were studied. The samples were taken from the same film casting, but they were distinct from one another and were studied using different permeation cells. For films of the same thickness, the aging behavior appears similar. Although there are differences in the calculated absolute permeability values, these differences amount to ~10% or less. Differences in permeation cell calibrations, as well as uncertainties associated with measurements of the area available for gas permeation and the film thickness (for both the PS and PDMS layers), can contribute to discrepancies in the calculated permeability values for nominally identical films. Differences in the permeability values of no more than ~10% are considered reasonably good agreement for two films measured on different permeation cells. The oxygen and nitrogen permeabilities of the 830 nm films are greater than those of either 417 nm film. This finding is similar to what was observed at early aging times by Huang and Paul in both PSF and Matrimid, where initial permeabilities were higher for ~1000 nm films than they were for ~400 nm films.[7]

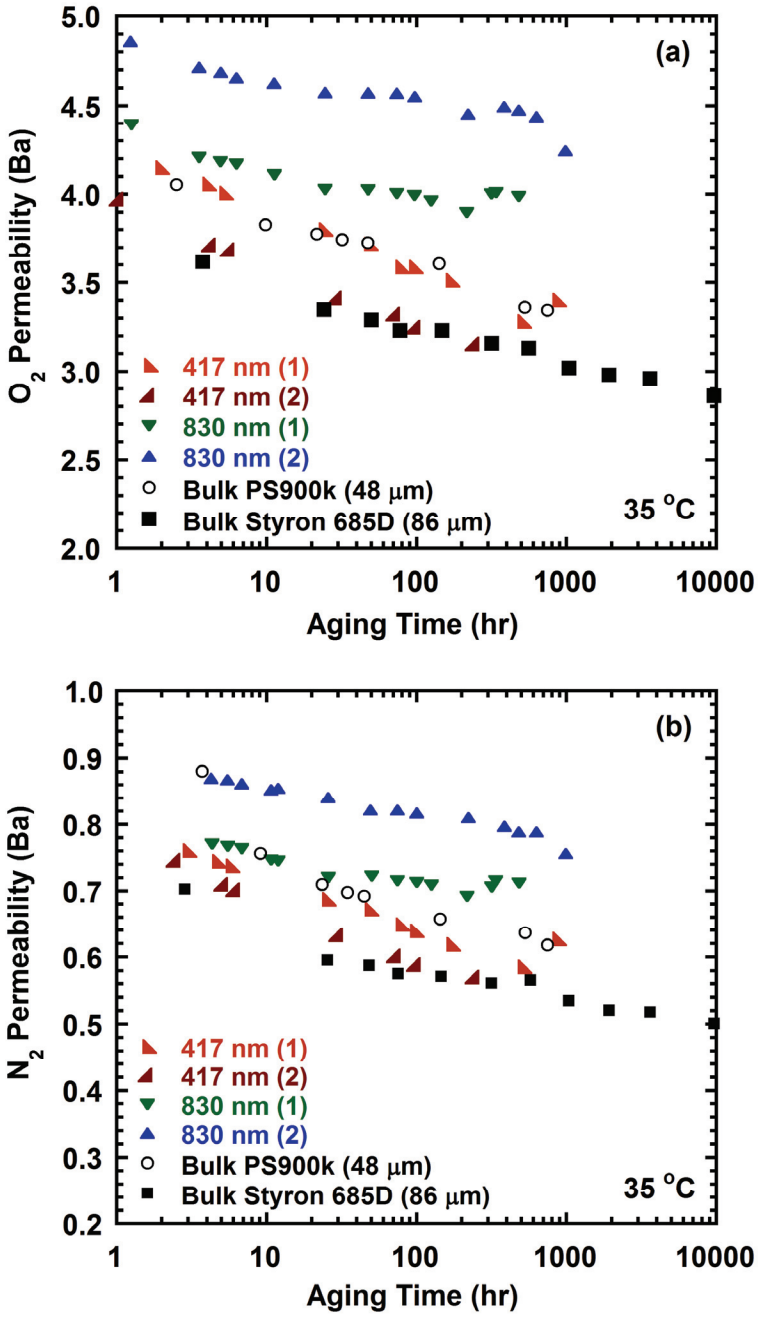

Figure 7.2: Effect of physical aging on (a) oxygen permeability and (b) nitrogen permeability for thin and bulk PS films.

The aging behavior of the thin PS films does not appear to differ as markedly from bulk as that of thin PSF or thin Matrimid films. Past studies on these materials and others have typically observed much greater differences in the aging behavior of thin versus bulk films.[1,2,7–9] The O_2/N_2 selectivity of PS films as a function of aging time is shown in Figure 7.3. The selectivity values for the thin PS films are similar to bulk values, indicating that the PDMS-coated PS layers are behaving like defect-free films. The initial selectivity of the bulk PS900k film is ~15% lower than that of the other films. The lower initial selectivity is due largely to difficulty in fully degassing a thick bulk film when it is first placed into the permeation cell (and in between permeation tests during the initial period of the aging study). This can result in slightly higher permeability values (more noticeable for nitrogen, as can be seen in Figure 7.2b) and lower selectivities. As the study progresses and the film is able to be fully degassed between tests and held under vacuum, this problem is eliminated. Thus, one should not over-interpret the fact that the bulk PS films show a slightly higher initial N_2 permeability and lower initial selectivity than would be expected based on extrapolation from the longer-time aging data. As would be expected from the bulk permeability data, the bulk Styron 685D film shows a slightly higher selectivity than the bulk PS900k film.

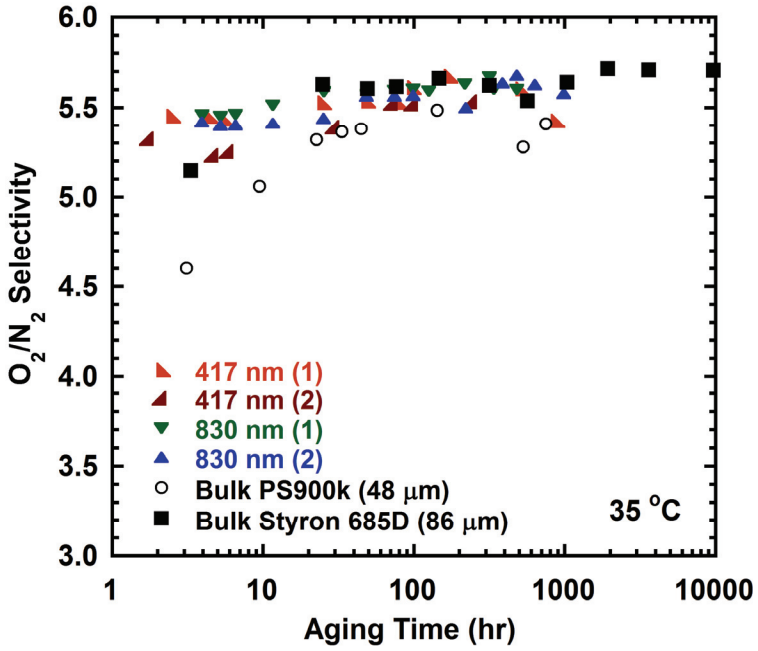

Figure 7.3: O_2/N_2 selectivity for thin and bulk PS films as a function of aging time.

The normalized oxygen permeability as a function of aging time for PS films is shown in Figure 7.4. Normalization facilitates comparison among films with different absolute permeability values by showing the relative decline in permeability over time. Figure 7.4 shows good agreement between films of the same thickness. The 417 nm films appear to undergo a slightly greater relative decline in permeability over time than either the 830 nm films or the bulk films. The 830 nm films appear to age in a manner that is generally similar to bulk. The relative changes in permeability for PS films are much less than those seen in PSF or Matrimid films of comparable thicknesses that were studied previously.[2,7,8]

Figure 7.5 shows a comparison of normalized oxygen permeability as a function of aging time for films of PS, PSF, and Matrimid that are around 400 nm in thickness (data for PSF and Matrimid are taken from Fig. 17 in Huang and Paul[7]). The permeability decline of the ~400 nm PS films is roughly linear with the logarithm of aging time and is less rapid than that of PSF or Matrimid. In contrast, Figure 7.1b shows that bulk PS undergoes a relative decline in permeability that is similar to Matrimid and

more rapid than PSF, demonstrating that the thickness dependence of aging is much more pronounced in polymers like PSF and Matrimid than in PS. Perhaps the gas permeation aging behavior of PS films would show greater deviation from bulk behavior if the films were much thinner (on the order of 100 nm or less), but experimental difficulties have prevented this possibility from being explored.

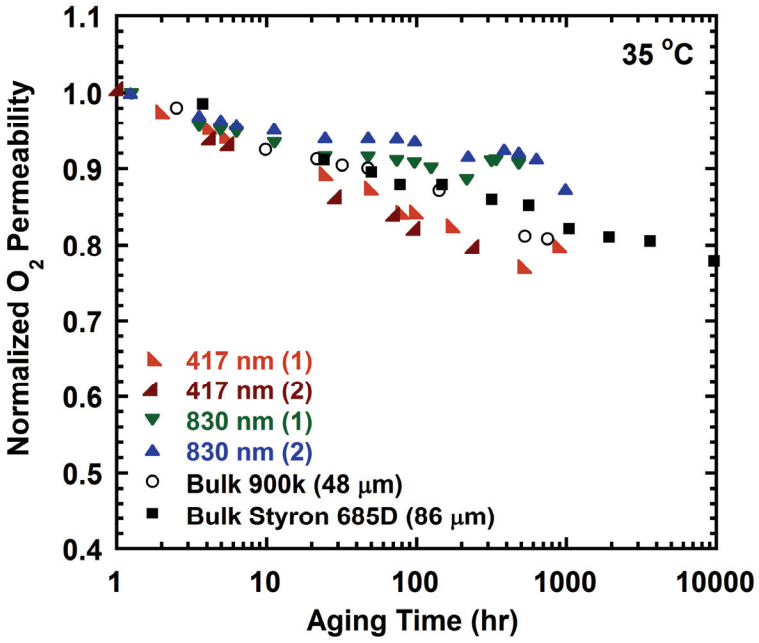

Figure 7.4: Normalized oxygen permeability for thin and bulk PS films as a function of aging time.

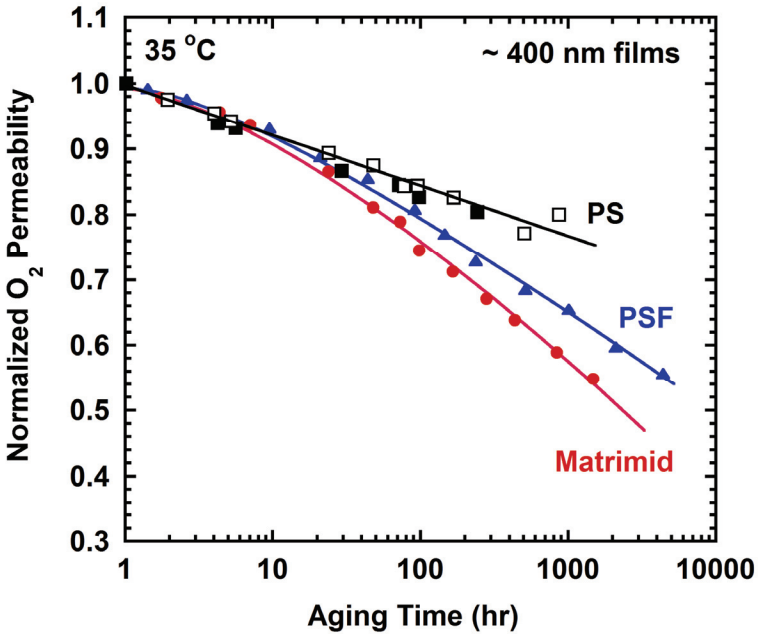

Figure 7.5: Normalized oxygen permeability as a function of aging time for PS, PSF, and Matrimid films of approximately 400 nm. Lines are provided to guide the eye. Data for PSF and Matrimid films are from Huang and Paul.[7]

There are many potential reasons why the aging behavior of PS films at 35 °C differs so markedly from that of other polymers. One significant difference between PS and PSF or Matrimid is that at the aging temperature used in nearly all gas permeation studies (35 °C), PS is much closer to its T_g (T_g - T_a ~ 70 °C) than PSF or Matrimid, which are ~150 °C and ~280 °C from their T_gs, respectively. Differences in the thickness dependence of aging for these polymers could be due in part to differences in $T_g - T_a$. Huang and Paul observed a weakening of the thickness dependence of the aging rate of PSF (based on oxygen permeability data) as the aging temperature was increased (i.e., T_g -T_a decreased).[10] Pye et al. also observed a smaller difference between the aging rates of relatively thick (2.4 μm) and ultrathin (29 nm) PS films as the aging temperature was increased.[11]

The ellipsometry studies of Gray et al. showed that PS films quenched in a freestanding state had aging rates that depended on thickness (where the aging rate, β, is

determined by the change in normalized film thickness, i.e., $\beta = -\frac{1}{h_0}\frac{\partial h}{\partial \log t}$).[12] The PS films in their work (T_g ~ 100 °C) were aged at 65 °C (T_g - T_a ~ 35 °C), and the data covered aging times up to ~7 hr. In our study, a lower aging temperature was used, and the permeability measurements were made over a longer period of time. The temperature dependence of aging in freestanding quenched PS films is not known. However, had the films of Gray et al. been aged at 35 °C, one could reasonably expect the aging to be slower. The changes in film thickness (which are directly related to density changes, since the film is biaxially constrained on a wafer) over the course of their experiments are quite small. Considering that the expected density changes would be even smaller for a film aged at 35 °C relative to one aged at 65 °C, it is not surprising that the PS films in this work show relatively little thickness dependence in permeation tests. In contrast to the ellipsometry experiments, permeation experiments may be less able to reliably capture such small differences in aging behavior. Using the aging rate calculation methodology of Gray et al., the ellipsometry data of Huang and Paul for a ~400 nm PSF film aged at 35 °C (see Fig. 6 in Huang and Paul[13]) show that it ages more rapidly than any of the PS films aged at 65 °C that were considered by Gray et al.[12] or Pye et al.[11] (β_{PSF} ~ 17 x 10^{-4}, while the largest value of β_{PS} is roughly 10 x 10^{-4}). Thus, both permeation experiments and ellipsometry experiments are in agreement that thin PSF films age more rapidly than PS films of comparable thicknesses.

As mentioned previously, there has been discussion in the literature regarding potential differences between the physical aging behavior of the relatively stiff-backbone polymers used in gas permeation studies and that of polymers with more flexible backbones, such as PS or poly(methyl methacrylate) (PMMA). Baker et al. measured the oxygen permeability of PMMA films ranging in thickness from 190 nm to ~6 μm over the course of roughly two months.[14] They observed no noticeable thickness dependence in the aging behavior and saw very little decrease in gas permeability over time. Additionally, Priestley et al. observed similar aging behavior between 500 nm and 20 nm PS films aged at 305 K (32 °C, very similar to the aging temperature in this work).[15]

Although these films were supported on silica and the 20 nm film was much thinner than any considered in this work, it is worth noting that thin PS films aged at nearly the same temperature used in this work have been shown to lack thickness dependence.

7.2.3 Comparison of aging data to the upper bound

A well-documented tradeoff exists between the gas permeability and permselectivity of polymeric membrane materials.[16–20] This tradeoff is typically discussed in terms of an "upper bound" line, which describes the current performance limits of polymer materials (i.e., the line is defined by the polymers with the highest selectivity at a given permeability, or vice-versa). The O_2 permeability and O_2/N_2 selectivity values for bulk and thin PS films are compared to the upper bound in Figure 7.6.[16] Data for a bulk PSF film and a 400 nm PSF film from Huang are also included for comparison.[7] The results for PS are similar to what has been observed previously in other gas permeation aging studies, which have shown that aging generally results in movement that parallels or deviates slightly away from the upper bound line.[2,21]

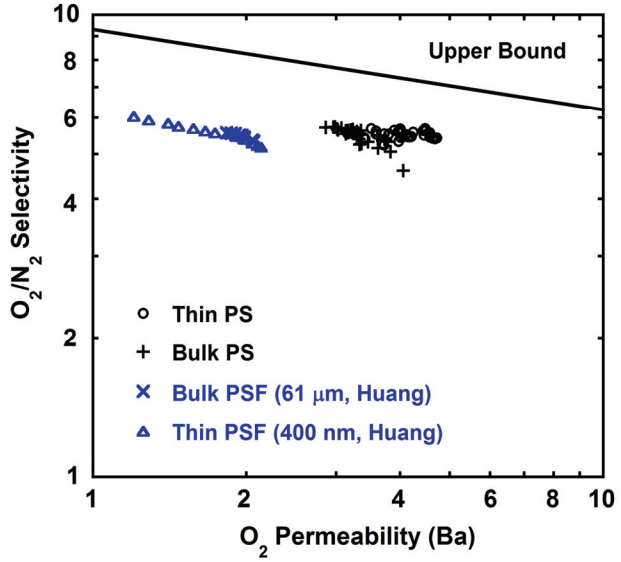

Figure 7.6: Comparison of the aging behavior of bulk and thin films of PS (this work) and PSF (from Huang and Paul[7]) to the upper bound line reported by Robeson.[16]

7.3 CONCLUSIONS

The physical aging of both thin and bulk PS films was studied as a function of aging time at 35 °C. The aging behavior of bulk films of PS and two samples each of ~400 nm and ~800 nm PS films coated with PDMS was characterized using gas permeation techniques. In contrast to thin films of PSF and Matrimid studied earlier by Rowe et al.[2] and Huang and Paul,[7,8,10,22] PS films do not show aging behavior that is strongly thickness-dependent and highly accelerated relative to bulk. The ~400 nm PS films in this work showed slightly faster aging than bulk PS; however, the slight acceleration seen here is much less than that observed in PSF and Matrimid films of similar thicknesses that were also aged at 35 °C. Additionally, comparison of the normalized oxygen permeability of PS, PSF, and Matrimid films of roughly 400 nm aged at 35 °C revealed that a ~400 nm PS film experiences a slower decline in relative permeability than a PSF or Matrimid film does. Bulk films of PS, however, aged more rapidly than PSF and at a rate similar to that of Matrimid (as assessed by their normalized oxygen permeabilities over time). Thus, at the thicknesses and aging temperature considered in this study, the aging behavior of PS shows much weaker thickness dependence than that seen in polymers like PSF and Matrimid. Comparisons to the Robeson upper bound showed that physical aging in PS produced changes with respect to the upper bound (for O_2/N_2 separation) similar to those reported previously in other polymers. Based on our findings, it would be difficult to use the results of PS aging studies to predict the aging behavior of typical gas separation polymers. Thus, PS, which is not used commercially as a membrane material due to its relatively poor mechanical properties, low chemical resistance, and low T_g, is not a good model for the aging behavior of useful membrane materials.

7.4 REFERENCES

1. McCaig MS, Paul DR. Effect of film thickness on the changes in gas permeability of a glassy polyarylate due to physical aging Part I. Experimental observations. *Polymer* **2000**, 41(2): 629–637.

2. Rowe BW, Freeman BD, Paul DR. Physical aging of ultrathin glassy polymer films tracked by gas permeability. *Polymer* **2009**, 50(23): 5565–5575.

3. Cui L, Qiu W, Paul DR, Koros WJ. Responses of 6FDA-based polyimide thin membranes to CO2 exposure and physical aging as monitored by gas permeability. *Polymer* **2011**, 52(24): 5528–5537.

4. Cui L, Qiu W, Paul DR, Koros WJ. Physical aging of 6FDA-based polyimide membranes monitored by gas permeability. *Polymer* **2011**, 52(15): 3374–3380.

5. Henis JMS, Tripodi MK. Composite hollow fiber membranes for gas separation: the resistance model approach. *Journal of Membrane Science* **1981**, 8(3): 233–246.

6. Huang Y. Physical Aging of Thin Glassy Polymer Films, The University of Texas at Austin, 2005.

7. Huang Y, Paul DR. Physical aging of thin glassy polymer films monitored by gas permeability. *Polymer* **2004**, 45(25): 8377–8393.

8. Huang Y, Paul DR. Effect of Film Thickness on the Gas-Permeation Characteristics of Glassy Polymer Membranes. *Industrial & Engineering Chemistry Research* **2007**, 46(8): 2342–2347.

9. Huang Y, Paul DR. Effect of molecular weight and temperature on physical aging of thin glassy poly(2,6-dimethyl-1,4-phenylene oxide) films. *Journal of Polymer Science Part B: Polymer Physics* **2007**, 45(12): 1390–1398.

10. Huang Y, Paul DR. Effect of Temperature on Physical Aging of Thin Glassy Polymer Films. *Macromolecules* **2005**, 38(24): 10148–10154.

11. Pye JE, Rohald KA, Baker EA, Roth CB. Physical Aging in Ultrathin Polystyrene Films: Evidence of a Gradient in Dynamics at the Free Surface and Its Connection to the Glass Transition Temperature Reductions. *Macromolecules* **2010**, 43(19): 8296–8303.

12. Gray LAG, Yoon SW, Pahner WA, Davidheiser JE, Roth CB. Importance of Quench Conditions on the Subsequent Physical Aging Rate of Glassy Polymer Films. *Macromolecules* **2012**, 45(3): 1701–1709.

13. Huang Y, Paul DR. Physical Aging of Thin Glassy Polymer Films Monitored by Optical Properties. *Macromolecules* **2006**, 39(4): 1554–1559.

14. Baker EA, Rittigstein P, Torkelson JM, Roth CB. Streamlined ellipsometry procedure for characterizing physical aging rates of thin polymer films. *Journal of Polymer Science Part B: Polymer Physics* **2009**, 47(24): 2509–2519.

15. Priestley RD, Broadbelt LJ, Torkelson JM. Physical Aging of Ultrathin Polymer Films above and below the Bulk Glass Transition Temperature: Effects of Attractive vs Neutral Polymer−Substrate Interactions Measured by Fluorescence. *Macromolecules* **2005**, 38(3): 654–657.

16. Robeson LM. Correlation of separation factor versus permeability for polymeric membranes. *Journal of Membrane Science* **1991**, 62(2): 165–185.

17. Freeman BD. Basis of Permeability/Selectivity Tradeoff Relations in Polymeric Gas Separation Membranes. *Macromolecules* **1999**, 32(2): 375–380.

18. Robeson LM. The upper bound revisited. *Journal of Membrane Science* **2008**, 320(1-2): 390–400.

19. Robeson LM, Freeman BD, Paul DR, Rowe BW. An empirical correlation of gas permeability and permselectivity in polymers and its theoretical basis. *Journal of Membrane Science* **2009**, 341(1-2): 178–185.

20. Rowe BW, Robeson LM, Freeman BD, Paul DR. Influence of temperature on the upper bound: Theoretical considerations and comparison with experimental results. *Journal of Membrane Science* **2010**, 360(1-2): 58–69.

21. Murphy TM, Langhe DS, Ponting M, Baer E, Freeman BD, Paul DR. Physical aging of layered glassy polymer films via gas permeability tracking. *Polymer* **2011**, 52(26): 6117–6125.

22. Huang Y, Paul DR. Experimental methods for tracking physical aging of thin glassy polymer films by gas permeation. *Journal of Membrane Science* **2004**, 244(1-2): 167–178.

Chapter 8: Conclusions and Recommendations

The physical aging of glassy polymers in confined environments has been investigated using gas permeability tracking and differential scanning calorimetry. A summary of the major conclusions from the studies described in Chapters 4, 5, 6, and 7 is provided in section 8.1. Section 8.2 discusses recommendations for future work related to physical aging in polymer glasses.

8.1 CONCLUSIONS

In order to compare the results of aging studies on multilayered films containing thin layers of polysulfone (PSF) to previous results from experiments that used free-standing thin films, the permeability of the rubbery co-layering material (Engage 8100) must be known so that the PSF layer permeability can be calculated. Because of initial difficulties measuring the gas permeability of Engage 8100 (EO), we wanted to verify the accuracy of our results and demonstrate that the measured values could be used to extract the PSF layer permeability from permeation measurements of layered films. Comparisons were made between the properties of EO and those of similar materials. The comparisons showed that the properties of our EO material followed the trends established by previous researchers, allowing us to confidently use them to calculate the permeability of PSF layers during aging experiments. Reasonably good agreement was seen between series model predictions and experimental permeability values in as-extruded PSF/EO films.

The physical aging of layered and bulk polysulfone (PSF) films at 35 °C was studied by measuring gas permeability over time. The layered films were composed of alternating layers of PSF and either Engage 8100 (EO) or Infuse 9007 (OBC). The

permeability of the PSF layers was calculated using a model based on mass transfer resistances in series. These layered films aged in a manner similar to that of bulk films, as demonstrated by the similar rates of permeability decline for these two types of films. Freestanding thin films of PSF (*i.e.*, those studied by Huang et al.[1] and Rowe et al.,[2] with overall thicknesses similar to the layer thicknesses of PSF/EO and PSF/OBC films) undergo more rapid aging than the films considered in this study. The aging rates of the thin PSF films studied by Huang et al. show a strong dependence on film thickness, and the absolute magnitudes of the aging rates are higher for all thin films than they are for any bulk or layered film.[1] Multilayered PSF/EO and PSF/OBC films show no dependence of aging rate on layer thickness, and the aging rates for the multilayered films are similar to those of bulk PSF films. In this study, the choice of confining polymer (EO or OBC) does not appear to affect the rate of aging. From this work, it appears that the effect of film thickness on physical aging stems from interfacial characteristics (i.e., free surfaces, weakly-adhering polymer-polymer interfaces, or strongly bonded polymer-polymer interfaces) and not merely thickness per se. The bulk-like aging behavior observed for multilayered films stands in sharp contrast to that of freestanding thin films, indicating that surfaces and interfaces play an important role during physical aging.

In addition to gas permeation aging studies of layered films, studies of the enthalpy relaxation behavior of multilayered PSF/OBC and bulk PSF films were performed using DSC. Isothermal aging studies at 170 °C and cooling rate studies were performed on both bulk and layered samples. The aging of thin PSF layers confined in these multilayered structures is largely similar to aging in bulk PSF for films for samples having PSF layer thicknesses of ~640 nm and ~260 nm. The film with 185 nm thick PSF layers showed a slightly higher aging rate than that of bulk PSF. Difficulties in preparing

layered films with PSF layers thinner than ~185 nm prevented us from determining if the higher aging rate observed in the 513-layer film was truly due to decreasing film thickness. Cooling rate studies on layered PSF/OBC and bulk PSF films were also performed by varying the cooling rate through T_g and then measuring the limiting fictive temperature (T_f') of the samples upon reheating. T_f' was similar (within 1 °C) among all samples at each cooling rate. The results of the DSC studies generally support the conclusions of our previous gas permeation aging studies of PSF/OBC and PSF/EO films aged at 35 °C, in which the aging rate was found to be independent of layer thickness and similar to the aging rate of bulk PSF. The absence of a strong thickness dependence of the aging rates in multilayered PSF films when studied by DSC at temperatures close to T_g (170 °C) or by gas permeability tracking at temperatures far from T_g (35 °C) tends to support the idea that accelerated aging in freestanding thin films relates to the presence of free surfaces (i.e., interfaces not in contact with, not adhering to, or only weakly interacting with a substrate). The multilayered films considered here and in our previous work are composed of PSF layers in intimate contact with rubbery confining layers and thus lack the large fraction of near-surface material that is present in freestanding films.

Most studies using gas permeability tracking to characterize physical aging in confined polymer films have focused on polymers of interest as membrane materials (*e.g.*, PSF and Matrimid). Many other physical aging studies focus on PS and use a variety of techniques other than gas permeation to characterize aging. In order to help bridge the gap between these two bodies of literature, the physical aging of polystyrene (PS) films was studied as a function of aging time at 35 °C using gas permeation techniques. The aging behavior of bulk films of PS and two samples each of ~400 nm and ~800 nm PS films coated with PDMS was characterized. In contrast to the thin films of PSF and Matrimid previously studied by Rowe et al.[2] and Huang and Paul,[1,3–5] PS

films do not exhibit aging behavior that is highly accelerated relative to bulk or strongly dependent on film thickness. The ~400 nm PS films showed slightly faster aging than bulk PS. However, the slight acceleration of aging that was observed is much less than that of PSF and Matrimid films of similar thicknesses. Additionally, comparison of the normalized oxygen permeability of PS, PSF, and Matrimid films of roughly 400 nm in thickness revealed that a ~400 nm PS film experiences a slower decline in relative permeability than a PSF or Matrimid film. Bulk films of PS, however, aged more rapidly than PSF and at a rate similar to that of Matrimid. Therefore, at the thicknesses and aging temperature considered in this study, the aging of PS shows much weaker thickness dependence than that seen in polymers like PSF and Matrimid. Based on our findings, it would be difficult to use the results of PS aging studies to predict the aging behavior of typical gas separation polymers. We propose that polystyrene, which is not used commercially as a membrane material due to its relatively poor mechanical properties, low chemical resistance, and low T_g, is not a good model for understanding the aging behavior of useful membrane materials.

8.2 RECOMMENDATIONS FOR FUTURE STUDIES

8.2.1 Gas permeation aging studies of multilayered films consisting of two glassy materials

Gas permeation aging studies have been performed on multilayered films consisting of alternating layers of PSF (glassy) and EO or OBC (both rubbery) that were produced via layer-multiplying co-extrusion. These studies suggested that the aging of the PSF layers was similar to bulk and independent of layer thickness for the

temperatures and layer thicknesses studied. The aging behavior of multilayered films consisting of two glassy materials has not been characterized using gas permeability. Langhe et al. performed DSC aging studies of layered films of polystyrene (PS) and polycarbonate (PC) and observed that the aging rate of the PS layers decreased with decreasing PS layer thickness when the films were aged at 80 °C.[6] The layered films, which had PS layers ranging in thickness from 50 nm to 500 nm, aged more slowly than bulk PS films despite having T_gs that were essentially identical to bulk (*N.B.*: substrate-supported PS films have been observed to undergo measurable T_g depression at thicknesses of 100 nm or less, so the invariant T_g in layered films with 50 nm or 100 nm PS layers is itself interesting and perhaps warrants further investigation). Because the findings of Langhe et al. differ from those of gas permeation and DSC aging studies of glass/rubber systems (which saw minimal effect of layer thickness on aging), it would be interesting to learn how aging affects gas permeability in glass/glass films at near-ambient temperatures. Although studies on glass/glass films would not allow for the aging of either component to be assessed individually as was done in the PSF/EO and PSF/OBC studies (due to both materials undergoing aging simultaneously), the aging behavior of the layered composite film could be characterized.

PS and PC could be used for initial experiments, since this type of film has been used in the aforementioned DSC aging studies. Films with a 50/50 PS/PC composition (and thus PS and PC layers of equal thickness) should be produced first. The aging behavior of bulk films of each component would need to be characterized, followed by aging studies of freestanding PS and PC films with thicknesses approximately equal to the PS and PC layer thicknesses in the multilayered films. Using data from aging experiments on the freestanding PS and PC films, a model (i.e., mass transfer resistances in series) could be used to predict the permeability response of the layered films,

assuming that they aged like freestanding films. Similarly, the bulk aging data could also be used to generate permeability data predictions (assuming that the aging of each layer was similar to bulk). The gas permeability of multilayered films could then be measured as a function of aging time, and comparisons of the responses could be made to predictions based on freestanding and bulk film results. Figure 8.1 depicts some possible aging responses for layered films based on hypothetical data for thin and bulk PS and PC films. PC has been observed to undergo accelerated aging in confinement,[7,8] while our initial studies with PS showed that its aging behavior was not strongly thickness dependent at the thicknesses and aging temperatures we considered.

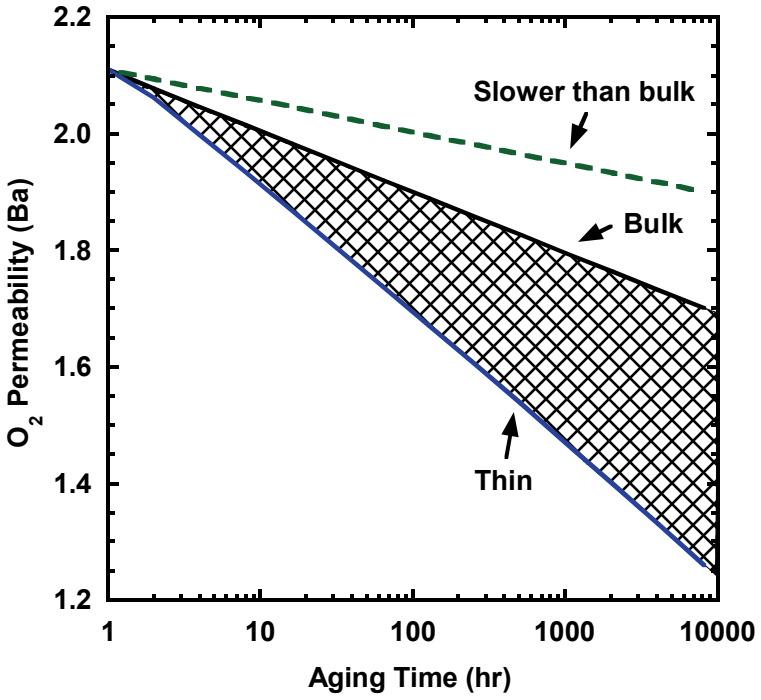

Figure 8.1: Illustration of possible aging responses in multilayered PS/PC films. Predictions of layered film aging behavior based on hypothetical bulk aging data (solid black line) and predictions based on hypothetical thin film data (solid blue line) are shown, with the area signifying an intermediate response between that of bulk and thin films. Dashed green line shows hypothetical experimental data for a film that ages slower than what is predicted based on aging data for bulk PS and PC films.

The study described above would entail annealing the films above the T_g of both PS and PC. However, another study could be performed in which the PS layers are selectively annealed at a temperature below the T_g of PC.

It could also be interesting to study layered films of other polymers, such as PSF and PC, which have similar permeabilities and chemical structures. Studies of PSF/PC films could be compared to studies of PSF/OBC and PSF/EO films, allowing a more direct comparison of glass/rubber vs. glass/glass films. The findings of studies like those

described above could provide further insight into understanding physical aging in confined geometries. Based on the results of the DSC studies of Langhe et al., it is possible that the glass/glass films may age even slower than bulk films. If so, the ability to make thin layers of polymer that age very slowly could be beneficial in applications where the stability of a glassy material is important, and understanding why layered films age differently than bulk or thin films would shed light on the role played by interfaces during physical aging.

8.2.2 Higher-temperature aging studies using gas permeation techniques

Nearly all gas permeation studies of the physical aging behavior of glass polymer films take place at temperatures well below the T_g of the material of interest. For materials like PSF and Matrimid, the aging temperatures are typically well over 100 °C below T_g. At such temperatures, it is impossible for the glass to reach an equilibrium state over any reasonable period of study. Most studies of physical aging that use other techniques (DSC, ellipsometry, etc.) take place much nearer to T_g, and in many of these cases the polymers do reach equilibrium within an experimentally-accessible period of time. Though Huang and Paul investigated the effect of temperature on physical aging in films of PSF and PPO, the highest temperature used was 55 °C.[5,9] In their studies, it was observed that the aging rate increased with increasing temperature, but that the sensitivity of the aging rate to changes in film thickness decreased with increasing temperature.

Higher-temperature aging studies of a polymer like PSF would likely be impossible using the techniques that have been historically used in gas permeation aging studies, due to limitations in the permeation cell setup and the materials used to mount the sample (i.e., the adhesive on the aluminum tape). However, recently-developed

techniques for sample mounting use thin brass plates and more heat-tolerant adhesives (such as epoxy or superglue), which would be much more appropriate for studies at elevated temperatures. One interesting study could involve aging films of PSF and PS (or other polymers) at aging temperatures that were equidistant from T_g (i.e., the values of $T_g - T_a$ would be identical, but T_a would be different for each polymer) and then comparing the resulting aging behavior. The stiffness of the polymer backbone has been discussed as a possible reason for differences in the aging behavior of polymers like PSF (stiffer backbone) and that of polymers like PS or PMMA (more flexible backbone).[10–12] However, studies using the latter polymers often take place in much different temperature regimes than studies using the former. A study of this sort could help elucidate the effect of backbone structure by eliminating differences in the quantity $T_g - T_a$. Initially, bulk films of the polymers of interest should be studied. Comparisons could be made to aging studies via DSC, which could be done in parallel with the gas permeation studies. However, it would also be interesting to understand how very thin films, such as those studied by Rowe et al., behave when aged at elevated temperatures.[2] Because these very thin films (~100 nm or less) would be expected to have T_gs that are depressed relative to bulk, increasing the aging temperature (i.e., moving towards T_g) could potentially have a dramatic effect on the aging behavior.

8.2.3 Gas permeation aging studies in ultrathin PS films

The aging behavior of PS films with thicknesses of 400 nm and 800 nm has been characterized using gas permeability measurements at an aging temperature of 35 °C. The aging behavior of the thin films did not appear to depend strongly on film thickness and was largely similar to bulk, though perhaps slightly accelerated for the 400 nm films.

Experimental difficulties and time constraints prevented thinner films from being investigated. It would be instructive to determine if ultrathin films (100 nm or less) show results that are similar to what was observed for 400 nm and 800 nm films. Rowe et al. observed that the thinnest PSF and Matrimid films they studied (~20 nm) showed rates of permeability decline that were slower than those of slightly thicker films, but that the absolute permeability values were also lower, suggesting a more "aged" (i.e., denser) film that had undergone rapid physical aging prior to the initial permeability measurements.[2] At 35 °C, PS is much closer to its T_g than PSF or Matrimid, and decreasing the PS film thickness below 100 nm (which is where T_g changes typically begin to occur) could result in significant deviations from bulk behavior. Many aging studies of supported PS films have focused on films thinner than 400 nm, so the aging responses of ultrathin PS films as assessed by gas permeability could be compared in a straightforward manner to the responses observed in studies using other techniques.

8.2.4 Effects of quench conditions on the physical aging of amorphous polymers via gas permeability tracking

Important differences exist between physical aging studies of thin films by researchers using gas permeation techniques and those using techniques such as ellipsometry and fluorescence spectroscopy. One such difference is that in the studies using the latter techniques, the film is typically supported on a substrate during annealing and quenching into the glassy state; in gas permeation studies, annealing and quenching takes place while the film is held on two sides by a wire frame (typically referred to as a "freestanding" state). Most of the gas permeation studies have observed thickness-dependent physical aging that is accelerated relative to bulk.[1–3,5,9,13] The onset of this thickness dependence typically occurs at relatively large length scales (on the order of ~1

μm or more) compared to those associated with changes in T_g or aging behavior in supported films. A study by Pye et al. showed that the aging behavior of supported PS films did not deviate from bulk until the film was ~100 nm thick and that further reductions in thickness decreased the aging rate.[14]

A recent study by Roth et al.[10] sought to address potential reasons for the differences in the aging behavior of PS and PSF films. Using ellipsometry to measure the change in thickness upon aging, it was demonstrated that the quench conditions (i.e., "freestanding" vs. fully supported) affect the physical aging behavior. Substrate-supported PS and PSF films showed similar aging behavior independent of thickness (down to ~400 nm), while PS films quenched in a "freestanding" state showed thickness-dependent aging that was slower than that of fully-supported films (PSF films quenched in a freestanding state were not studied by Gray et al.). When the films quenched in a freestanding state were then reheated above T_g (after aging) and re-quenched in a supported state, their subsequent aging behavior was essentially identical to that of supported films, lending credibility to the notion that the quench conditions are important in determining aging behavior. It was suggested that stresses resulting from the quenching step affect the aging behavior. Preliminary calculations showed that, for supported films, the stresses should be independent of sample thickness, whereas the stress in freestanding films would increase as the film thickness decreased but be generally lower in magnitude than that of supported films.

It would be informative to study how gas permeability is affected by different quench conditions. During the initial phases of their work on aging in thin films, Huang and Paul measured the time-dependent gas permeability of films supported during quenching.[4] Though they did not adopt that methodology for their subsequent studies, it demonstrates that such measurements should be possible. In contrast to what Gray et al.

observed in PS films, Huang and Paul observed that a 400 nm PSF film quenched while supported aged more slowly than a film quenched in a freestanding state. However, Huang and Paul used an aging temperature that was much deeper into the glassy state than that used by Gray et al., and they also considered aging times that were much longer (over 1000 hr for Huang and Paul, compared to ~6 hr for Gray et al.). Additionally, the measurements of Gray et al. begin earlier in the aging process (~10 minutes after annealing above T_g) than those of Huang and Paul (~1 hr after annealing). Gas permeation studies on PSF films supported during quenching could be compared to previous results with freestanding films. Also, ellipsometry studies of freestanding-quenched and supported-quenched PSF films (like those performed by Gray et al. for PS films) could be conducted. These studies could potentially help us understand why different types of aging experiments show what sometimes appear to be conflicting results, and they would be of use in understanding the role of glass formation conditions on physical aging behavior.

8.3 REFERENCES

1. Huang Y, Paul DR. Physical aging of thin glassy polymer films monitored by gas permeability. *Polymer* **2004**, 45(25): 8377–8393.

2. Rowe BW, Freeman BD, Paul DR. Physical aging of ultrathin glassy polymer films tracked by gas permeability. *Polymer* **2009**, 50(23): 5565–5575.

3. Huang Y, Paul DR. Effect of Film Thickness on the Gas-Permeation Characteristics of Glassy Polymer Membranes. *Industrial & Engineering Chemistry Research* **2007**, 46(8): 2342–2347.

4. Huang Y, Paul DR. Experimental methods for tracking physical aging of thin glassy polymer films by gas permeation. *Journal of Membrane Science* **2004**, 244(1-2): 167–178.

5. Huang Y, Paul DR. Effect of Temperature on Physical Aging of Thin Glassy Polymer Films. *Macromolecules* **2005**, 38(24): 10148–10154.

6. Langhe DS, Murphy TM, Shaver A, LaPorte C, Freeman BD, Paul DR, Baer E. Structural relaxation of polystyrene in nanolayer confinement. *Polymer* **2012**, 53(9): 1925–1931.

7. Rezac ME, Pfromm PH, Costello LM, Koros WJ. Aging of thin polyimide-ceramic and polycarbonate-ceramic composite membranes. *Industrial & Engineering Chemistry Research* **1993**, 32(9): 1921–1926.

8. Rezac ME. Update on the Aging of a Thin Polycarbonate-Ceramic Composite Membrane. *Industrial & Engineering Chemistry Research* **1995**, 34(9): 3170–3172.

9. Huang Y, Paul DR. Effect of molecular weight and temperature on physical aging of thin glassy poly(2,6-dimethyl-1,4-phenylene oxide) films. *Journal of Polymer Science Part B: Polymer Physics* **2007**, 45(12): 1390–1398.

10. Gray LAG, Yoon SW, Pahner WA, Davidheiser JE, Roth CB. Importance of Quench Conditions on the Subsequent Physical Aging Rate of Glassy Polymer Films. *Macromolecules* **2012**, 45(3): 1701–1709.

11. Baker EA, Rittigstein P, Torkelson JM, Roth CB. Streamlined ellipsometry procedure for characterizing physical aging rates of thin polymer films. *Journal of Polymer Science Part B: Polymer Physics* **2009**, 47(24): 2509–2519.

12. Priestley RD. Physical aging of confined glasses. *Soft Matter* **2009**, 5(5): 919–926.

13. Cui L, Qiu W, Paul DR, Koros WJ. Physical aging of 6FDA-based polyimide membranes monitored by gas permeability. *Polymer* **2011**, 52(15): 3374–3380.

14. Pye JE, Rohald KA, Baker EA, Roth CB. Physical Aging in Ultrathin Polystyrene Films: Evidence of a Gradient in Dynamics at the Free Surface and Its Connection to the Glass Transition Temperature Reductions. *Macromolecules* **2010**, 43(19): 8296–8303.

Appendix A: DSC Aging Studies of Physical Aging in PSF/EO Films

This chapter has been adapted with permission from the supplemental material to an article published in Polymer, **2012,** 53(18): 4002-4009.

SUMMARY

Multilayered films of polysulfone (PSF) and Dow Engage 8100, an ethylene-1-octene copolymer (EO), were made using a layer-multiplying co-extruder. The aging behavior of two layered film samples (with ~410 and ~180 nm PSF layers) and a bulk PSF sample was studied using DSC, which is a common and useful technique for characterizing aging in many types of polymer samples.[1–4] The aging temperature used in this study was 170 °C, which is the same temperature used in the DSC aging studies of PSF/OBC films discussed in Chapter 6. The enthalpy recovered upon heating an aged sample through its T_g was measured as a function of time. The aging behavior of PSF/EO layered films was similar to that of bulk PSF films. Additionally, comparisons between the aging of PSF/OBC and PSF/EO films revealed that the aging behavior of the two film types was similar, suggesting that when the confinement is provided by a relatively "soft" rubbery material (like EO or OBC), the choice of material for the confining layer does not significantly affect the aging behavior. The aging rates for all layered films were very similar to the aging rates for the two bulk films (with the exception of the 513-layer PSF/OBC sample, which had a slightly higher aging rate). This finding led us to conclude that the effect of layer thickness on aging in multilayered PSF films is minimal at the temperatures and layer thicknesses considered here. The aging behavior observed here for layered films differs from that of thin, freestanding PSF films studied via gas permeability tracking, which show thickness-dependent aging that is accelerated relative to bulk.

MATERIALS AND FILM CHARACTERIZATION

Multilayered films were prepared on a layer-multiplying co-extruder using Udel P-3700 PSF and Dow Engage 8100, an ethylene-1-octene copolymer (EO). The

isothermal physical aging of bulk PSF and two multilayered PSF/EO films was studied using DSC (T_a = 170 °C). The PSF/EO films both contained 257 layers. The PSF layer thickness in the PSF/EO films was changed by varying the feed composition to the extruder. The nominal volumetric compositions in the layered films studied here were 50% and 20% PSF, and the films possessed ~410 and ~180 nm PSF layers, respectively. PSF/EO films with 50% and 20% PSF are referred to in the following plots as 50/50 and 20/80, respectively.

RESULTS AND DISCUSSION

Figure A.1 shows the recovered enthalpy data as a function of aging time at 170 °C for the three aforementioned films. As was the case with layered PSF/OBC films discussed in Chapter 6, the slopes of the best-fit lines for the bulk and multilayered films are similar. Figure A.2 shows the combined data for PSF/EO, PSF/OBC, and bulk PSF films aged at 170 °C. The data for PSF/EO, PSF/OBC, and bulk PSF films are reasonably well-aligned (i.e., the slope of the ΔH vs log t_a data and the absolute ΔH values at any particular aging time are reasonably similar among all films). This suggests two things: (1) the choice of confining material (EO or OBC) does not significantly influence the aging behavior when the confinement for the PSF layers is provided by a relatively "soft" rubbery material, and (2) the aging rate in these multilayered films is independent of layer thickness and similar to bulk.

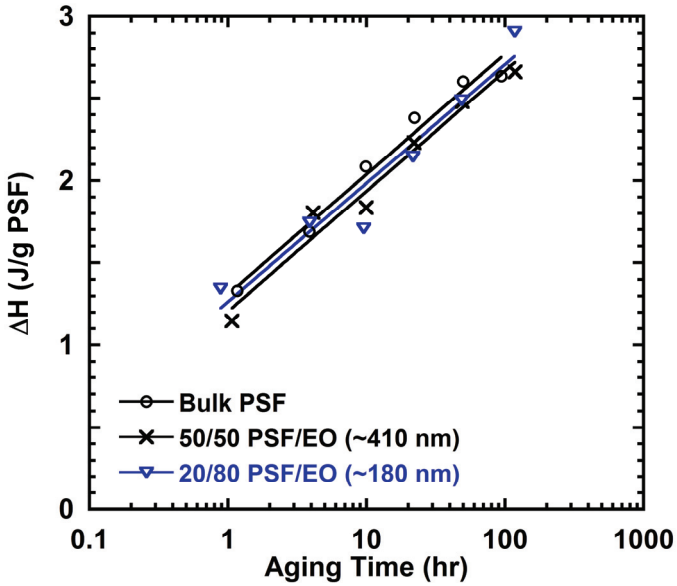

Figure A.1: Recovered enthalpy (ΔH) data as a function of aging time for bulk PSF and PSF/EO films aged at 170 °C. Results normalized by the mass fraction of PSF in the samples. PSF layer thickness is given in parentheses.

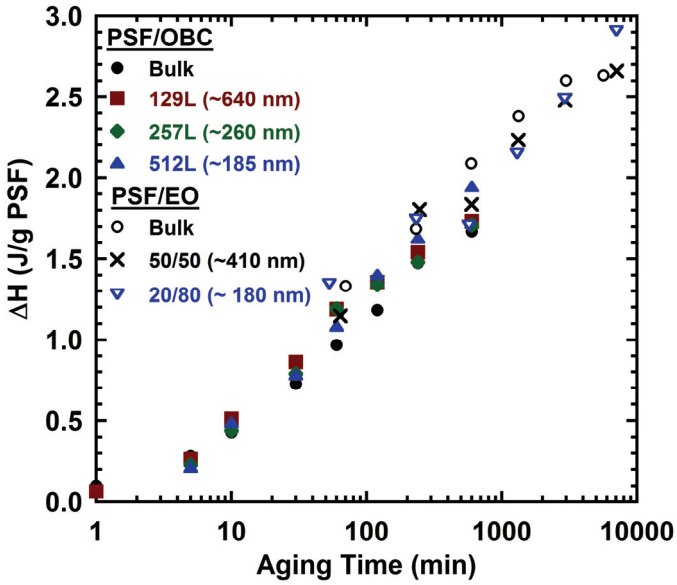

Figure A.2: Recovered enthalpy data as a function of aging time for bulk PSF, PSF/EO, and PSF/OBC films aged at 170 °C. ΔH values were normalized by the mass of PSF in the samples. Average PSF layer thickness is given in parentheses.

Figure A.3 shows a plot of the aging rates at 170 °C as a function of PSF layer thickness for PSF/EO, PSF/OBC, and bulk PSF films. The bulk samples produced during the PSF/EO and PSF/OBC extrusion runs had aging rates of 0.73 and 0.75, respectively. The aging rates for all films except for the 513-layer PSF/OBC sample are very similar to the bulk aging rates. The similarity of the aging rates for nearly all of the PSF/EO, PSF/OBC, and bulk PSF films led us to conclude that the effect of layer thickness on aging in multilayered PSF is minimal. This behavior differs from that observed in free-standing thin PSF films studied using gas permeability measurements, in which aging is accelerated relative to bulk and dependent on film thickness.

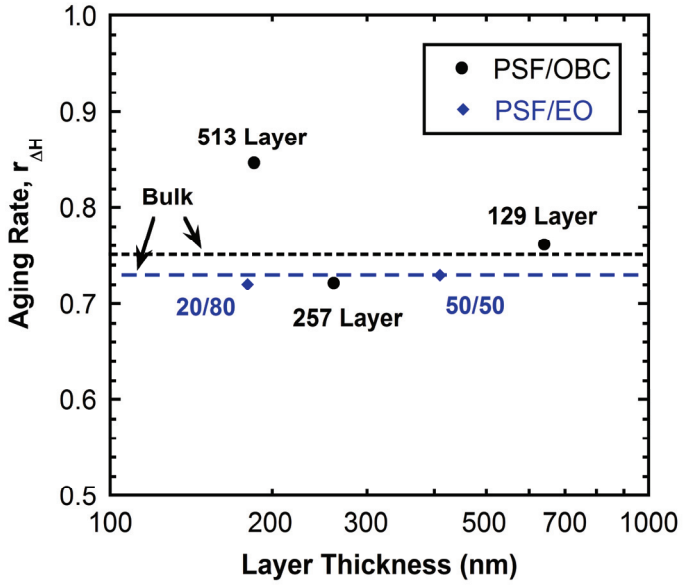

Figure A.3: Aging rates as a function of layer thickness for bulk PSF, PSF/EO, and PSF/OBC films aged at 170 °C. The definition of the aging rate ($r_{\Delta H}$) is given by Eq. 6.4 in Chapter 6. Bulk PSF aging rates are shown as dashed lines.

REFERENCES

1. Petrie SEB. Thermal behavior of annealed organic glasses. *Journal of Polymer Science Part A-2: Polymer Physics* **1972**, 10(7): 1255–1272.

2. Hutchinson JM. Physical aging of polymers. *Progress in Polymer Science* **1995**, 20(4): 703–760.

3. Koh YP, Simon SL. Structural relaxation of stacked ultrathin polystyrene films. *Journal of Polymer Science Part B: Polymer Physics* **2008**, 46(24): 2741–2753.

4. Langhe DS, Murphy TM, Shaver A, LaPorte C, Freeman BD, Paul DR, Baer E. Structural relaxation of polystyrene in nanolayer confinement. *Polymer* **2012**, 53(9): 1925–1931.

Appendix B: Additional Information on PS Thin Film Studies

SUMMARY

Aging studies on polystyrene (PS) films using gas permeability tracking at 35 °C were performed, and the results of these studies are presented in Chapter 7. Although PS is commonly used in other types of aging studies (e.g., studies using ellipsometry, fluorescence spectroscopy, or DSC to study substrate-supported films), its aging behavior as assessed by gas permeability measurements had never before been reported. Many difficulties were encountered during the initial phases of the work described in Chapter 7. This appendix describes some of those difficulties and how they were overcome, and it is intended to serve as a guide for future investigators who may conduct studies of aging in thin PS films.

INITIAL ATTEMPTS TO STUDY THIN PS FILMS

Styron 685D was used in our early attempts to prepare thin PS films. Styron 685D (M_w = 300,000, M_w/M_n = 2.3) is a commercial grade of PS that was used by our colleagues in DSC studies[1] that were performed on layered polystyrene/polycarbonate (PS/PC) films. Initially, we attempted to prepare thin, freestanding PS films with no coating layer. A variety of annealing times (ranging from 5-40 minutes) and temperatures (ranging from 110 to 150 °C) were tested to see if conditions that produced usable films for aging studies could be identified, but no such conditions could be found. Despite our efforts, we were unable to prepare any uncoated thin films that could be used in gas permeation studies.

The frequent failures were likely due in no small part to the brittleness of PS. According to the manufacturer datasheets, the elongation at break for Styron 685D PS is 3%, whereas for Solvay P-3500 NT LCD polysulfone (the grade of polysulfone (PSF)

used in previous thin film aging studies[2,3]), a value of 50-100% is reported. The Izod impact strength of PS is also reported as being roughly 3 times lower than that of PSF (21 J/m for PS, 69 J/m for PSF). PSF is clearly a much tougher and less brittle polymer than PS, so it is perhaps not surprising that PS films failed before sufficient data could be collected, even though permeability measurements on uncoated thin films of PSF have been made in the past.[3,4] PS also has a tendency to craze quite easily, and evidence of this could be seen in thick films that formed semi-opaque white regions when flexed or handled improperly.

DEVELOPMENT OF PDMS COATING PROCEDURE FOR PS FILMS

Identification of an appropriate solvent

One of the most commonly encountered difficulties in aging studies of thin films using gas permeability measurement is the existence of pinhole defects in the film. Such defects obscure the true permeability of the material and cause the measured selectivity to be much lower than it would be in the absence of such defects. Additionally, the thin films are fragile, and preparing a sample for permeation testing requires the film to be handled and manipulated without tearing or otherwise ruining it. The relatively long duration of aging studies (coupled with a practical limit on the number of permeation cells) also requires inserting and removing the film sample from the permeation cell many times. Thus, sample failure is an unfortunate but frequent occurrence, regardless of whether or not the film originally has any defects. Recent studies of aging and CO_2 plasticization in thin films have used a polydimethylsiloxane (PDMS) coating technique to mitigate the effects of pinhole defects and increase success rates in thin film studies.[2,5–7] The PDMS coating layer, which is typically on the order of 3-5 μm, also provides

mechanical support for the delicate glassy films. It was highly desirable to use PDMS on thin PS films, as it could significantly increase the probability that a given film would be suitable for aging studies via gas permeation techniques. However, the aforementioned studies used solutions of PDMS in cyclohexane to coat films of polysulfone and various polyimides. Cyclohexane, though a rather weak solvent for PS, could still potentially affect the PS thin films in a detrimental way during the PDMS coating step by changing the film thickness, causing non-uniformity of the PS-PDMS interface, or causing stress cracking or crazing. In order to avoid these problems, it was necessary to find a different solvent for the PDMS solutions used to coat PS films.

After initial assessment of the solubility of PS and PDMS in various solvents, iso-octane was identified as the best candidate for our purposes. To verify that the iso-octane would not change the underlying PS layer during the spinning of the PDMS layer, a test was performed using pure iso-octane and the same spinning procedure used for PDMS coating. Iso-octane was deposited onto the PS-coated wafer from a sterile dropper and then spun for 60 s at 1000 rpm. The PS thickness was measured at three locations on three separate wafers both before and after the iso-octane rinse. Figure B.1 shows the results of the test, which indicated that the thickness of the PS layer was essentially unchanged (within 1% of the pre-rinse thickness) at each measurement location. Therefore, iso-octane was used in preparing the PDMS solutions used in this work.

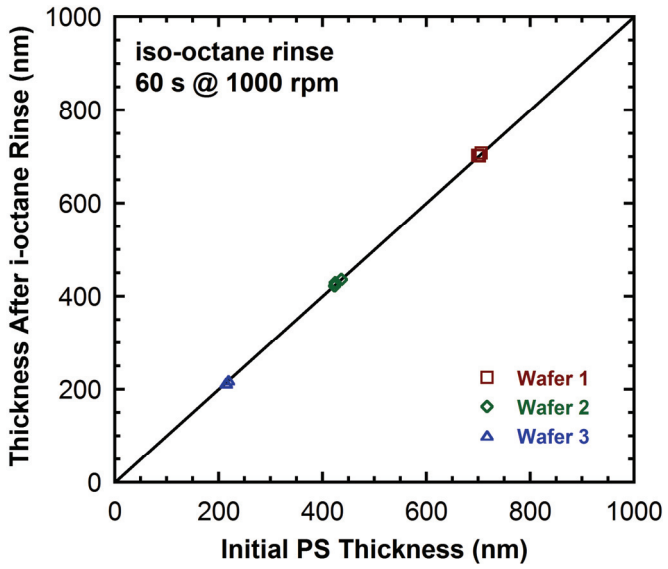

Figure B.1: Effect of pure iso-octane spin-coating procedure on PS thickness for films supported on three different silicon wafers. Three measurements were made per wafer. The solid line is the parity line.

Making PDMS solutions

Solutions of PDMS in iso-octane (12 wt. % PDMS) were prepared by mixing Wacker Dehesive 944 with iso-octane and then adding an appropriate amount of the crosslinker and catalyst solutions supplied with Dehesive 944. Typically, the solutions were prepared in 20 mL scintillation vials. A magnetic stir bar was used to mix the solution of iso-octane and Dehesive 944 in the vial. Prior to addition of catalyst and crosslinker, the vial was placed in an ice bath (to minimize the rate of unwanted crosslinking). First, one drop of crosslinker solution was added to the vial and slowly mixed until homogenous. Next, one drop of catalyst solution was added and mixed in similarly. After roughly 10-20 minutes of mixing in an ice bath, the solution was removed from the bath and placed in freezer until needed.

PDMS coating of thin PS films

The PDMS coating/crosslinking procedure that was eventually used successfully in the studies described in Chapter 7 differs from the original procedure. A brief description of the original procedure, the reasons why that procedure was changed, and the results of aging studies using the original procedure are discussed in more detail in the following sections. The procedure described below was used to prepare the coated PS films discussed in Chapter 7, and it is the procedure that would be recommended as a starting point for anyone who desired to perform additional gas permeation aging studies of thin PS films.

After measuring the thickness of the spin-coated PS (*via* ellipsometry), a layer of poly(dimethylsiloxane) (PDMS) was spun atop the previously-deposited glassy layer from a ~12% solution of PDMS in iso-octane (spin time = 1 minute, spin speed = 1000 rpm). After coating with PDMS, the wafer-supported two-layer film was placed under vacuum at ambient temperature for 10-15 minutes to facilitate the removal of air bubbles and residual solvent from the PDMS layer and to ensure good contact between the PDMS and PS layers. Next, the PDMS was crosslinked at 100 °C for approximately 35 minutes in a temperature-controlled oven. The thickness of the crosslinked PDMS layer was measured using a Dektak 6M stylus profilometer. The PDMS layers produced by this coating and crosslinking procedure were ~5 μm in thickness. Lifting and storage of the films is described in Chapter 3 (section 3.3.2.4).

ORIGINAL PROCEDURE AND RESULTS

Original PDMS coating procedure

The original procedure used to apply the PDMS coating differs from the one depicted above. Originally, the PDMS solution was spun onto the wafer as described above. Next, the wafer was placed on a hotplate that was set at 115 °C for 15 minutes. This procedure was adopted based on its use in previous studies of PSF and Matrimid films that were coated with Dehesive 940A PDMS (rather than Dehesive 944, which was used after production of 940A was discontinued). While PSF and Matrimid have T_gs that are well above the crosslinking temperature of 115 °C, this temperature is above the T_g of PS. For this reason (and also because of frequent sample failure), a new coating procedure was developed. This new methodology involved placing the freshly coated PS films under vacuum (prior to crosslinking) to remove any air bubbles from the PDMS layer, and the crosslinking step was performed in an oven at 100 °C (below the PS T_g) for a longer period of time (30-40 minutes). Additionally, the films were stored under vacuum (rather than at ambient conditions) for at least one day prior to beginning an aging study. The following section presents some of the data that was gathered when using the original PDMS coating procedure.

Unexpected Results

Even with a PDMS coating, we found that many of the films failed during permeation testing. Typically, film failure was evident upon beginning the first permeation test (i.e., the rate of pressure increase in the downstream side of the permeation cell was far too high), and no further tests were performed using these films. However, other film samples appeared to fail at around 100-300 hr of aging time. In

aging experiments, sample failure typically becomes evident when the selectivity begins to decrease sharply, indicating that the glassy layer is no longer behaving as an effectively defect-free film. Typically, the permeability would also begin to increase rapidly due to the selectivity-destroying defects in the film. In some of our experiments, however, we observed a decrease in O_2/N_2 selectivity that was accompanied by a simultaneous decrease in O_2 and N_2 permeability. This type of behavior, which was not expected, is illustrated by the data shown in Figure B.2.

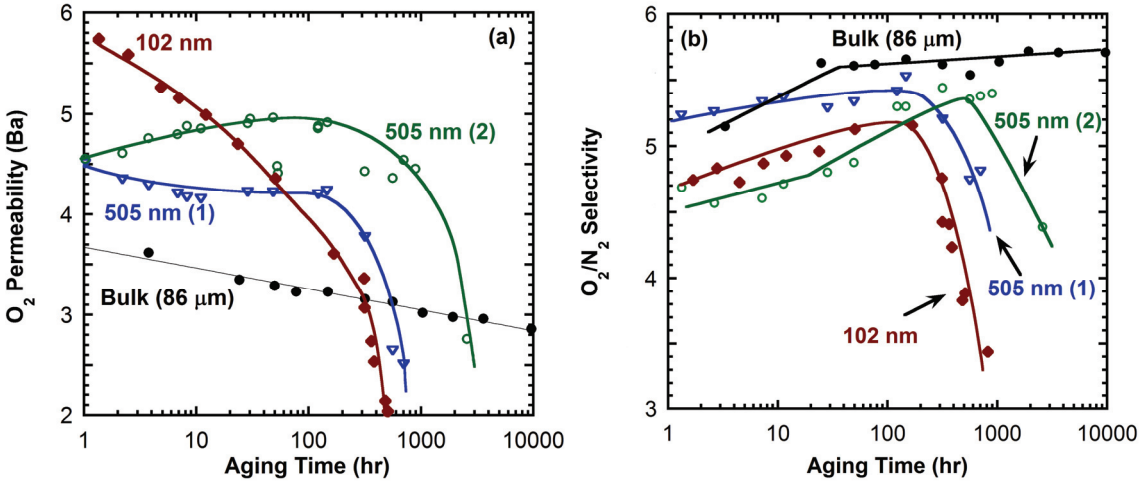

Figure B.2: (a) O_2 permeability data for thin films of Styron 685D coated using original PDMS coating procedure. (b) O_2/N_2 selectivity data for the same films. Simultaneous decrease in both permeability and selectivity was not expected.

These results are counterintuitive and not easily explained. One possible explanation involves the effective thickening of the PDMS layer with time. This could happen *via* intrusion of PDMS into the permeation area or extrusion of PDMS into the pores of the 60 μm thick Anopore disc (this is more likely to occur if any unreacted or oligomeric material is still present in the PDMS layer). An increase in the PDMS layer thickness

increases the mass transfer resistance of the composite film. Because this effective thickness change is not accounted for in the permeability calculations, the result is a decrease in the calculated PS permeability for both O_2 and N_2. Additionally, this thickness change would have a greater effect on the calculated O_2 permeability than it does on N_2 permeability, thus resulting in a decreased O_2/N_2 selectivity. The equations below provide what may be a clearer explanation of how an unexpected thickness change would affect the calculated PS permeability.

$$P_{i,calc}^{PS} = \ell_{measured}^{PS}\left[\left(\frac{N_i}{\Delta p}\right)_{measured}^{-1} - \frac{\ell_{nominal}^{PDMS}}{P_i^{PDMS}}\right]^{-1} \tag{B.1}$$

$$P_{i,calc}^{PS} = \left[\frac{1}{P_{i,actual}^{PS}} + \frac{(\ell_{actual}^{PDMS} - \ell_{nominal}^{PDMS}) / \ell_{measured}^{PS}}{P_i^{PDMS}}\right]^{-1} \tag{B.2}$$

As seen in Equation B.1, the measured permeance of gas *i* ($N_i/\Delta p$), which depends on the actual thickness and permeability of the composite films, is adjusted by a term that depends on the PDMS permeability and the nominal value of the PDMS thickness in order to calculate the permeability of the PS layer. Assuming that the PS layer does not change in thickness and that the PDMS permeability is constant, the calculated PS permeability will be lower than the "actual" value when the PDMS thickness change is unaccounted for. Equation B.2 shows the Equation B.1 recast in terms of the "actual" PS permeability. When the actual and nominal PDMS thicknesses are identical (or very similar), the calculated and "actual" PS permeability values will be identical (or nearly so, for small differences in nominal and actual PDMS thickness). For example, consider a 500 nm PS film coated with a PDMS layer that has a nominal thickness of 5 μm. Assuming that the "actual" O_2 and N_2 permeabilities for the PS layer are 4 Ba and 0.75 Ba, respectively, the "actual" O_2/N_2 selectivity would be 5.3 (these values are similar to

what was measured at ~ 100 hr of aging time for the film labeled "505 nm (1)" in Figure B.2). If, however, the PDMS layer began thickening over time such that the effective PDMS thickness became 35 μm, the calculated O_2 and N_2 permeabilities for the PS layer would be 3.1 Ba and 0.67 Ba, respectively, with a calculated selectivity of 4.6. These values are similar to the interpolated values for the film labeled '505 nm (1)" in Figure B.2 at an aging time of roughly 400 hr. Unexpected changes in the PDMS thickness would have a greater effect on the calculated values for thinner films (i.e., the 102 nm film), which is consistent with the data shown in Figure B.2. Whether or not this mechanism was truly the cause of our unexpected results has not been determined, but it is one of the few explanations that make sense physically and mathematically. Because of these unexpected results and their possible causes (coupled with the frequent film failures), we chose to modify the crosslinking procedure and began to explore different grades of PS for our study.

CHOOSING A NEW GRADE OF PS

One proposed remedy for frequent film failures was to prepare films using a grade of PS with a higher molecular weight than that of Styron 685D. Three different grades of PS were obtained from Pressure Chemical. The grades obtained are shown in the table below.

Table B.1: High molecular weight polystyrene standards obtained from Pressure Chemical

Grade	$\overline{M_w}$	$\overline{M_w} / \overline{M_n}$
PS 61120 (PS650k)	650,000	1.06
PS 80323 (PS900k)	900,000	1.1
PS 61111 (PS2000k)	2,000,000	1.3

Spin-coating experiments using the various grades revealed that PS900k (M_w = 900,000, M_w/M_n = 1.1) produced films that had the fewest visible defects and appeared most uniform. Thus, it was chosen for use in the studies described in Chapter 7. Use of this grade of PS, in conjunction with the modified PDMS coating procedure, led to better success rates in preparing usable films for aging experiments. However, film failure was still a rather frequent occurrence.

ADDITIONAL INFORMATION ABOUT FILM PREPARATION AND MEASUREMENT

Although Chapter 3 describes the process of producing thin films and preparing them for measurement, the following section provides a more detailed discussion of certain aspects of film preparation and permeation testing that could be useful for future researchers.

Preparation of thin PS films

Thin films of PS were prepared by spin casting from toluene solutions onto 5-inch silicon wafers. The spin time was 60 s, and the spinning rates were between 500 and 1000 rpm. Although it was desirable to produce films of different thickness by varying

the solution concentration and using a constant spin rate, as has been done in previous thin film aging studies that used gas permeation techniques, sample failure was so frequent that new preparation methodologies were explored until finding something that worked. Prior to applying the PDMS coating layer, the thickness of the PS films was measured using a J.A. Woollam M-2000 spectroscopic ellipsometer (see Chapter 3 for more information). Figure B.3 shows the PS film thickness as a function of solution concentration for a spin speed of 1000 rpm.

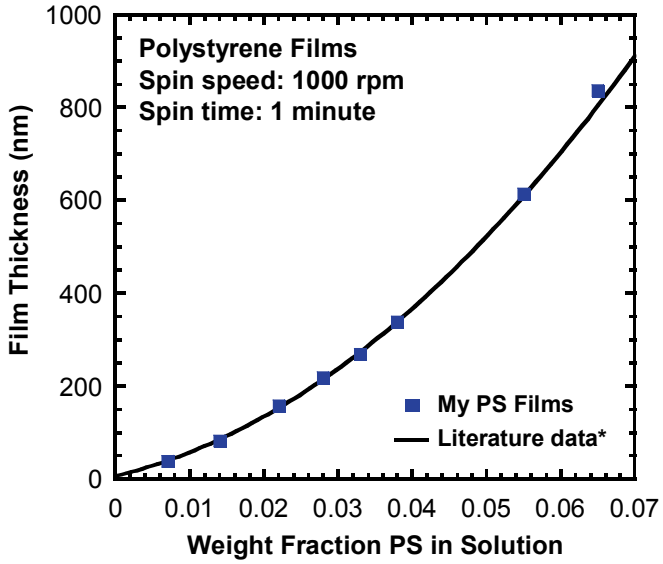

Figure B.3: PS film thickness as a function of solution concentration for a spin speed of 1000 rpm and a spin speed of 1 minute. Literature data taken from Hall et al.[8]

After coating with PDMS and crosslinking, the PS films were removed from the wafer, collected, and stored as described in Chapter 3. To begin an aging experiment, the film was annealed at 120 °C (~15 °C above the PS Tg) for 20 minutes. Because the aging behavior depends on the process of glass formation, it is often useful to know the cooling rate experienced by a film as it passes through T_g upon removal from the

annealing oven. Using the methodology outlined by Gray et al.,[9] the cooling rate through T_g experienced by an 800 nm PS film coated with a 5 μm layer of PDMS (when it is removed from the annealing oven) is estimated to be on the order of 5000 °C/min.

Permeation testing of thin PS films

One of the first steps in permeation tests that use a constant-volume, variable-pressure permeation cell involves pulling vacuum on a sample to fully degas it (and to allow the system tubing to be evacuated) before introducing the test gas on the upstream side of the sample. Because of the way thin films are mounted for permeation testing (see Figure 3.3), it is imperative that the downstream (DS) side of the sample remains at a lower pressure than the upstream (US) side (since there is no support for the fragile film on the upstream side, whereas the Anopore disc supports the downstream side of the film). Concerns about film breakage led us to modify the procedure of sample degassing. Figure B.4 shows the valve manifold for the permeation cells used in this work (see Figure 3.4 for complete permeation cell diagram).

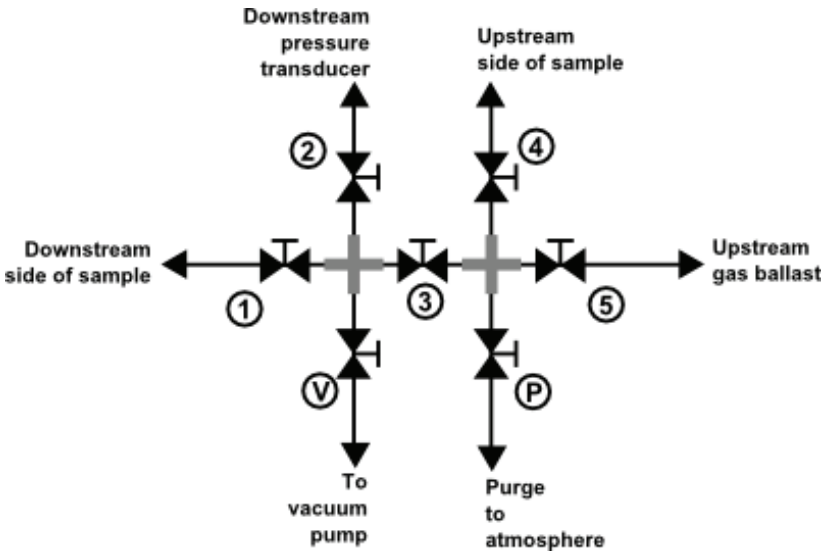

Figure B.4: Permeation cell valve manifold with labels.

The following steps outline the recommended procedure for degassing a thin PS film that has just been placed into the permeation cell, assuming that the entire system is at atmospheric pressure and that all valves are closed. The valve numbers refer to Figure B.4 (note: the pressure transducers used in this work were MKS Baratron 627 models that have a reading range of 0-10 torr).

Sample degassing

1. Make sure valve 3 is closed (to isolate the US side of the system from the DS)
2. Open valves V, 1, and 2 (to evacuate the downstream side of the sample and allow the DS pressure to be measured)
3. Continue pulling vacuum until the DS pressure is no longer changing (typically, the DS pressure will be ~0.1 torr, but this depends on the system volume and the vacuum pump)
4. Close valve 1

5. Make sure that valve P is closed, and open valves 4 and 5 (US side should still be at atmospheric pressure, and no US pressure change should be detectable unless the film itself is broken or not well-sealed in the sample holder)
6. Open valve 3 (to allow the US side to be slowly evacuated – having valve 5 open results in a slower decrease in US pressure, due to the large ballast volume)
7. Once the pressure transducer reads ~10 torr, close valve 5 (to allow for quicker evacuation)
8. Allow the pressure to decrease until the transducer reads ~1 torr, and then close valve 4 (at this point, the pressure on the DS side of the sample should still be ~0.1 torr, while the US side of the sample is now at ~1 torr)
9. Allow the pressure reading to continue to decrease for a few seconds and then slowly open valve 1 (the pressure reading will decrease more sharply upon opening valve 1, since that section of tubing is a lower pressure)
10. Wait a few more seconds, and then open valve 4 *only slightly* (the pressure reading will begin to increase, since the US side of the sample is at a higher pressure)
11. Once the pressure begins decreasing again (typically within 2-5 seconds), slowly open valve 4 until it is fully open (at this point, valves V, 1, 2, 3, and 4 will all be fully open, and the entire system except the ballast volume will be undergoing evacuation)
12. Allow the system to be evacuated completely until the pressure reading no longer changes

13. Once the entire system (except the ballast) is at its minimum pressure, allow another 20-30 minutes for full degassing of the sample (Note: for a thick film, 20-30 minutes may not be sufficient. Additionally, if one is interested in characterizing the transient permeation behavior rather than simply measuring the steady-state permeability of a thick film, it may be necessary to pull vacuum on the sample overnight, i.e., for 8 or more hours)

Permeation testing procedure

The permeation test pressure used for the thin PS films was also changed. The upstream pressure was set at ~20 psia for thin films (to decrease the likelihood of film failure) and ~30 psia for the bulk films (to ensure a readily detectable gas flux through the film, because these films are considerably thicker). This small difference in upstream gas pressure, which is accounted for in permeability calculations, is not expected to produce any appreciable changes in the aging behavior for low-sorbing gases like O_2 or N_2.

To begin a permeation test after degassing, the upstream ballast and test gas supply line must first be evacuated before introducing the test gas. The following steps outline this procedure in detail.

1. Close valves 4, 2, and 1 (valve V and valve 3 should still be open, but valve 5 will still be closed)
2. Ensure that the upstream ballast is connected to the test gas supply line but that the supply line is NOT pressurized (i.e., shut off the regulator connected to the gas cylinder or close the valve on the gas cylinder, and depressurize the gas supply line if necessary)

3. Open valve 5 and open the valve that allows gas from the unpressurized supply line into the ballast volume
4. Allow the US ballast volume and gas supply line to be evacuated until the US pressure gauge reads essentially zero pressure (~2-3 minutes).
5. Close valve 3 and close the valve that connects the gas supply line to the US ballast volume (leave valve V open)
6. Open the valve on the gas cylinder (if closed) and set the gas cylinder regulator to an appropriate pressure (typically ~100-120 psig)
7. Open the gas ballast supply valve and allow gas into the US ballast (valves 3 and 4 should still be closed)
8. Once the US pressure gauge reads ~60-80 psia, close US ballast supply valve, and then open valve P to purge the gas to atmospheric pressure
9. Repeat steps 7-8 two or three times and then close valve P.
10. Introduce gas into the US ballast until the pressure is approximately at the desired test pressure and close the US ballast supply valve.
11. Close valve V and open valve 2, allowing the pressure reading on the DS transducer to stabilize (~2-5 seconds)
12. Open valve 4 (to expose the US side of the sample to the test gas)
13. Open valve 1 (at this point, valves 1, 2, 4, and 5 will be open, and valves 3, P, and V will be closed)
14. Record the upstream pressure and begin collecting data

CONCLUSIONS

The procedures developed for producing PDMS-coated PS films for aging tests *via* gas permeability tracking have been described in detail. This purpose of this appendix was to describe some of the difficulties associated with this work and provide useful information to any future investigators who may wish to repeat the studies described in Chapter 7 or perform similar studies. Additionally, the section detailing the process of degassing a film and beginning a permeation test could be useful to anyone who wishes to learn how to measure gas permeability using a constant-volume, variable-pressure permeation cell.

REFERENCES

1. Langhe DS, Murphy TM, Shaver A, LaPorte C, Freeman BD, Paul DR, Baer E. Structural relaxation of polystyrene in nanolayer confinement. *Polymer* **2012**, 53(9): 1925–1931.

2. Rowe BW, Freeman BD, Paul DR. Physical aging of ultrathin glassy polymer films tracked by gas permeability. *Polymer* **2009**, 50(23): 5565–5575.

3. Huang Y, Paul DR. Physical aging of thin glassy polymer films monitored by gas permeability. *Polymer* **2004**, 45(25): 8377–8393.

4. Huang Y, Paul DR. Experimental methods for tracking physical aging of thin glassy polymer films by gas permeation. *Journal of Membrane Science* **2004**, 244(1-2): 167–178.

5. Horn NR, Paul DR. Carbon dioxide plasticization and conditioning effects in thick vs. thin glassy polymer films. *Polymer* **2011**, 52(7): 1619–1627.

6. Cui L, Qiu W, Paul DR, Koros WJ. Responses of 6FDA-based polyimide thin membranes to CO2 exposure and physical aging as monitored by gas permeability. *Polymer* **2011**, 52(24): 5528–5537.

7. Cui L, Qiu W, Paul DR, Koros WJ. Physical aging of 6FDA-based polyimide membranes monitored by gas permeability. *Polymer* **2011**, 52(15): 3374–3380.

8. Hall DB, Underhill P, Torkelson JM. Spin coating of thin and ultrathin polymer films. *Polymer Engineering & Science* **1998**, 38(12): 2039–2045.

9. Gray LAG, Yoon SW, Pahner WA, Davidheiser JE, Roth CB. Importance of Quench Conditions on the Subsequent Physical Aging Rate of Glassy Polymer Films. *Macromolecules* **2012**, 45(3): 1701–1709.

Bibliography

Algers J, Suzuki R, Ohdaira T, Maurer FHJ. Characterization of free volume and density gradients of polystyrene surfaces by low-energy positron lifetime measurements. *Polymer* **2004**, 45(13): 4533–4539.

Amerongen GJ van. The Permeability of Different Rubbers to Gases and Its Relation to Diffusivity and Solubility. *Journal of Applied Physics* **1946**, 17(11): 972.

Andreozzi L, Faetti M, Giordano M, Palazzuoli D. A calorimetric study of structural relaxation in the glassy state of a liquid-crystal polymer. *Philosophical Magazine B Physics of Condensed Matter Statistical Mechanics, Electronic, Optical and Magnetic Properties* **2002**, 82(4): 397–407.

Andreozzi L, Faetti M, Giordano M, Palazzuoli D. Physical Aging in Side-Chain Liquid Crystal Polymers: A DSC Investigation of the Enthalpy Relaxation. *Macromolecules* **2002**, 35(24): 9049–9056.

Baker EA, Rittigstein P, Torkelson JM, Roth CB. Streamlined ellipsometry procedure for characterizing physical aging rates of thin polymer films. *Journal of Polymer Science Part B: Polymer Physics* **2009**, 47(24): 2509–2519.

Baker RW. Future directions of membrane gas separation technology. *Ind. Eng. Chem. Res* **2002**, 41(6): 1393–1411.

Berens AR, Hodge IM. Effects of annealing and prior history on enthalpy relaxation in glassy polymers. 1. Experimental study on poly(vinyl chloride). *Macromolecules* **1982**, 15(3): 756–761.

Bernardo P, Drioli E, Golemme G. Membrane Gas Separation: A Review/State of the Art. *Industrial & Engineering Chemistry Research* **2009**, 48(10): 4638–4663.

Bero CA, Plazek DJ. Volume-dependent rate processes in an epoxy resin. *Journal of Polymer Science Part B: Polymer Physics* **1991**, 29(1): 39–47.

Boersma A, Cangialosi D, Picken SJ. Mobility and solubility of antioxidants and oxygen in glassy polymers. Part II. Influence of physical aging on antioxidant and oxygen mobility. *Polymer Degradation and Stability* **2003**, 79(3): 427–438.

Boucher VM, Cangialosi D, Alegría A, Colmenero J. Enthalpy Recovery of PMMA/Silica Nanocomposites. *Macromolecules* **2010**, 43(18): 7594–7603.

Boucher VM, Cangialosi D, Alegría A, Colmenero J. Enthalpy Recovery in Nanometer to Micrometer Thick Polystyrene Films. *Macromolecules* **2012**, 45(12): 5296–5306.

Boucher VM, Cangialosi D, Alegría A, Colmenero J, González-Irun J, Liz-Marzan LM. Accelerated physical aging in PMMA/silica nanocomposites. *Soft Matter* **2010**, 6(14): 3306.

Boucher VM, Cangialosi D, Alegría A, Colmenero J, Pastoriza-Santos I, Liz-Marzan LM. Physical aging of polystyrene/gold nanocomposites and its relation to the calorimetric Tg depression. *Soft Matter* **2011**, 7(7): 3607.

Cangialosi D, Boucher VM, Alegría A, Colmenero J. Enhanced physical aging of polymer nanocomposites: The key role of the area to volume ratio. *Polymer* **2012**, 53(6): 1362–1372.

Cangialosi D, Wübbenhorst M, Groenewold J, Mendes E, Picken SJ. Diffusion mechanism for physical aging of polycarbonate far below the glass transition temperature studied by means of dielectric spectroscopy. *Journal of Non-Crystalline Solids* **2005**, 351(33-36): 2605–2610.

Cangialosi D, Wübbenhorst M, Groenewold J, Mendes E, Schut H, Veen A van, Picken SJ. Physical aging of polycarbonate far below the glass transition temperature: Evidence for the diffusion mechanism. *Physical Review B* **2004**, 70 224213.

Cangialosi D, Wübbenhorst M, Schut H, Veen A van, Picken S. Dynamics of polycarbonate far below the glass transition temperature: A positron annihilation lifetime study. *Physical Review B* **2004**, 69(13): 1–9.

Cao H, Yuan J-P, Zhang R, Sundar C., Jean Y., Suzuki R, Ohdaira T, Nielsen B. Free volumes and holes near the polymer surface studied by positron annihilation. *Applied Surface Science* **1999**, 149(1-4): 116–124.

Cui L, Qiu W, Paul DR, Koros WJ. Physical aging of 6FDA-based polyimide membranes monitored by gas permeability. *Polymer* **2011**, 52(15): 3374–3380.

Cui L, Qiu W, Paul DR, Koros WJ. Responses of 6FDA-based polyimide thin membranes to CO2 exposure and physical aging as monitored by gas permeability. *Polymer* **2011**, 52(24): 5528–5537.

Debolt MA, Easteal AJ, Macedo PB, Moynihan CT. Analysis of Structural Relaxation in Glass Using Rate Heating Data. *Journal of the American Ceramic Society* **1976**, 59(1-2): 16–21.

Dorkenoo KD, Pfromm PH. Experimental evidence and theoretical analysis of physical aging in thin and thick amorphous glassy polymer films. *Journal of Polymer Science Part B: Polymer Physics* **1999**, 37(16): 2239–2251.

Dorkenoo KD, Pfromm PH. Accelerated Physical Aging of Thin Poly[1-(trimethylsilyl)-1-propyne] Films. *Macromolecules* **2000**, 33(10): 3747–3751.

Echeverria I, Su P-C, Simon SL, Plazek DJ. Physical aging of a polyetherimide: Creep and DSC measurements. *Journal of Polymer Science Part B: Polymer Physics* **1995**, 33(17): 2457–2468.

Efremov MY, Warren JT, Olson EA, Zhang M, Kwan AT, Allen LH. Thin-Film Differential Scanning Calorimetry: A New Probe for Assignment of the Glass Transition of Ultrathin Polymer Films. *Macromolecules* **2002**, 35(5): 1481–1483.

Ellison CJ, Kim SD, Hall DB, Torkelson JM. Confinement and processing effects on glass transition temperature and physical aging in ultrathin polymer films: novel fluorescence measurements. *The European Physical Journal E - Soft Matter* **2002**, 8(2): 155–66.

Ellison CJ, Torkelson JM. The distribution of glass-transition temperatures in nanoscopically confined glass formers. *Nature Materials* **2003**, 2(10): 695–700.

Flory AL, Ramanathan T, Brinson LC. Physical Aging of Single Wall Carbon Nanotube Polymer Nanocomposites: Effect of Functionalization of the Nanotube on the Enthalpy Relaxation. *Macromolecules* **2010**, 43(9): 4247–4252.

Forrest JA, Dalnoki-Veress K. The glass transition in thin polymer films. *Advances in Colloid and Interface Science* **2001**, 94(1-3): 167–195.

Forrest JA, Dalnoki-Veress K, Stevens JR, Dutcher JR. Effect of free surfaces on the glass transition temperature of thin polymer films. *Physical Review Letters* **1996**, 77(10): 2002–2005.

Freeman BD. Basis of Permeability/Selectivity Tradeoff Relations in Polymeric Gas Separation Membranes. *Macromolecules* **1999**, 32(2): 375–380.

Freeman BD, Pinnau I. Separation of gases using solubility-selective polymers. *Trends in Polymer Science* **1997**, 5(5): 167–173.

Fukao K, Miyamoto Y. Glass transitions and dynamics in thin polymer films: dielectric relaxation of thin films of polystyrene. *Physical Review E* **2000**, 61(2): 1743–54.

Fukao K, Sakamoto A. Aging phenomena in poly(methyl methacrylate) thin films: Memory and rejuvenation effects. *Physical Review E* **2005**, 71(4): 41803.

Gopalakrishnan TR, Beiner M. Effects of quenching and physical aging on the relaxation behavior of nanophase-separated side chain polymers. *Journal of Physics Conference Series* **2006**, 40 67–75.

Gray LAG, Yoon SW, Pahner WA, Davidheiser JE, Roth CB. Importance of Quench Conditions on the Subsequent Physical Aging Rate of Glassy Polymer Films. *Macromolecules* **2012**, 45(3): 1701–1709.

Greiner R, Schwarzl FR. Volume relaxation and physical aging of amorphous polymers I. Theory of volume relaxation after single temperature jumps. *Colloid & Polymer Science* **1989**, 267(1): 39–47.

Hall DB, Underhill P, Torkelson JM. Spin coating of thin and ultrathin polymer films. *Polymer Engineering & Science* **1998**, 38(12): 2039–2045.

Henis JMS, Tripodi MK. Composite hollow fiber membranes for gas separation: the resistance model approach. *Journal of Membrane Science* **1981**, 8(3): 233–246.

Hodge IM. Physical aging in polymer glasses. *Science* **1995**, 267(5206): 1945–1947.

Hodge IM. Effects of annealing and prior history on enthalpy relaxation in glassy polymers. 4. Comparison of five polymers. *Macromolecules* **1983**, 16(6): 898–902.

Hodge IM. Enthalpy relaxation and recovery in amorphous materials. *Journal of Non-Crystalline Solids* **1994**, 169(3): 211–266.

Hodge IM, Huvard GS. Effects of annealing and prior history on enthalpy relaxation in glassy polymers. 3. Experimental and modeling studies of polystyrene. *Macromolecules* **1983**, 16(3): 371–375.

Horn NR, Paul DR. Carbon dioxide plasticization and conditioning effects in thick vs. thin glassy polymer films. *Polymer* **2011**, 52(7): 1619–1627.

Huang Y. Physical Aging of Thin Glassy Polymer Films, The University of Texas at Austin, 2005.

Huang Y, Paul DR. Physical Aging of Thin Glassy Polymer Films Monitored by Optical Properties. *Macromolecules* **2006**, 39(4): 1554–1559.

Huang Y, Paul DR. Physical aging of thin glassy polymer films monitored by gas permeability. *Polymer* **2004**, 45(25): 8377–8393.

Huang Y, Paul DR. Effect of Temperature on Physical Aging of Thin Glassy Polymer Films. *Macromolecules* **2005**, 38(24): 10148–10154.

Huang Y, Paul DR. Effect of Film Thickness on the Gas-Permeation Characteristics of Glassy Polymer Membranes. *Industrial & Engineering Chemistry Research* **2007**, 46(8): 2342–2347.

Huang Y, Paul DR. Effect of molecular weight and temperature on physical aging of thin glassy poly(2,6-dimethyl-1,4-phenylene oxide) films. *Journal of Polymer Science Part B: Polymer Physics* **2007**, 45(12): 1390–1398.

Huang Y, Paul DR. Experimental methods for tracking physical aging of thin glassy polymer films by gas permeation. *Journal of Membrane Science* **2004**, 244(1-2): 167–178.

Huang Y, Wang X, Paul DR. Physical aging of thin glassy polymer films: Free volume interpretation. *Journal of Membrane Science* **2006**, 277(1-2): 219–229.

Hutchinson JM. Physical aging of polymers. *Progress in Polymer Science* **1995**, 20(4): 703–760.

Jackson CL, McKenna GB. The glass transition of organic liquids confined to small pores. *Journal of Non-Crystalline Solids* **1991**, 131-133 221–224.

Jarus D, Hiltner A, Baer E. Barrier properties of polypropylene/polyamide blends produced by microlayer coextrusion. *Polymer* **2002**, 43(8): 2401–2408.

Jin Y, Tai H, Hiltner A, Baer E, Shirk JS. New class of bioinspired lenses with a gradient refractive index. *Journal of Applied Polymer Science* **2007**, 103(3): 1834–1841.

Kawana S, Jones RAL. Effect of physical ageing in thin glassy polymer films. *The European Physical Journal E - Soft Matter* **2003**, 10(3): 223–30.

Kawana S, Jones RAL. Character of the glass transition in thin supported polymer films. *Physical Review E* **2001**, 63(2): 21501.

Kim JH, Jang J, Zin W-C. Estimation of the Thickness Dependence of the Glass Transition Temperature in Various Thin Polymer Films. *Langmuir* **2000**, 16(9): 4064–4067.

Kim JH, Koros WJ, Paul DR. Physical aging of thin 6FDA-based polyimide membranes containing carboxyl acid groups. Part II. Optical properties. *Polymer* **2006**, 47(9): 3104–3111.

Kim JH, Koros WJ, Paul DR. Physical aging of thin 6FDA-based polyimide membranes containing carboxyl acid groups. Part II. Optical properties. *Polymer* **2006**, 47(9): 3104–3111.

Koh YP, McKenna GB, Simon SL. Calorimetric glass transition temperature and absolute heat capacity of polystyrene ultrathin films. *Journal of Polymer Science Part B: Polymer Physics* **2006**, 44(24): 3518–3527.

Koh YP, Simon SL. Structural relaxation of stacked ultrathin polystyrene films. *Journal of Polymer Science Part B: Polymer Physics* **2008**, 46(24): 2741–2753.

Kovacs A. Transition vitreuse dans les polymeres amorphes. Etude phenomenologique. *Fortschritte Der Hochpolymeren-Forschung* **1963**, 394–507.

Kovacs AJ. The isothermal volume contraction of amorphous polymers. *J. Polymer Sci.* **1958**, 30(131-147):

Kuzmychov O, Koplin C, Jaeger R, Büchner H, Gopp U. Physical aging and the creep behavior of acrylic bone cements. *Journal of Biomedical Materials Research Part B: Applied Biomaterials* **2009**, 91B(2): 910–917.

Labahn D, Mix R, Schönhals A. Dielectric relaxation of ultrathin films of supported polysulfone. *Physical Review E* **2009**, 79(1): 1–9.

Laguna MF, Cerrada ML, Benavente R, Perez E, Quijada R. Permeation measurements in ethylene-1-hexene, ethylene-1-octene, and ethylene-1-dodecene copolymers synthesized with metallocene catalysts. *Journal of Polymer Science Part B: Polymer Physics* **2003**, 41(18): 2174–2184.

Langhe DS, Murphy TM, Shaver A, LaPorte C, Freeman BD, Paul DR, Baer E. Structural relaxation of polystyrene in nanolayer confinement. *Polymer* **2012**, 53(9): 1925–1931.

Lee C-H, Park J-J. The Properties of DSC and DMA for Epoxy Nano-and-Micro Mixture Composites. *Transactions on Electrical and Electronic Materials* **2010**, 11(2): 69–72.

Lee WM. Selection of barrier materials from molecular structure. *Polymer Engineering and Science* **1980**, 20(1): 65–69.

Li Q, Simon SL. Enthalpy recovery of polymeric glasses: is the theoretical limiting liquid line reached? *Polymer* **2006**, 47(13): 4781–4788.

Lu H, Nutt S. Restricted Relaxation in Polymer Nanocomposites near the Glass Transition. *Macromolecules* **2003**, 36(11): 4010–4016.

Mackey M, Hiltner A, Baer E, Flandin L, Wolak MA, Shirk JS. Enhanced breakdown strength of multilayered films fabricated by forced assembly microlayer coextrusion. *Journal of Physics D: Applied Physics* **2009**, 42(17): 175304.

Marshall AS, Petrie SEB. Rate-determining factors for enthalpy relaxation of glassy polymers. Molecular weight. *Journal of Applied Physics* **1975**, 46(10): 4223.

Matteucci S, Yampolskii Y, Freeman BD, Pinnau I. in:, Y. Yampolskii, I. Pinnau, B.D. Freeman (Eds.), Materials Science of Membranes for Gas and Vapor Separation, John Wiley & Sons, Ltd, 2006, pp. 1–49.

Mattsson J, Forrest JA, Borjesson L. Quantifying glass transition behavior in ultrathin free-standing polymer films. *Physical Review E* **2000**, 62(4): 5187.

McCaig M., Paul DR, Barlow JW. Effect of film thickness on the changes in gas permeability of a glassy polyarylate due to physical aging Part II. Mathematical model. *Polymer* **2000**, 41(2): 639–648.

McCaig MS, Paul DR. Effect of film thickness on the changes in gas permeability of a glassy polyarylate due to physical aging Part I. Experimental observations. *Polymer* **2000**, 41(2): 629–637.

McGonigle EA, Daly JH, Jenkins SD, Liggat JJ, Pethrick RA. Influence of physical aging on the molecular motion and structural relaxation in poly (ethylene terephthalate) and related polyesters. *Macromolecules* **2000**, 33(2): 480–489.

McHattie JS, Koros WJ, Paul DR. Gas transport properties of polysulphones: 1. Role of symmetry of methyl group placement on bisphenol rings. *Polymer* **1991**, 32(5): 840–850.

Merkel TC, Bondar VI, Nagai K, Freeman BD, Pinnau I. Gas sorption, diffusion, and permeation in poly(dimethylsiloxane). *Journal of Polymer Science Part B: Polymer Physics* **2000**, 38(3): 415–434.

Michaels AS, Bixler HJ. Flow of gases through polyethylene. *Journal of Polymer Science* **1961**, 50(154): 413–439.

Moynihan CT, Easteal AJ, DeBolt MA, Tucker J. Dependence of the Fictive Temperature of Glass on Cooling Rate. *Journal of the American Ceramic Society* **1976**, 59(1-2): 12–16.

Moynihan CT, Macedo PB, Montrose CJ, Gupta PK, DeBolt MA, Dill JF, Dom BE, Drake PW, Easteal AJ, Elterman PB, Moeller RP, Sasabe H, Wilder JA. Structural relaxation in vitreous materials. *Annals of the New York Academy of Sciences* **1976**, 279(The Glass Transition and the Nature of the Glassy State): 15–35.

Murphy TM, Langhe DS, Ponting M, Baer E, Freeman BD, Paul DR. Physical aging of layered glassy polymer films via gas permeability tracking. *Polymer* **2011**, 52(26): 6117–6125.

Narayanaswamy OS. A Model of Structural Relaxation in Glass. *Journal of the American Ceramic Society* **1971**, 54(10): 491–498.

Park JY, Paul DR. Correlation and prediction of gas permeability in glassy polymer membrane materials via a modified free volume based group contribution method. *Journal of Membrane Science* **1997**, 125(1): 23–39.

Petrie SEB. Thermal behavior of annealed organic glasses. *Journal of Polymer Science Part A-2: Polymer Physics* **1972**, 10(7): 1255–1272.

Pfromm PH, Koros WJ. Accelerated physical ageing of thin glassy polymer films: evidence from gas transport measurements. *Polymer* **1995**, 36(12): 2379–2387.

Pfromm PH, Koros WJ. Accelerated physical aging of thin glassy polymer films. *Polymeric Materials Science and Engineering* **1994**, 71 401–402.

Priestley RD. Evidence for the molecular-scale origin of the suppression of physical ageing in confined polymer: fluorescence and dielectric spectroscopy studies of polymer-silica nanocomposites. *Journal of Physics: Condensed Matter* **2007**, 19(20): 205120.

Priestley RD. Physical aging of confined glasses. *Soft Matter* **2009**, 5(5): 919–926.

Priestley RD, Broadbelt LJ, Torkelson JM. Physical Aging of Ultrathin Polymer Films above and below the Bulk Glass Transition Temperature: Effects of Attractive vs Neutral Polymer−Substrate Interactions Measured by Fluorescence. *Macromolecules* **2005**, 38(3): 654–657.

Priestley RD, Ellison CJ, Broadbelt LJ, Torkelson JM. Structural relaxation of polymer glasses at surfaces, interfaces, and in between. *Science* **2005**, 309(5733): 456–9.

Priestley RD, Mundra MK, Barnett NJ, Broadbelt LJ, Torkelson JM. Effects of nanoscale confinement and interfaces on the glass transition temperatures of a series of poly (n-methacrylate) films. *Australian Journal of Chemistry* **2007**, 60(10): 765–771.

Pye JE, Rohald KA, Baker EA, Roth CB. Physical Aging in Ultrathin Polystyrene Films: Evidence of a Gradient in Dynamics at the Free Surface and Its Connection to the Glass Transition Temperature Reductions. *Macromolecules* **2010**, 43(19): 8296–8303.

Rezac ME. Update on the Aging of a Thin Polycarbonate-Ceramic Composite Membrane. *Industrial & Engineering Chemistry Research* **1995**, 34(9): 3170–3172.

Rezac ME, Pfromm PH, Costello LM, Koros WJ. Aging of thin polyimide-ceramic and polycarbonate-ceramic composite membranes. *Industrial & Engineering Chemistry Research* **1993**, 32(9): 1921–1926.

Rittigstein P, Torkelson JM. Polymer-nanoparticle interfacial interactions in polymer nanocomposites: confinement effects on glass transition temperature and suppression of physical aging. *Journal of Polymer Science Part B: Polymer Physics* **2006**, 44(20): 2935–2943.

Robeson LM. Correlation of separation factor versus permeability for polymeric membranes. *Journal of Membrane Science* **1991**, 62(2): 165–185.

Robeson LM. The upper bound revisited. *Journal of Membrane Science* **2008**, 320(1-2): 390–400.

Robeson LM, Freeman BD, Paul DR, Rowe BW. An empirical correlation of gas permeability and permselectivity in polymers and its theoretical basis. *Journal of Membrane Science* **2009**, 341(1-2): 178–185.

Rowe BW, Freeman BD, Paul DR. Physical aging of ultrathin glassy polymer films tracked by gas permeability. *Polymer* **2009**, 50(23): 5565–5575.

Rowe BW, Freeman BD, Paul DR. Influence of previous history on physical aging in thin glassy polymer films as gas separation membranes. *Polymer* **2010**, 51(16): 3784–3792.

Rowe BW, Pas SJ, Hill AJ, Suzuki R, Freeman BD, Paul DR. A variable energy positron annihilation lifetime spectroscopy study of physical aging in thin glassy polymer films. *Polymer* **2009**, 50(25): 6149–6156.

Rowe BW, Robeson LM, Freeman BD, Paul DR. Influence of temperature on the upper bound: Theoretical considerations and comparison with experimental results. *Journal of Membrane Science* **2010**, 360(1-2): 58–69.

Royal JS, Torkelson JM. Monitoring the molecular scale effects of physical aging in polymer glasses with fluorescence probes. *Macromolecules* **1990**, 23(14): 3536–3538.

Royal JS, Torkelson JM. Photochromic and fluorescent probe studies in glassy polymer matrices. 5. Effects of physical aging on bisphenol A polycarbonate and poly(vinyl acetate) as sensed by a size distribution of photochromic probes. *Macromolecules* **1992**, 25(18): 4792–4796.

Royal JS, Torkelson JM. Physical aging effects on molecular-scale polymer relaxations monitored with mobility-sensitive fluorescent molecules. *Macromolecules* **1993**, 26(20): 5331–5335.

Royal JS, Victor JG, Torkelson JM. Photochromic and fluorescent probe studies in glassy polymer matrices. 4. Effects of physical aging on poly(methyl methacrylate) as sensed by a size distribution of photochromic probes. *Macromolecules* **1992**, 25(2): 729–734.

Schrenk W, Chisholm D, Cleereman K, Alfrey Jr. T. METHOD OF PREPARING MULTILAYER PLASTIC ARTICLES, U.S. Patent Number 3565985, 1971.

Schrenk W, Chisholm D, Cleereman K, Alfrey Jr. T. MULTILAYER IRIDESCENT PLASTIC ARTICLES, U.S. Patent Number 3576707, 1971.

Schrenk W, Chisholm D, Cleereman K, Alfrey Jr. T. MULTILAYER PLASTIC ARTICLES, U.S. Patent Number 3647612, 1972.

Schut JH. Microlayer films: New uses for hundreds of layers. *Plastics Technology* **2006**, 52(3): 54–57.

Sepúlveda A, Leon-Gutierrez E, Gonzalez-Silveira M, Rodríguez-Tinoco C, Clavaguera-Mora M, Rodríguez-Viejo J. Accelerated Aging in Ultrathin Films of a Molecular Glass Former. *Physical Review Letters* **2011**, 107(2): 1–4.

Serghei A, Huth H, Schick C, Kremer F. Glassy Dynamics in Thin Polymer Layers Having a Free Upper Interface. *Macromolecules* **2008**, 41(10): 3636–3639.

Simon SL. Enthalpy Recovery of Poly(ether imide): Experiment and Model Calculations Incorporating Thermal Gradients. *Macromolecules* **1997**, 30(14): 4056–4063.

Simon SL, Park J-Y, McKenna GB. Enthalpy recovery of a glass-forming liquid constrained in a nanoporous matrix: negative pressure effects. *The European Physical Journal E - Soft Matter* **2002**, 8(2): 209–16.

Simon SL, Sobieski JW, Plazek DJ. Volume and enthalpy recovery of polystyrene. *Polymer* **2001**, 42(6): 2555–2567.

Singer KD, Kazmierczak T, Lott J, Song H, Wu Y, Andrews J, Baer E, Hiltner A, Weder C. Melt-processed all-polymer distributed Bragg reflector laser. *Optics Express* **2008**, 16(14): 10358–10363.

Struik LCE. *Physical Aging in Amorphous Polymers and Other Materials*. Amsterdam, Elsevier, 1978.

Svoboda R, Pustková P, Málek J. Structural relaxation of polyvinyl acetate (PVAc). *Polymer* **2008**, 49(13-14): 3176–3185.

Tool AQ. RELATION BETWEEN INELASTIC DEFORMABILITY AND THERMAL EXPANSION OF GLASS IN ITS ANNEALING RANGE. *Journal of the American Ceramic Society* **1946**, 29(9): 240–253.

Tool AQ, Eicitlin CG. VARIATIONS CAUSED IN THE HEATING CURVES OF GLASS BY HEAT TREATMENT. *Journal of the American Ceramic Society* **1931**, 14(4): 276–308.

Tress M, Erber M, Mapesa EU, Huth H, Müller J, Serghei A, Schick C, Eichhorn K-J, Voit B, Kremer F. Glassy Dynamics and Glass Transition in Nanometric Thin Layers of Polystyrene. *Macromolecules* **2010**, 43(23): 9937–9944.

Victor JG, Torkelson JM. Photochromic and fluorescent probe studies in glassy polymer matrices. 3. Effects of physical aging and molar weight on the size distribution of local free volume in polystyrene. *Macromolecules* **1988**, 21(12): 3490–3497.

Wang H, Keum JK, Hiltner A, Baer E, Freeman B, Rozanski A, Galeski A. Confined crystallization of polyethylene oxide in nanolayer assemblies. *Science* **2009**, 323(5915): 757–60.

Wijmans J. The solution-diffusion model: a review. *Journal of Membrane Science* **1995**, 107(1-2): 1–21.

Wolak M a., Pan M-J, Wan A, Shirk JS, Mackey M, Hiltner A, Baer E, Flandin L. Dielectric response of structured multilayered polymer films fabricated by forced assembly. *Applied Physics Letters* **2008**, 92(11): 113301.

Wypych A, Duval E, Boiteux G, Ulanski J, David L, Mermet A. Effect of physical aging on nano- and macroscopic properties of poly(methyl methacrylate) glass. *Polymer* **2005**, 46(26): 12523–12531.

Vita

Thomas Matthew (Tom) Murphy was born in Cincinnati, Ohio. In 1995, his family relocated to Conway, Arkansas, where he attended middle school and high school. Tom graduated from Conway High School in 2001. Upon completion of high school, he attended the University of Arkansas at Fayetteville as a Bodenhamer Fellow. In 2004, Tom worked as a summer engineering intern at Potlatch Corp., a paper mill located in McGehee, Arkansas. Tom graduated with a Bachelor of Science in Chemical Engineering, *summa cum laude*, in May 2005 and received the First-Ranked Senior Scholar award for chemical engineering. After completing his undergraduate study, he worked as an intern and associate engineer in the Process Technology group at E&J Gallo Winery in Modesto, California. Tom entered the University of Texas at Austin in 2006 to pursue a doctoral degree in chemical engineering. Under the direction and tutelage of Dr. Donald R. Paul and Dr. Benny D. Freeman, he received the degree of Doctor of Philosophy in Chemical Engineering in Fall 2012. After completion of his degree, Tom will begin his career with the Dow Chemical Company in Freeport, Texas, in a rotational program within the Performance Plastics group.

Permanent email address: thomas.matthew.murphy@gmail.com

This dissertation was typed by the author.